An Investigation into the Axial Capacity of Eccentrically Loaded Concrete Filled Double Skin Tube Columns

by

Johan Alexander Koen

Dissertation presented for the degree of
Master of Science in Engineering at
Stellenbosch University

Supervisor: Dr Trevor Haas
Faculty of Engineering
Department of Civil Engineering

March 2015

DECLARATION

By submitting this thesis/dissertation electronically, I declare that the entirety of the work contained therein is my own, original work, that I am the sole author thereof (save to the extent explicitly otherwise stated), that reproduction and publication thereof by Stellenbosch University will not infringe any third party rights and that I have not previously in its entirety or in part submitted it for obtaining any qualification.

March 2014

Signature:

SUMMARY

Concrete filled double skin tube (CFDST) columns is a new method of column construction. CFDST columns consists of two steel hollow sections, one inside the other, concentrically aligned. The cross-sections of the two hollow sections does not have to be the same shape. Concrete is cast in between the two hollow sections resulting in a CFDST. This study only considers CFDST columns constructed with circular steel hollow sections. The advantages of CFDST construction include:

- The inner and outer steel hollow sections replaces the traditional steel reinforcement that would be used in a normal reinforced concrete column. This reduces the construction time since there is no need to construct a reinforcing cage.
- The steel hollow sections acts as a stay in place formwork, eliminating the need for traditional formwork. This also reduces construction time.
- The steel hollow sections confine the concrete, making it more ductile and increasing its yield strength.

The objective of this study is to identify methods that can predict the axial capacity of eccentrically loaded circular CFDST columns. Methods chosen for the investigation are:

1. Finite element model (FEM). A model was developed to predict the behaviour of eccentrically loaded CFDST columns. The FE model uses a concrete material model proposed in literature for stub columns. The aim was to determine whether the material model is suited for this application.
2. The failure load of CFDST columns under concentric loading was calculated using a model obtained in literature. These capacities were compared to the experimental test results of eccentrically loaded CFDST columns to establish a correlation.

This study found that the concrete material model used does not adequately capture the behaviour resulting in the axial response of the column being too stiff. The difference between the eccentrically loaded experimental test results and the calculated concentrically loaded capacity showed a clear trend that could be used to predict the capacity of eccentrically loaded CFDST columns.

OPSOMMING

Beton-gevulde dubbel laag pyp (BGDLP) kolomme is 'n nuwe metode van kolom konstruksie. BGDLP kolomme bestaan uit twee staal pyp snitte, die een binne die ander geplaas met hul middelpunte opgelyn, die dwarssnit van die twee pype hoef nie dieselfde vorm te wees nie. Beton word dan in die wand tussen die twee pyp snitte gegiet. Die resultaat is 'n hol beton snit. Hierdie studie handel slegs oor BGDLP kolomme wat met ronde pyp snitte verwaardig is. Die volgende voordele kan aan BGDLP toegeken word:

- Die binne en buite staalpype vervang die tradisionele staal bewapening was in normale bewapende-beton gebruik sou word. Dus verminder dit die tyd wat dit sal neem om die kolom op te rig.
- Die staalpypsnitte is ook permanente vormwerk. Dit doen dus weg met die gebruik van normale bekisting, wat ook konstruksie tyd spaar.
- Die buite-staalpypsnit bekamp die uitsetting van die beton onder las. Hierdie bekamping veroorsaak dat die beton se gedrag meer daktiel is en 'n hoër falings spanning kan bereik.

Die doel van die studie is om metodes te identifiseer wat gebruik kan word om die aksiale kapasiteit onder eksentriese laste van BGDLP kolomme te bepaal. Twee metodes was gekies:

1. Eindige element model. 'n Model was ontwikkel om die gedrag van BGDLP kolomme te voorspel. Die mikpunt was om te bepaal of 'n beton materiaal gedrag model vanuit die literatuur gebruik kan word om BGDLP kolomme te modelleer.
2. Die swiglas van BGDLP kolomme onder konsentriese belasting was bereken vanaf vergelykings uit die literatuur. Hierdie swiglaste was vergelyk met die eksperimentele toets resultate vir eksentriese belaste BGDLP kolomme om 'n korrelasie te vind.

Hierdie studie het bewys dat die beton materiaal model uit die literatuur kan nie gebruik word om die swiglaste van BGDLP kolomme te bepaal nie. Die model het die gedrag te styf gemodelleer. Die verskil tussen die berekende konsentriese belaste swiglas en die eksperimentele resultate van eksentriese BGDLP kolomme was voorspelbaar en kan gebruik word om die swiglas van eksentriese belaste BGDLP kolomme te voorspel.

ACKNOWLEDGEMENTS

I would like to thank the following people for their assistance and support during this study:

- My supervisor, Dr. Trevor Haas for his patience, guidance and support throughout this study.

- The workshop and laboratory staff at the Civil Engineering Department of Stellenbosch University, for their assistance during the experimental work.

- My Wife, for her support, understanding and patience.

- Finally, my Creator, for giving me the ability to complete this study.

TABLE OF CONTENTS

LIST OF FIGURES

Chapter 1

INTRODUCTION

Concrete and steel composite sections are widely used to construct columns for an array structures. The most common composite used in the Civil Engineering industry, is reinforced concrete (RC), where steel reinforcement is embedded within the concrete. This study investigates a different type of composite section, namely concrete infill tubular sections. These composite sections consist of a hollow steel profile filled with unreinforced concrete. In particular, this study considers concrete filled double skin tube (CFDST) columns. This type of composite section consists of two hollow steel sections (HSS), one placed inside the other, with the cavity between the two HSS filled with unreinforced concrete, leaving the smaller HSS unfilled. A comprehensive overview of work conducted on circular CFDST columns is presented due to the newness of these composite sections.

The literature study confirms that this is a new field of investigation. The majority of research focused on stub CFDST columns and limited intermediate to slender columns, which in concentrically loaded. The literature study found one paper which addresses eccentrically loaded CFDST columns. Thus the investigation confirmed that the case of eccentrically loaded CFDST columns required further research.

The objective of this study is to investigate the capacity of eccentrically loaded concrete filled double skin tube (CFDST) columns and identify methods of predicting their capacities. In order to achieve this goal a literature study was conducted on CFDST. From the literature study two methods were identified to analyse CFDSTs, namely finite element modelling and a model from literature (Zhao, et al., 2010). Experimental tests were conducted and compared to the two chosen methods for comparison.

The report contains the following content layout:

Chapter 2:   Provides a literature review on CFDST columns, focusing on circular cross sections.

Chapter 3:   Presents the experimental work conducted which includes the test setup and the results.

Chapter 4:   Discusses the development of the finite element model (FEM) used in this study to predict the response of eccentrically loaded CFDST columns.

Chapter 5:   Draws comparisons between the different methods and the experimental results.

Chapter 6:   Provides the final conclusions and discusses future recommendations.

Chapter 2

LITERATURE REVIEW

2.1. INTRODUCTION

Concrete-filled double skin tubes (CFDST) is a relatively new method of constructing columns. The literature review explores research conducted on single skin concrete-filled steel tubes (CFST), where after CFDST sections are reviewed. The origins of this composite section is also briefly discussed. It is shown that the work conducted on CFST was adopted with minor changes to predict the behaviour of CFDST members. The literature review found that the behaviour of CFDST members predicted by these adopted methods show good correlation with experimental results when stub columns were investigated.

2.2. BACKGROUND

A column is a vertical structural member that resists compressive axial loads, with or without moments applied to it. The cross-sectional dimensions of a column are generally significantly smaller than the height of a column. The purpose of a column is to transfer vertical loads from floor slabs, beams and roof structures to the structure's foundations. The shape and size of a column's cross-section is typically square, circular or rectangular although elliptical, diamond, triangular and other shapes have also been used. The cross sectional shape of a column depends on aesthetics and the loads the column is expected to resist.

Under seismic loading, columns with circular cross-sections perform better than similar square cross-section columns. This is due to circular cross-sections providing better confinement than square cross-sections (Xiao & Zhang, 2008). In cases where larger moments need to be resisted, a deeper rectangular cross-section is favoured about the axis generating the larger moment. Bending moments in columns is caused by eccentric and lateral loading. Column to beam connections and point loads that are eccentrically applied to the cross-section of the column are examples of eccentric loading. Typically horizontal loads are resisted by shear walls. However, when moment frames are used, the columns are required to resist moments caused by horizontal loads. In South Africa, moment frames are typically used in framed structures such as warehouses, apartments and office buildings. Since columns can be constructed from different materials, any material that is strong enough can be used to transfer vertical loads

from floors and roofs to the structure's foundation. For this study only columns that use concrete and steel as a construction material is considered.

Concrete is a complex material with many factors affecting its dimensional stability; such as creep and shrinkage which can be exacerbated by environmental conditions and cause cracking in the concrete (Mehta & Monteiro, 2006). The main factors that affect the strength of concrete are:

- The water-cement ratio.
- The porosity of the concrete, which is affected by the compaction of the concrete.

Concrete is an isotropic material. The tensile strength of concrete varies between 7% and 11% of the compressive strength (Mehta & Monteiro, 2006).

To minimise cracking in concrete caused by tensile stresses due to shrinkage and loading conditions, structural members are typically constructed from concrete and steel, where steel is used to resists the tensile stresses. The most common concrete-steel composite uses steel reinforcement embedded in the concrete to reinforce the structural member where tensile forces are present. This type of composite is commonly known as reinforced concrete (RC). In seismic prone regions reinforcing steel in RC columns is arranged to provide confinement by placing stirrups close together, approximately 30mm apart. The reason for this is that confined concrete is more ductile than unconfined concrete (Mirmiran & Shahawy, 1997).

Fibre reinforced concrete (FRC) is an advancement in concrete technology, where fibres (either steel or polymer) are added to the concrete mix to control cracking in the matrix. However, reinforcing steel is still required to resist larger tensile forces.

RC is not the only steel-concrete composite which exists. Other types of steel and concrete composite sections include; encased composite sections and filled composite sections presented in Figure 2-1. Encased sections consist of a steel section, typically an H-section, encased in concrete. Concrete filled sections consist of a hollow steel section filled with concrete. Self-compacting concrete (SCC) enables concrete to fill a mould without the need for mechanical compaction. This is achieved by an additive that polarises the particles in the concrete, making is more workable. SCC would thus be favourable to use in concrete filled sections. This study deals with concrete-filled sections with no reinforcing in the infill, as shown in Figure 2-1.
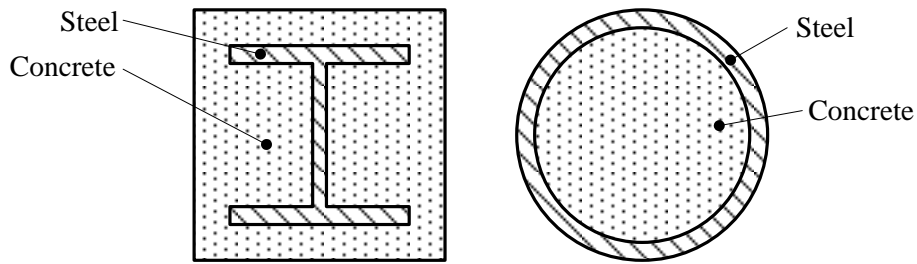
Figure 2-1: Examples of concrete-encased (left) and concrete-filled (right) sections

2.3.   CONCRETE-FILLED STEEL TUBES

Concrete-filled steel tubes (CFSTs) have been used in many structural engineering applications, such as columns in high-rise buildings, industrial buildings, electricity transmitting towers and bridges (Zhao, et al., 2010). CFST sections have the following advantages:

- During construction the steel tube provides permanent formwork for the concrete.
- Prior to pumping wet concrete into the members, the steel tube can carry significant construction loads.
- Increased strength and ductility. The steel tube offers confinement to the concrete which increases the capacity of the concrete. The concrete also supports the steel tube, reducing or eliminating local buckling of the steel section resulting in increased load carrying capacity, ductility and energy absorption during earthquakes.
- The thermal properties of concrete increase the fire resistance of the steel tube.

These advantages result in quick and efficient construction as opposed to traditional RC construction. Numerous research projects were conducted on CFST columns to determine the advantages that this construction method offers. Research investigating the axial capacity of square, rectangular, circular and even elliptical steel tubes filled with concrete was conducted by (Vrcelj & Uy, 2002), (Zhao & Packer, 2009), (Ellobody & Young, 2006) , (Giakoumelis & Lam, 2004) and (Gupta, et al., 2007).

Numerous researchers investigated the influence of several parameters on the behaviour of circular CFST stub columns. Some of the columns were filled with SCC and others with normal concrete (NC), (Yu, et al., 2007). The parameters that were investigated included measurement methods of deformation and concrete strength. The affect of small holes or full slots notched in the hoop direction of the steel tube on the confinement of the concrete core and compression shared by the steel tube was also investigated. It was found that by increasing the compressive

strength of the concrete, for both SCC and NC, resulted in a significant increase in load capacity. Increasing the compressive strength of concrete had little affect on the residual capacity after failure. The results also showed that a significant confinement effect was present for most specimens after the axial load reached a certain percentage of the ultimate capacity of the stub column. Once the steel tube was notched with small holes at mid-height region, the confinement affect was enhanced and occurred earlier, but the axial compressive stiffness was reduced. However, the ultimate capacity and residual capacity were insignificantly influenced. When the steel tube was notched around the full perimeter at mid-height region, the axial capacity and axial compressive stiffness decreased. The confinement affect is enhanced when the dimension of the full slot was small. However, increasing the slot dimension gradually resulted in insignificant confinement from the steel tube. The authors also investigated different loading conditions, namely:

a) Where both the steel and concrete were loaded simultaneously.
b) Initially only the concrete is loaded, thereafter both materials resisted the compression force.
c) Initially only the steel was loaded, thereafter both materials resisted the compression force.
d) The concrete section only. Only the concrete was loaded through the entire test.

When case (a) is compared, the results showed that:

- For case (c).
  - The confinement takes effect earlier but is reduced.
  - The ultimate capacity is comparable to case (a).
- For case (b) and (d).
  - The confinement affect is enhanced but delayed.
  - The ultimate capacity increased insignificantly from that observed in case (a).
- For all cases.
  - The residual capacity of the stub column is hardly influenced.

Other research includes work on creep modelling in CFST (Mirmiran & Naguib, 2003). Using the rate of flow method and the double power law creep function, Naguib and Mirmiran (Mirmiran & Naguib, 2003) developed an algorithm to determine the creep of CFST columns by adhering to strain compatibility and static equilibrium. Their proposed model shows good

agreement with previous creep tests on bonded and un-bonded CFSTs. Some research was conducted into the behaviour of CFST sections using other metals beside carbon steel for the tube. Experimental tests on short and slender concrete filled stainless steel tubular columns shows that, compared to conventional carbon steel CFST columns, stainless steel composite columns show more ductile behaviour and have a much higher residual strength. However, for slender columns there is no obvious difference between the stainless steel and conventional carbon steel concrete-filled columns in terms of test observations and failure modes (Uy, et al., 2011). Zhou and Young investigated concrete-filled aluminium tubes filled with concrete (Zhou & Young, 2009). Forty-two stub column specimens were tested with diameter-to-thickness ratios and cylinder strengths ranging from 9.7 to 59.7 and 40.7 to 100 MPa, respectively. The test results were compared to design approaches using the American and the Australian/New Zealand specifications, which generally yielded conservative estimates of the capacity of the columns.

Work was also conducted that investigates the design and construction of moment-resisting joints used in two low-rise buildings in Vancouver, Washington U.S.A (Schneider, et al., 2004).

The above paragraphs informs us of the different research topics conducted in the field of concrete-filled sections. To limit the focus of this investigation only the axial capacity of CFST columns will be elaborated on.

The overall behaviour of CFST members in compression is similar to that of unfilled tubular columns. The strength of the columns depends significantly on the member's length and the end support conditions. The bending stiffness of CFST columns increase, compared to unfilled tubes, due to the concrete infill, which results in increased column capacity (Zhao, et al., 2010).

The local buckling of tubular sections in compression is well documented. The typical inelastic local buckling mode for square hollow sections (SHS) is the so called "roof mechanism" where two opposite faces buckle outward and the other two opposite faces buckle inward. For circular hollow sections (CHS) the so called "elephant's foot" failure occurs, where the entire section perimeter buckles outward. The typical failure mode for short CFSTs is an outward folding mechanism, because the concrete core supports the steel tube from inward buckling (Zhao, et al., 2005). These failure mechanisms are shown below in Figure 2-2 and Figure 2-3. Similar failure modes are observed for concrete-filled sections.

<p align="center">(a)   (b)   (c)   (d)</p>
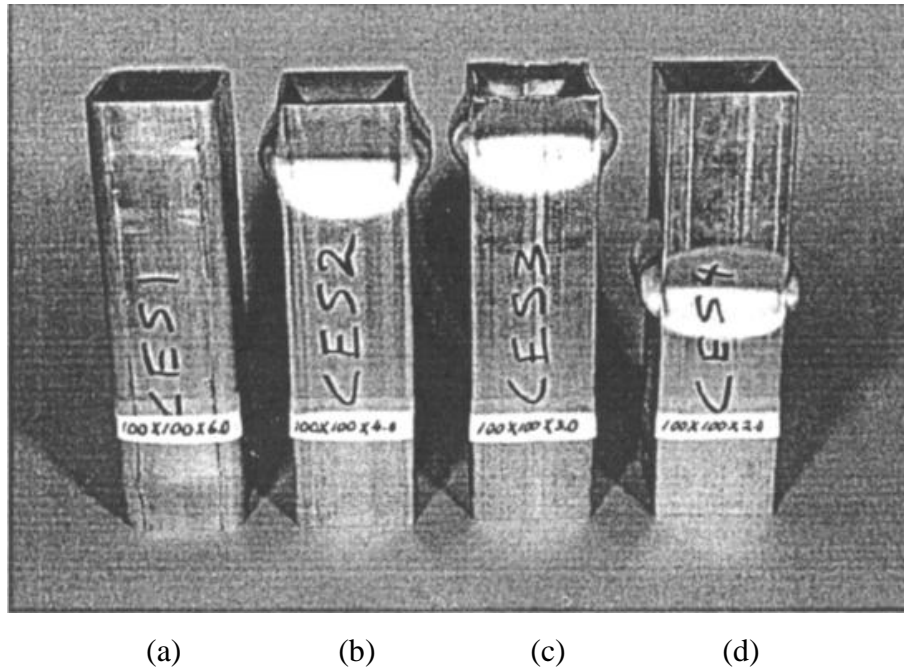
Figure 2-2: Typical local buckling failure modes for cold-formed rectangular hollow sections (Zhao, et al., 2005)

(a)   Slight local buckling near bottom end of column.

(b)   Significant local buckling near top end of column. Clearly demonstrates the roof mechanism discussed earlier.

(c)   Significant local buckling near top end of column. Clearly demonstrates the roof mechanism discussed earlier.

(d)   Significant local buckling near midspan of column. Clearly demonstrates the roof mechanism discussed earlier.

<p align="center">(a)   (b)   (c)   (d)   (e)   (f)   (g) (h)</p>
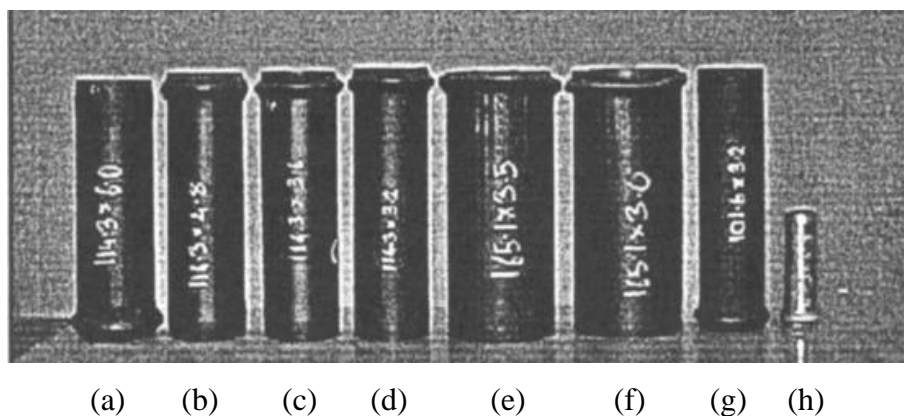
Figure 2-3: Typical local buckling modes for cold-formed circular hollow sections (Zhao, et al., 2005)

The elephant's foot mechanism discussed earlier is presented in columns (a)-(h) of Figure 2-3. In columns (b)-(f) the local failure mechanism occurs near the top end of the columns and for specimen (a), (g) and (h) it occurs near the bottom of the column.

The local buckling modes depicted in Figure 2-2 and Figure 2-3 can be described by St Venant's principle. The principle states that the stresses are concentrated at the point where the load is applied and reduces to a constant stress across the entire cross section at a dimension equal to the largest dimension of the cross section away from the point where the load is applied.

A schematic view of the stress strain curves of CFST sections in compression is presented in Figure 2-4, where ξ is the constraining factor defined as:

$$\xi = (A_{so} \cdot f_{syo})/(A_c \cdot f_{ck}) \qquad\qquad \text{EQ 2-1.}$$

where A_{so} is the cross-sectional area of the outer steel tube; A_c is the cross-sectional area of the concrete core, f_{syo} is the yield strength of the outer steel tube and f_{ck} is the characteristic strength of the concrete taken as 67% of the cube compression strength (f_{cu}). For circular hollow sections (CHS) the constraining factor ξ_o is approximately 1.1, while rectangular hollow sections (RHS) has a ξ_o of 4.5. This indicates that confinement is greater in CHS than in RHS (Zhao, et al., 2010).
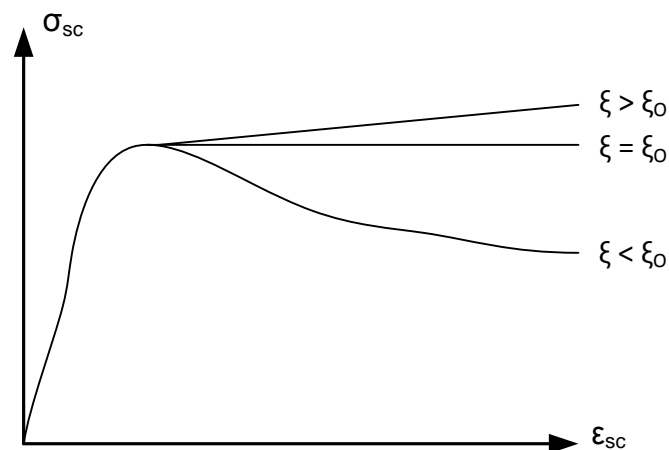
Figure 2-4: Schematic view of stress-strain curves of CFST

When CHSs confine concrete a tensile stress develops in the hoop direction of the tube as a reaction to the expanding concrete. The confinement provided by the steel tube to the concrete core reduces as the steel reaches its yield strength. For slender columns that fail as a result of flexural buckling it can be assumed that the steel remains elastic and therefore will still provide significant confinement to the concrete core. In certain design codes a reduced steel capacity is considered due to the hoop stress caused by the expansion of the concrete core under compression.

pg. 9

CFST columns can be classified as short, intermediate or long. For short (stub) columns the axial capacity of the column is directly related to the section capacity of the CFST. For long (slender) columns the capacity is proportional to the bending stiffness of the section as opposed to the section capacity. Thus, a larger elastic buckling load is expected from CFST columns as a result of its increased bending stiffness as opposed to a regular RC section where the reinforcing steel is closer to the centre of the cross section. For intermediate length columns the concept of interaction of local buckling and member buckling also applies to CFST columns. However, the local buckling is delayed, and could be eliminated, as a result of the support that the concrete core provides the steel tube. The member capacity of CFST columns are calculated in a familiar manner; i.e. the member's capacity is equal to the product of the section capacity and a slenderness reduction factor. The Chinese code DBJ13-51 uses a slenderness reduction factor, (called the column stability factor ϕ) that is a function of steel yield stress, concrete strength, steel ratio (area of steel over area of concrete) and the member slenderness.

A publication by Y.C. Wang (Wang, 1999) compares three codes of practice for designing slender composite columns, for both encased and single skin concrete-filled tubes. The three codes are:

- Eurocode 4 (EC 4): Part 1.1.
- BS 5400: Part 5.
- A modification of the British Standard for steel BS 5950 Part 1 which contains a design method for steel columns that is simple to use, clear to understand, well calibrated, and well accepted by the steelwork design profession in Britain.

The basis of the modification is to replace the appropriate steel section properties with those of the composite section. This method has been fully presented in a paper by Wang and Moore (Wang & Moore, 1997) and its validity is supported by comparing the results from this method against a large number of tests on concrete filled composite columns. The paper by Wang concluded that all three methods, the EC4, BS 5400 and the proposed modified method, yields conservative predictions when compared to experimental data. The closest predictor is the EC4 method followed by the proposed modified method and then the BS 5400 method. However, the proposed modified method gives a clear understanding of the behaviour of composite columns and is much easier to use than both the BS 5400 and the EC4 methods.

A more recent investigation into the behaviour of eccentrically loaded slender CFST columns using fibre reinforced concrete (FRC) with CHS found that the use of FRC resulted in a significant improvement in the structural behaviour of slender composite columns subjected to eccentric loading (Gopal & Manoharan, 2006). It was also found that the slenderness ratio has a significant affect on the strength and behaviour of CFST columns under eccentric loading. FRC filled steel tubular columns have a relatively high stiffness when compared to normal CFST columns. As we know, ductility is defined as the ability to possess non-linear deformation under loading and the energy absorption as the work done by the external load up to the failure of the column specimen. Using FRC had an insignificant influence on the ductility of the specimens compared to the normal concrete filled steel tube columns. However the test reviled an increase in the energy absorption of the column.

From available journal articles it is evident that extensive research was conducted on CFST columns. However, a variant of CFST sections that have not received the same amount of attention is concrete filled double skin tube (CFDST) sections. The advantages of CFST columns are clear and should hold for concrete-filled double skin tube columns as well, with the added benefit that it is lighter due to the void in the centre of the column. The specific focus of this investigation is on CFDST columns which is now elaborated upon.

2.4.   CONCRETE-FILLED DOUBLE SKIN TUBULAR (CFDST) SECTIONS

Recently a concept named concrete-filled double skin tubes (CFDST) was developed using two steel tubes while filling the annulus with concrete. CFDST may provide the following advantages (Zhao & Han, 2006):

- Lighter weight.
- High bending stiffness due to inner tube.
- Good cyclic performance.
- High fire resistance due to concrete protection of inner tube.
- High energy absorption due to the concrete infill and deformation of the inner tube.
- High local buckling stability due to the support offered to the steel by the concrete infill
- High global stability due to an increased section modulus.

One major challenge of CFDSTs is the susceptibility to the influence of poor concrete compaction. In reinforced concrete columns compaction only affects the concrete's mechanical properties. However, with CFDST columns, the steel-concrete interaction is vital. Not only are

the concrete infill's mechanical properties influenced, but the steel-concrete interaction may also be affected thereby changing the overall behaviour of the column by introducing imperfections. One way of avoiding this would be to use SCC.

2.5.   BEHAVIOUR OF CFDST COLUMNS

The behaviour of CFDST columns is derived from the behaviour of single skin concrete filled tube columns, discussed in *Section 2.3*. This section discusses the theoretical models derived to predict the behaviour of circular CFDST columns and observations made by other authors regarding the behaviour of CFDST columns from experimental tests.

2.5.1.   CFDST COLUMNS UNDER STATIC LOADING

Zhao and Han (Zhao & Han, 2006) reported on tests conducted by other authors on CFDST stub columns with four combinations of outer and inner tubes shown in Figure 2-5. It was observed that the outer tube of the CFDST behaves similarly to the tube in CFST while the inner tube of CFDST behaves like an unfilled tube. A significant increase in the ultimate load and ductility was observed when comparing the behaviour of a typical CFDST stub column to the corresponding unfilled outer steel tube. It was also observed that a larger increase in ductility and energy absorption is experienced for slender CFDST columns.
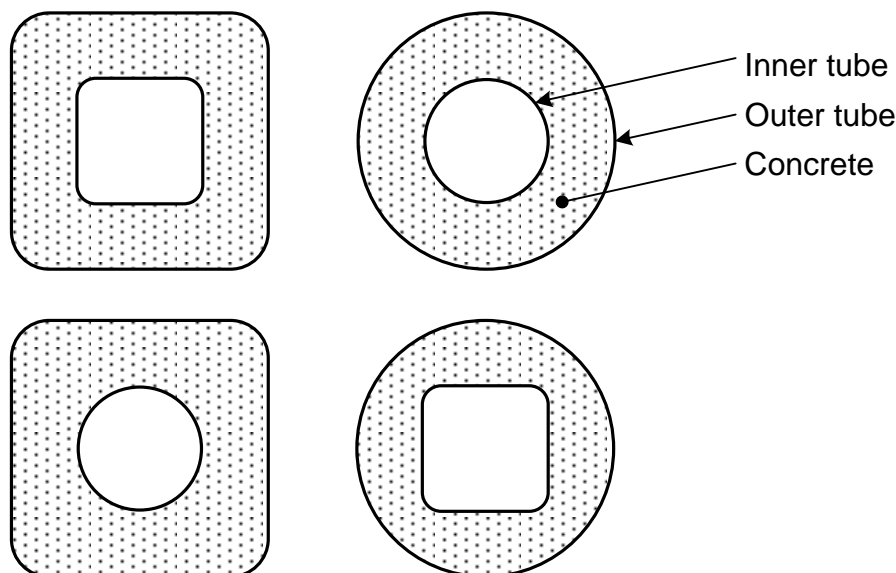
Figure 2-5: Different combinations of inner and outer tubes used in CFDST sections

A unified theory is described by Tao (Tao, et al., 2007) which was used to develop a theoretical model for CFDST stub columns. The interaction between the steel tubes and the sandwiched concrete was first examined. The structural behaviour of CFDSTs under axial loading is

pg. 12

significantly influenced by the different Poisson's ratio of the steel and concrete. The initial Poisson's ratio of concrete is approximately 0.2 while that of steel is approximately 0.3. Thus, the initial lateral expansion of the steel will be greater than that of the concrete causing the outer steel tube to provide no confinement effect while causing the inner tube to press against the inner face of the concrete core. The affect of the inner tube applying an outward force on the concrete is negligible because the concrete soon enters the elasto-plastic state, thus the pressure stops increasing and then decreases gradually. As the longitudinal strain in the column increases the lateral expansion of the concrete starts to exceed that of the outer steel tube due to lateral cracking of the concrete. Compression will develop between the concrete core and the outer steel tube while the pressure between the inner tube and the concrete decreases until it changes to tension. Since the bond between the two surfaces is small, it becomes reasonable to negate the tension between them until they delaminate. In single skin CFST columns the stress in the concrete is assumed to be constant along the radial direction (moving from the outer tube to the centre of the concrete core). It is evident from the fact that there is no stress between the inner tube and the concrete that, in the case of CFDST columns the stress is not constant along the radial direction. The uneven distribution of stress is concentrated mainly near the inner part of the concrete core and may be ignored if the hollow section ratio (the ratio between the inner and outer tube diameters) is not too large. This was verified by test results (Tao, et al., 2007). When considering the steel tubes, the propensity for local buckling is reduced by the concrete infill. The outer tube can only buckle outward while the inner tube can only buckle inward. However, if the concrete infill is too thin the inner tube could buckle outward in the same region where the outer tube buckles (Zhao, et al., 2002).

Considering the discussion above, it is assumed that the inner tube acts independently and can develop its full yielding strength due to the concrete infill. Conversely, the outer tube and the sandwiched concrete have the same behaviour as a standard CFST column. Thus, the confined state of the concrete is the same in a CFDST as for CFST, as long as the hollow section ratio is not greater than 0.8 (Tao, et al., 2007).

The assumptions above are used to develop an equivalent stress strain relationship. The equivalent stress-strain model presented in Figure 2-6 is taken from (Tao, et al., 2007). The model uses the same confinement factor for CFST, which is presented in equation 2-1 (pg9), however uses nominal concrete area not the actual concrete area, presented as:

$$\xi = \frac{A_{so} \cdot f_{syo}}{A_{c,nominal} \cdot f_{ck}} \qquad \text{EQ 2-2}$$

where:

- A_{so} is the cross-sectional area of the outer steel tube
- $A_{c,nominal}$ is the nominal cross-sectional area of the concrete given by $\pi(D_o - 2t_{so})^2/4$, where t_{so} is the thickness of the outer tube.
- f_{syo} is the yield strength of the outer steel tube and f_{ck} is the characteristic strength of the concrete, taken as 67% of the cube compression strength (f_{cu}).

The effects of changes in the confinement factor on the stress-strain relationship is shown in Figure 2-6.
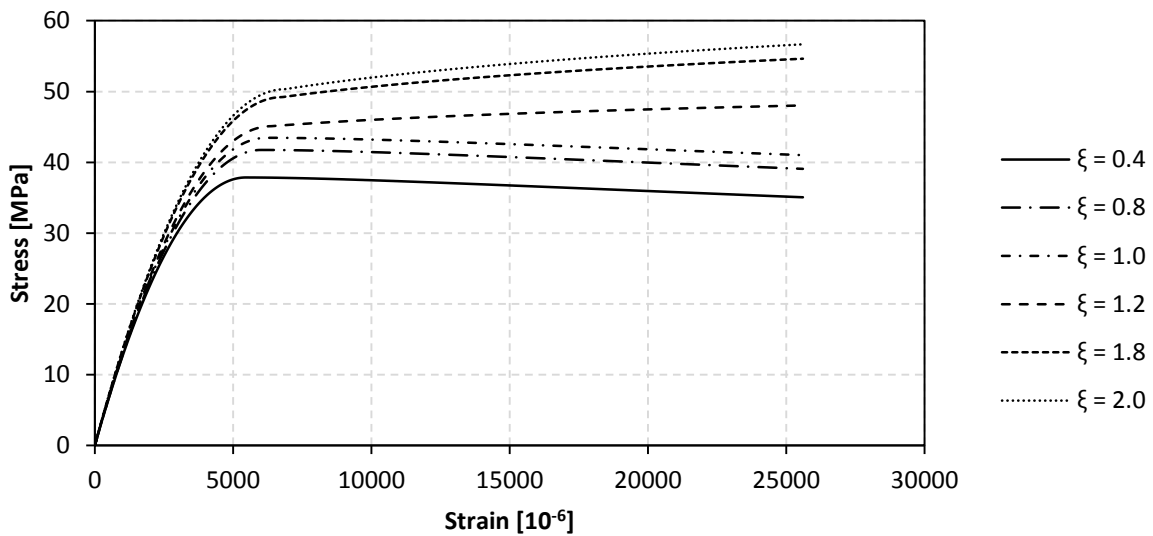
Figure 2-6: Stress versus strain relations of concrete core.

The stress strain relationship depicted in Figure 2-6 is described as:

$$y = 2x - x^2 \qquad (x \leq 1) \qquad \text{EQ 2-3}$$

$$y = \begin{cases} 1 + q \cdot \left(x^{0.1\xi} - 1\right) & (\xi \geq 1.12) \\ \dfrac{x}{\beta \cdot (x-1)^2 + x} & (\xi < 1.12) \end{cases} \quad (x > 1) \qquad \text{EQ 2-4}$$

where $y = \sigma/\sigma_o$, $x = \varepsilon/\varepsilon_o$

with $\quad \sigma_o = \left[1 + (-0.054\xi^2 + 0.4\xi) \cdot \left(\frac{24}{f_c}\right)^{0.45}\right] \cdot f_c$

$\quad \varepsilon_o = \varepsilon_{cc} + \left[1400 + 800 \cdot \left(\frac{f_c}{24} - 1\right)\right] \cdot \xi^{0.2}$

pg. 14

$$\varepsilon_{cc} = 1300 + 12.5 f_c$$

$$q = \xi^{0.745}/(2 + \xi);$$

$$\beta = (2.36 \times 10^{-5})^{[0.25+(\xi-0.5)^7} \cdot f_c^2 \cdot 3.51 \times 10^{-4}$$

From Figure 2-6 it is evident that a higher confinement factor results in a greater compressive strength. It is also noticeable that the ductility of the concrete core also increases with the confinement factor. From the stress strain relationships, the load versus axial strain behaviour is obtained based on the following assumptions:

1. There is no slip between the steel and concrete.
2. Longitudinal stress-strain models of steel and concrete are determined using the relationships discussed above.
3. The force equilibrium and deformation constraints are considered along the longitudinal direction and presented as:

$$N_{CFDST} = N_{outer} + N_{inner} + N_{concrete} \qquad\qquad \text{EQ 2-5}$$

$$\varepsilon_{CFDST} = \varepsilon_{outer} = \varepsilon_{inner} = \varepsilon_{concrete} \qquad\qquad \text{EQ 2-6}$$

where N_{outer}, N_{inner} and $N_{concrete}$ are the longitudinal forces supported by the outer steel tube, inner steel tube and concrete infill, while ε_{outer}, ε_{inner} and $\varepsilon_{concrete}$ is the strain in each material respectively.

Toa (Tao, et al., 2007) used these equations to plot prediction curves for the axial load versus strain of CFDST stub columns. Good agreement was achieved between the predicted curves and experimental test curves. However, the post peak behaviour of the specimens that are more susceptible to local buckling does not agree well with the prediction curves.

Han (Han, et al., 2009) used the fibre-based model from Tao (Tao, et al., 2007) to conduct parametric studies for CFDSTs to attain a design approach. It was found that the design formulae for CFDSTs could be obtained by modifying the formulae from CFSTs.

2.5.1.1. SECTIONAL CAPACITY

The force equilibrium of equation 2-5 can be written as equation 2-7.

$$N_{CFDST,u} = N_{oc,u} + N_{i,u} \qquad\qquad \text{EQ 2-7}$$

pg. 15

where: $\qquad N_{oc,u} = A_{osc} \cdot f_{osc}$

$\qquad\qquad N_{i,u} = A_{si} \cdot f_{yi}.$

f_{yi} and A_{si} are the yield strength and cross sectional area of the inner steel tube. A_{osc} is the cross-sectional area of the outer steel tube and the concrete infill. f_{osc} is the yield stress of the outer tube and concrete composite, given for circular CFDSTs as;

$$f_{osc} = C_1 \cdot \chi^2 \cdot f_{yo} + C_2 \cdot (1.14 + 1.02\xi)f_{ck} \qquad\qquad \text{EQ 2-8}$$

where: $C_1 = \alpha/((1 + \alpha))$;

$\qquad C_2 = (1 + \alpha_n)/(1 + \alpha);$

$\qquad \alpha = A_{so}/A_c$;

$\qquad \alpha = A_{so}/A_{c,nominal}$

The confinement factor ξ was defined earlier in 2-1 and χ is the hollow section ratio described previously as $D_i/(D_o - 2 \cdot t_o)$ for circular CFDSTs. A_c is the area of the concrete given as; $\pi[(D_o - 2t_{so})^2 - D_i^2]/4.$

2.5.2. CFDST BEAM COLUMN

Four point bending tests were conducted on CFDST beams (Zhao, et al., 2010). It was concluded that the outer tube and the concrete infill behaves in a similar manner as a single skin concrete-filled steel tube while the inner tube behaves similar to an unfilled tube. Based on these observations the ultimate moment capacity of CFDST sections can be estimated using the sum of the section capacity of the inner tube and that of the outer tube filled with concrete. Figure 2-7 shows the stress distribution over the section at ultimate capacity. From here equilibrium formulas can be derived. The formulas were adopted from (Zhao, et al., 2010).

pg. 16
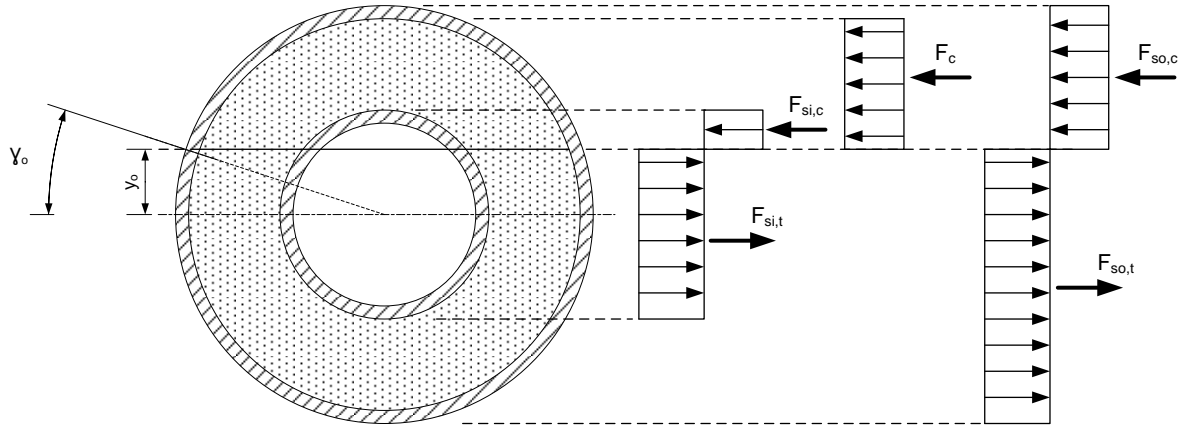
Figure 2-7: Neutral axis and stress distribution on CFDST section

The compression forces in the tubes is described as:

$$F_{si,c} = f_{yi} \cdot t_i \cdot r_{im} \cdot (\pi - 2 \cdot \gamma_i) \qquad \text{EQ 2-9a}$$

$$F_{so,c} = f_{yo} \cdot t_o \cdot r_{om} \cdot (\pi - 2 \cdot \gamma_o) \qquad \text{EQ 2-9b}$$

$$F_{s,c} = F_{si,c} + F_{so,c} \qquad \text{EQ 2-9c}$$

The concrete in compression is presented as:

$$F_{co} = f_{ck} \cdot r_{oi}^2 \cdot \left(\frac{\pi}{2 - \gamma_o - 0.5 \cdot \sin(2 \cdot \gamma_o)} \right) \qquad \text{EQ 2-10a}$$

$$F_{ci} = f_{ck} \cdot r_{io}^2 \cdot \left(\frac{\pi}{2 - \gamma_i - 0.5 \cdot \sin(2 \cdot \gamma_i)} \right) \qquad \text{EQ 2-10b}$$

$$F_c = F_{co} - F_{ci} \qquad \text{EQ 2 10c}$$

The tensile forces in the tubes is described as:

$$F_{si,t} = f_{yi} \cdot t_i \cdot r_{im} \cdot (\pi + 2 \cdot \gamma_i) \qquad \text{EQ 2-11a}$$

$$F_{so,t} = f_{yo} \cdot t_o \cdot r_{om} \cdot (\pi + 2 \cdot \gamma_o) \qquad \text{EQ 2-11b}$$

$$F_{s,t} = F_{si,t} + F_{so,t} \qquad \text{EQ 2-11c}$$

The equilibrium equation is then written as:

$$F_{s,t} = F_{s,c} + F_c \qquad \text{EQ 2-12}$$

pg. 17

- where f_{yi} and f_{yo} are the yield strength of the inner and outer steel tubes.
- t_i and t_o are the thicknesses of the inner and outer steel tubes.
- r_{im} and r_{om} are the radius to the centre of the inner and outer tube.
- f_{ck} is the characteristic strength of the concrete core, taken as 67% of the cube strength.
- r_{oi} is the inside radius of the outer tube.
- r_{io} is the outer radius of the inside tube.

The resultant force of the concrete is obtained by assuming the entire section is filled with concrete (F_{co}) and subtracting the force that would have been carried by the void and inner tube (F_{ci})

The angle γ_i can be written in terms of γ_o presented in equation 2-13 as:

$$\gamma_i = \sin^{-1}\left(\sin(\gamma_o) \cdot \frac{r_{om}}{r_{im}}\right) \leq \frac{\pi}{2} \qquad \text{EQ 2-13}$$

Substituting this relationship into the equilibrium equation the depth of the neutral axis (y_n) can be obtained through incrementing γ_o from zero. Once y_n is known the ultimate moment can be determined from equation 2-14.

$$M_{CFDST} = F_{si,t} \cdot d_{si,t} + F_{so,t} \cdot d_{so,t} + F_{si,c} \cdot d_{si,c} + F_{so,c} \cdot d_{so,c} + F_{co} \cdot d_{co} - F_{ci} \cdot d_{ci}$$

$$\text{EQ 2-14}$$

where *d* denotes the distance to the respective resultant forces.

2.5.2.1. FLEXURAL CAPACITY

According to Han (Han, et al., 2009), Tao and Yu published a paper in 2006 titled "New types of composite columns – experiments, theory and methodology" in which the flexural strength of CFDST is derived. Unfortunately the paper in question, published in Science Press, is in Chinese. This paper could not be obtained, thus Han (Han, et al., 2009) is referenced for these formulae. The flexural capacity (ultimate moment) of CFDST columns can be estimated using equation 2-15 as:

$$M_{CFDST,u} = \gamma_{m1} \cdot W_{scm} \cdot f_{scy} + \gamma_{m2} \cdot W_{si} \cdot f_{yi} \qquad \text{EQ 2-15}$$

where W_{scm} is the section modulus of the outer steel tube and the sandwiched concrete while W_{si} is the plastic section modulus of the inner tube. γ_{m1} and γ_{m2} are parameters given by equation 2-16a and 2-16b as:

pg. 18

$$\gamma_{m1} = 0.48 \cdot \ln(\xi + 0.1) \cdot (-0.85 \cdot \chi^2 + 0.06 \cdot \chi + 1) + 1.1.$$

<div align="right">EQ 2-16a</div>

$$\gamma_{m2} = -0.02 \cdot \chi^{-2.76} \cdot \ln \xi + 1.04 \cdot \chi^{-0.67}$$ EQ 216b

2.5.3. MEMBER CAPACITY AND INTERACTION CURVES

Tests on CFDST beam-columns were conducted by Han, Yao and Tao (Han & Yao, 2004), (Tao, et al., 2007). The main parameters that were varied in their studies are:

a) The hollow section ratio, which is the ratio between the inner and outer tube diameters.
b) Outer tube diameter to thickness ratio.
c) Column slenderness.
d) Load eccentricity.

Mechanical models were developed to predict the behaviour CFDST stub columns, beams, columns and beam-columns. The unified theory from Han (Han, et al., 2001) was adopted in the formulation given in Zhao (Zhao, et al., 2010) and Han (Han, et al., 2009) for the interaction curve of circular CFDST columns. The member capacity of CFDST columns can be calculated using the section capacity $N_{CFDST,u}$ (defined in *Section 2.5.1.1*) with a stability reduction factor (φ):

$$N_{CFDST,cr} = \varphi \cdot N_{CFDST,u}$$ EQ 2-17

where the stability reduction factor is given by equation 2-18a as:

$$\varphi \begin{cases} 1.0 & (\lambda \leq \lambda_o) \\ a \cdot \lambda^2 + b \cdot \lambda + c & (\lambda_o < \lambda \leq \lambda_p) \\ d \cdot \frac{-0.23 \cdot \chi^2 + 1}{(\lambda + 35)^2} & (\lambda > \lambda_p) \end{cases}$$ EQ 2-18a

where $\lambda = L/i$ is the slenderness ratio, in which L is the effective buckling length and i is the radius of gyration of the CFDST section.

The parameters given in equation 2-18a are defined in equation 2-18b to 2-18h as:

$$a = \frac{1 + (35 + 2 \cdot \lambda_p - \lambda_o) \cdot e}{(\lambda_p - \lambda_o)^2}$$ EQ 2-18b

$$b = e - 2 \cdot a \cdot \lambda_p$$ EQ 2-18c

<div align="right">pg. 19</div>

$$c = 1 - a \cdot \lambda_o^2 - b \cdot \lambda_o \qquad \text{EQ 2-18d}$$

$$d = \left[13000 + 4657 \cdot \ln \frac{235}{f_{yo}} \right] \cdot \left(\frac{25}{f_{ck}+5} \right)^{0.3} \cdot \left(\frac{\alpha_n}{0.1} \right)^{0.05} \qquad \text{EQ 2-18e}$$

$$e = \frac{-d}{(\lambda_p + 35)^3} \qquad \text{EQ 2-18f}$$

where λ_p and λ_o are given by:

$$\lambda_p = 1743 / \sqrt{f_{yo}} \qquad \text{EQ 2-18g}$$

$$\lambda_o = \pi / \sqrt{(420 \cdot \xi + 550) / f_{osc}} \qquad \text{EQ 2-18h}$$

the unit for f_{yo} and f_{osc} is MPa.

The interaction equations are presented as:

when $\qquad N / N_{CFDST,u} \geq 2 \cdot \varphi^3 \cdot \eta_o$:

$$\frac{N}{\varphi \cdot N_{CFDST,u}} + \frac{C_1}{C_4} \cdot \frac{M}{M_{CFDST,u}} = 1 \qquad \text{EQ 2-19a}$$

when $\qquad \overline{N} / N_{CFDST,u} < 2 \cdot \varphi^3 \cdot \eta_o$:

$$-C_2 \cdot \left(\frac{N}{N_{CFDST,u}} \right)^2 - C_3 \cdot \frac{N}{N_{CFDST,u}} + \frac{1}{C_4} \cdot \frac{M}{M_{CFDST,u}} = 1 \qquad \text{EQ 2-19b}$$

with $\quad C_1 = 1 - 2 \cdot \varphi^2 \cdot \eta_o$

$$C_2 = \frac{(1 - \zeta_o)}{(\varphi^3 \cdot \eta_o^2)}$$

$$C_3 = \frac{2 \cdot (\zeta_o - 1)}{\eta_o}$$

$$C_4 = 1 - 0.4 \cdot \frac{N}{N_E}$$

where

$$\zeta_o = 1 + (0.18 - 0.2 \cdot \chi^2) \cdot \xi^{-1.15}$$

$$\eta_o = \begin{cases} 0.5 - 0.2445 \cdot \xi & \xi \leq 0.4 \\ 0.1 + 0.14 \cdot \xi^{-0.84} & \xi > 0.4 \end{cases}$$

$$N_E = \pi^2 \cdot E_{sc}^{elastic} \cdot A_{sc}/\lambda^2$$

where $E_{sc}^{elastic}$ is the elastic modulus of the CFDST section given by:

$$E_{sc}^{elastic} = \frac{E_s \cdot (A_{so} + A_{si}) + E_c \cdot A_c}{A_{sc}}$$

2.5.4. CFDST MEMBERS UNDER CYCLIC LOADING

A study conducted on 28 concrete-filled double skin tubular beam-columns under constant axial load and cyclic flexural loading showed a significant increase in strength, ductility and dissipated energy over the outer tubes only (Han, et al., 2006). It was also found that in general, the ductility and energy dissipation of specimens with CHS outer tubes are higher than specimens with SHS outer tubes.

Han (Han, et al., 2009) developed a mechanic model for CFDST beam-columns under constant axial load and cyclically increasing flexural loading. They found good agreement between the predicted response and the test results. Parametric analysis was performed to finally produce simplified models to predict the moment versus curvature and lateral load versus lateral displacement curves of the composite member.

2.5.5. CFDST COLUMNS SUBJECTED TO LONG-TERM LOADING

Concrete is a complex material with many factors affecting its dimensional stability such as creep and shrinkage. Thus, CFDST columns under service loads in a structure will also experience the effects of creep and shrinkage of the concrete in-fill. An experimental study to determine the affects of long-term loading was conducted by Han, Liao and Tao (Han & Li, 2011). Tests were conducted on six different CFDST columns; namely:

- 2 x circular CFDST columns,
- 2 x square CFDST columns
- 2 x single skin CFST columns,

The columns were placed under sustained long-term axial loading. The tests comprised of two stages:

- In stage one, the columns are subjected to a long-term service load.
- In stage two, the ultimate axial load of the columns is determined.

Ten additional CFDST and CFST columns were tested to determine their ultimate load bearing capacity without being subjected to long-term service loading. Which served as a comparison. The study showed that the long-term deformation of CFDST columns increased relatively fast at an early stage and stabilised after approximately 100 days. The study also showed that the ultimate strength of the column is decreased by long-term loading and that long-term loading affects both the CFDST columns and the single skin CFST columns in a similar manner.

2.6.   FINITE ELEMENT MODELLING

In order to accurately simulate the actual behaviour of concrete-filled double skin columns it is important to model the three main aspects of the section correctly. These aspects are:

- The confinement of the concrete.
- The steel tubes
- The interaction between the concrete and each steel tube.

Once these three aspects are modelled correctly, choosing a mesh size and element type will help achieve accurate and computationally efficient result. The assumptions made in the development of the theoretical models earlier in this chapter can be used as a starting point, together with the literature study into previous work conducted. The finite element modelling performed by other authors on normal concrete-filled steel tube columns could be useful to gain insight into the tube-concrete interaction.

2.6.1.   MATERIAL MODELLING OF CONCRETE

The two main failure mechanism of concrete are cracking under tension and crushing under compression. The strength of concrete in a simple stress state, uniaxial compression or tension, differs from its strength under biaxial loading, which in turn differs from the strength under triaxial loading. Boundary surfaces are presented in three dimensional space to define the strength of concrete in three dimensions. Typically two boundary surfaces are described:

- *Failure surface*:   The stress state corresponding to material failure lie on this surface.
- *Plastic potential surface*:   The stress state corresponding to yielding lie on this surface

The plastic potential surface is inside the failure surface. Thus, the stress state must cross the plastic potential surface before it reaches the failure surface.

pg. 22

One of the strength hypotheses often used to model concrete is the Drucker-Prager hypothesis. According to it, failure is determined by a non-dimensional strain energy and the boundary surface in the stress strain space assumes the shape of a cone. Figure 2-8 shows a schematic presentation of the Drucker-Prager boundary surfaces.
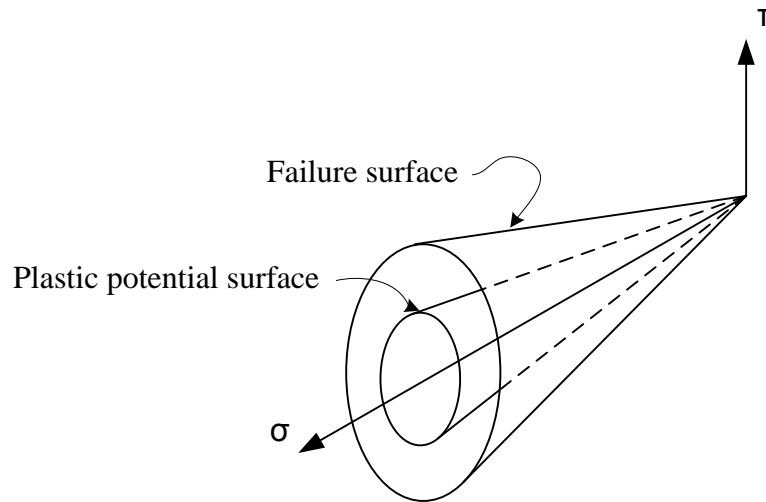
Figure 2-8: Schematic presentation of Drucker-Prager boudary surfaces

In Figure 2-8 the σ-axis is the hydrostatic-axis which denotes a line where the three principle stresses are equal. The T-axis is an axis in the deviatoric plane, which lies perpendicular to the hydrostatic-axis.

Finite element software ABAQUS, uses the Concrete Damaged Plasticity (CDP) model, which is a modification of the Drucker-Prager strength hypothesis. The modifications includes:

- The parameter K_c which changes the shape of the failure surface in the deviatoric plane. Parameter K_c can range from 0.5 to 1.0. If $K_c = 1.0$ then the failure surface is circular, as in the Drucker-Prager model.
- In a similar manner the shape of the surface's meridians in the stress space can be changed by adjusting the plastic potential eccentricity. Which is a small positive number. When the eccentricity is zero the surface's meridians are linear, as with the Drucker-Prager model.
- A parameter that can be specified if the point in which the concrete undergoes failure under biaxial compression (f_{b0}/f_{c0}) is the ratio of strength in the biaxial state to strength in the uniaxial state.

- The last parameter characterizing the performance of the concrete under multi-axial stress in the dilation angle. This is the angle of inclination of the failure surface towards the hydrostatic axis measured in the meridional plane.

These parameters are elaborated on in Chapter 4.

It is known that confined concrete reacts differently than unconfined concrete (confined concrete is loaded triaxially) and that there exist different degrees of confinement which in turn results in different stress-strain relationships for each level of confinement. There are two types of confinement namely active confinement and passive confinement. Active confinement actively confines the concrete member by applying an external confining pressure. Active confinement typically applies a constant confining pressure regardless of axial load or concrete expansion. Passive confinement is where the concrete only experiences a confining pressure when the concrete expands into the confining material. Thus, for passive confined concrete there would be no confining pressure at the start of loading, but as loading increases and the concrete expands due to the Poisson effect the passive confinement system will resist the expansion causing a confining effect. Passive confinement is present in CFDST and CFST columns.

2.6.1.1. CONCRETE CORE OF SINGLE SKIN CFST MEMBERS

Ellobody [(Ellobody, et al., 2006), (Ellobody & Young, 2006)] uses an approach from Hu, (Hu, et al., 2003) that likely originated from Mander (Mander, et al., 1988) where the confined concrete behaviour is determined using equation 2-21 as;

$$f'_{cc} = f'_{c} + k_1 \cdot f_l \qquad\qquad \text{EQ 2-21}$$

where f'_{cc} is the peak stress of the stress-strain curve for confined concrete, f'_{c} is the cylinder strength of the concrete and f_l is the lateral stress representing the confining pressure on the concrete. The constant k_1 is obtained from experimental data. A similar expression for the strain at peak stress is also given. It is important to notice that the peak stress changes with changing confinement pressures. Using this approach in an analysis would require that the peak stress of the stress-strain curve for the confined concrete be re-calculated with every change in the confining pressure. This would result in a re-calculation of the peak stress after every step of the analysis, because the confining pressure changes as the axial load increases. However, it is known that the lateral confining stress depends heavily on the diameter over thickness ratio

of the tube confining the concrete. Hu (Hu, et al., 2003) used this assumption to find empirical equations to define f_l based on experimental data. Thus, a single peak stress for a cross-section with a particular diameter over thickness ratio and steel yield stress can be obtained, saving computational time. However, Liang (Liang & Fragomeni, 2009) states that the model by Hu (Hu, et al., 2003) over estimates the confining pressure while Liang (Liang & Fragomeni, 2009) proceeds to propose a more accurate model for the confining pressure which takes into account the changing Poisson's ratio of the concrete core. Liang (Liang & Fragomeni, 2009) uses the equation from Mander (Mander, et al., 1988) to find f'_{cc} but added a strength reduction factor to the f'_c term and made adjustments to the work by Hu (Hu, et al., 2003). The design formula proposed by Liang provides a very good estimation of the ultimate axial loads of circular CFST (Liang & Fragomeni, 2009).

2.6.1.2. CONCRETE CORE OF CFDST MEMBERS

The confinement factor (ξ) defined in 2-2 is a method of estimating the confinement pressure that will act on the concrete infill. In order to simulate the behaviour of the confined concrete the stress-strain relationship presented by Han [(Han & Huo, 2003), Han's expressions (Han, et al., 2005)] was modified based on a large number of calculations on CFST stub-column test results to obtain an equivalent stress-strain model which is suitable for FE analysis (Han, et al., 2007). This equivalent stress-strain model was then used in Huang (Huang, et al., 2010) to model CFDST stub columns and found good agreement with test results. The same FE model used by Han (Han, et al., 2007) was also used by Xiong (Xiong & Zha, 2007) to model CFST columns and in Li (Li, et al., 2012) to model CFDST columns. Li verified his model against various published experimental results with column slenderness (λ, defined in *Section 2.5.3*) varying from 6.4 − 56.5 and found good agreement between predicted and measured results.

2.6.2. MATERIAL MODELLING OF STEEL

The steel tube in CFST and CFDST columns is bi-axially stressed due to the concrete expanding under axial loading and the axial load itself. The expanding concrete causes a hoop stress in the steel tube which reduces the yield strength in the longitudinal direction of the steel tube (Liang & Fragomeni, 2009). Liang (Liang & Fragomeni, 2009) proposes a three part linear-rounded-linear stress-strain curve for steel. Han (Han, et al., 2007) used different stress-strain relationships for different steels. For carbon steel an elasto-plastic stress-strain model that consists of five stages was used. A simplified model that consists only of two linear stages

was used for high strength steel; and an idealized multi-linear stress-strain model was adopted for cold formed steel tubes.

2.6.3. MODELLING OF THE STEEL-CONCRETE INTERFACE

Ellobody [(Ellobody & Young, 2006), (Ellobody, et al., 2006)] used interface elements that allows the two surfaces to separate under tension and to penetrate each other under compression. The friction between the two faces is maintained as long as the surfaces remain in contact. The coefficient of friction is taken as 0.25 in the analysis by Ellobody. No research was found on the bond behaviour of CFDST columns. It is expected that the behaviour of CFDST stub-columns is not sensitive to the bond between the concrete and inner or outer tube, since the three components are loaded together. This is confirmed by the FE modelling of Huang (Huang, et al., 2010). Han (Han, et al., 2007) also uses a surface based interaction with a contact pressure model in the normal direction, and a Coulomb friction model in the tangential direction to model the interface between the concrete and steel tube for CFST columns. A kind of "gap element" with high stiffness in the normal direction was adopted to simulate the contact and separation between the two surfaces

2.7. COLUMN AXIAL LOAD ACCORDING TO EULER THEORY AND SECANT FORMULA

The critical buckling load, P_{cr} of a slender column subjected to concentric loading can be determined using Euler theory presented in equation 2-22 as

$$P_{cr} = \frac{\pi^2 EI}{\left(L_{eff}\right)^2}$$
EQ 2-22

where E = Young's Modulus.

I = Second moment of inertia of the cross section

L_{eff} = Effective length of the column, defined as the distance between two points of zero moment.

The Euler theory cannot be used since:

  i.   An eccentric load is applied to the cross section.
 ii.   The cross section is not homogeneous.
iii.   It does not capture the complete interaction between the tubes and the concrete.

iv.   It does not capture the confinement of the concrete, which significantly affects the ultimate load capacity.

v.   Euler theory predicts the yield load and not the ultimate load of the column.

The Secant formula can be used to determine the critical load when a column is subjected to eccentric load, by determining the maximum stress in the section presented as;

$$\sigma_{max} = \frac{P}{A}\left[1 + \left(\frac{ec}{r^2}\right)\sec\left(\frac{L}{2r}\sqrt{\frac{P}{AE}}\right)\right]$$ EQ 2-23

where σ_{max} = Maximum compressive stress.

P = Axial compressive load.

A = Cross section area of the member.

e = Eccentricity of the load.

c = Distance from the centroid to the extreme compression fibre.

E = Young's Modulus.

I = Second moment of inertia of the cross section.

r = Radius of gyration.

L = Length of the member.

In a similar manner to the Euler theory the Secant formula cannot be used since:

i.   The cross section is not homogeneous.

ii.   It does not capture the complete interaction between the tubes and the concrete.

iii. It does not capture the confinement of the concrete, which significantly affects the ultimate load capacity.

Therefore, to determine the ultimate load of CFDST columns, we are forced to use more advanced theories developed by other researchers.

2.8.   CONCLUDING SUMMARY

A literature study was conducted to determine the state of current knowledge on CFDST columns. This study revealed that significant research was done into the behaviour of CFST columns. However, CFDST columns are a newer development in this type of steel-concrete composite construction. The design formulae that describe the behaviour of CFST columns was modified, to predict the capacities of CFDST stub columns. These formulae show good correlation to experimental tests by various authors. Research shows that finite element analysis (FEA) of CFDST stub columns is very similar to FEA of CFST, such that the stress strain behaviour of confined concrete was incorporated without any changes and delivered good results.

Work done on long (slender) CFDST columns loaded eccentrically is limited. Tao (Tao, et al., 2007) does discuss the behaviour of CFDST beam columns that were loaded eccentrically and includes results from two other authors. However, the theoretical model used to predict the behaviour is poorly presented and could not be used in this study. It is the goal of this study to use the knowledge gained from the literature review to:

1.   Conduct experimental tests on four different column configurations which are subjected to eccentric loading.

2.   To develop a FE model that implements the concrete material model proposed by Han (Han, et al., 2007) to predict the failure load of CFDST columns subjected to eccentric loading.

3.   Calculate the capacity of the CFDST column specimen under concentric loading with the model described by the equations provided in *Section 2.5.3* and compare the calculated capacities to the experimental test results from the eccentrically loaded CFDST specimens.

Chapter 3

EXPERIMENTAL WORK

3.1. INTRODUCTION

This chapter describes the objectives of the experimental work with the composition of the specimens. Due to of the simplicity of the test configuration the experimental results and discussion thereof are also included in this chapter.

3.2. TEST OBJECTIVE

An insignificant amount of experimental work on slender eccentrically loaded CFDST columns was discovered during the literature study (Tao, et al., 2007). Thus, the objective of the experimental tests were to specifically determine the axial behaviour of slender CFDST columns under eccentric loading. The experimental results would also be used to determine the validity of the finite element model developed in this study.

3.3. COMPOSITION OF CFDST COLUMNS

This section describes the construction of the CFDST test specimen as well as the materials used. CFDST columns consist of two steel tubes of different diameters, one placed inside the other with their centres aligned. One end of both tubes are sealed with a base-plate and the cavity between the inner and outer tube is filled with concrete as shown in Figure 3-1.

3.3.1. GENERAL DESCRIPTION

The two parameters that were changed in the experimental tests are;

- The length (L) of the specimen.
- The hollow-section ratio (χ) of the specimen.

  The hollow section ratio is defined by equation 3-1 as,

$$\chi = D_i/(D_o - 2 \cdot t_o) \qquad\qquad \text{EQ 3-1}$$

where D_i = Diameter of the inner tube

               D_i = Diameter of the outer tube.

t_o = Wall thickness of the outer tube.

A brief description of the specimens is now presented:

- Of the two lengths the shorter length was designated as short (S) while the longer length as long (L). Please note that the "short" designation does not imply that the column is a short or stub column. It merely refers to the shorter of the two chosen lengths. The shorter columns have a length of 2.5m while the longer columns have a length of 3.5m.
- Of the two hollow section ratios, the one concrete infill is thicker than the other. The thicker infill was designated as thick (TK) and the thinner infill as thin (TN). The diameter and thickness of the tubes are presented in *Section 3.5*.
- To summarize, the STK model refers to the shorter length column with the thicker concrete infill.

For each combination of length and hollow-section ratio three test specimens were constructed. A summary of the test specimen with the length, hollow section ratio, number of specimens and designation of each test specimen is given in Table 3-1. Figure 3-1 shows the different cross sections of the TN and TK models.
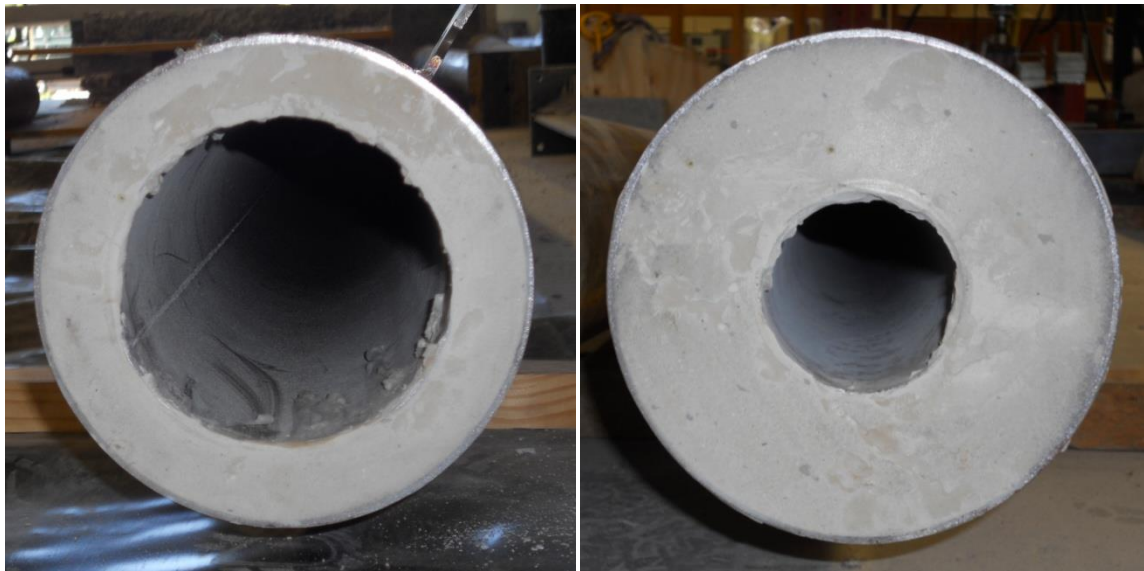

Figure 3-1: Different cross sections tested (left: Thin concrete annulus. right: thick concrete annulus)

Table 3-1: Summary of test specimens

Column Designation	Length [mm]	Hollow-section ratio	Number of test specimen.
STK (Short, Thick)	2500	0.444	3
LTK (Long, Thick)	3500	0.444	3
STN (Short, Thin)	2500	0.739	3
LTN (Long, Thin)	3500	0.739	3

3.3.2. MATERIALS

This section describes the materials used to construct the CFDST column specimens, which includes the concrete mix design and tests conducted on the fresh concrete.

3.3.2.1. CONCRETE

Ordinary Portland cement of strength class 52.5 classified with a normal setting time (OPC CEM I 52.5N) and a relative density of 3.14 was used for all experimental tests.

A cement extender, namely Fly Ash (FA) was also used in the concrete mix. FA is collected from the flues of modern power stations. FA is generally in the form of small glassy spheres. When mixed with Portland cement and water, FA reacts with calcium hydroxide (CH) produced from the cement hydration process to produce calcium oxide-silica-water (C-S-H) gel. This reaction is called pozzolanic and FA may be described as pozzolan. The finer FA particles act as nuclei for the growth of C-S-H and thus promote a more even distribution of C-S-H which results in a denser aggregate paste interface. The way FA is used in a concrete mix is by substituting some of the Portland cement with FA. Using FA in a concrete mix affects the properties of fresh concrete in the following ways: (Cement and Concrete Institute, 2009)

- Workability is improved.
- Slightly prolonged setting time.

 FA was used in these experiments because it improves workability and prolongs setting time. The process of filling each CFDST by hand was laborious and time consuming. Therefore a concrete with good workability and prolonged setting time was desirable.

Natural sand (Malmesbury Sand) with a relative density of 2.64 was used as the fine aggregate in the concrete mix. Natural sand is formed by the natural weathering of rock and therefore has

rounded particle shape and good grading. Natural sand is commonly used in South Africa as the fine aggregate in concrete.

Greywacke stone with a nominal size of 6mm and a relative density of 2.7 was used as the coarse aggregate in all experimental tests. The stone was graded in accordance with SANS 1083 (2002).

To minimize or eliminate the need for vibration self compacting concrete (SCC) was designed for use in CFDST columns. Table 3-2 provides the mix design of the concrete used in the experimental tests. Two tests were performed to identify whether the mix would be suited for filling the CFDST sections. A slump flow test was performed to judge the fluidity of the concrete mix and a segregation test to ensure the concrete will not segregate when poured into the column. The fluidity of the concrete is important because of the relatively small space between the inner and outer skin of the thin CFDST column specimens, especially in the LTN and STN specimens. Segregation is particularly important since the concrete is poured manually into the cavity of the CFDSTs. When the concrete is poured between the tubes it falls freely for before it reaches the bottom of the column or the level of wet concrete. The momentum from the freefall could cause the coarse aggregate to segregate to the bottom of the column. Table 3-3 presents the results of the tests performed on the fresh concrete with its classification (Cement and Concrete Institute, 2009).

Table 3-2: Mix proportions for SCC.

Constituents	Relative density	[kg/m³]
Cement: CEM I 52.5N (PPC)	3.14	246.4
Fly Ash DuraPozz (Ash Resources)	2.2	115.10
Water	1	190.00
Malmesbury Sand	2.64	990.00
6mm Greywacke stone	2.7	800.00
Super Plasticiser: SP1 (Mapei Dynamon)	1.09	2.89

Table 3-3: Results of tests performed on fresh concrete

Test	Result	Classification
Slump flow	690mm	SF2
Segregation	3%	SR2

The classifications of SCC are according to European guidelines for self-compacting concrete (Cement and Concrete Institute, 2009), (Okamura & Ouchi, n.d.). The slump flow test is carried out with a normal slump cone. The measurement of the ultimate spread diameter is taken. The concrete spread is also evaluated visually to detect any segregation. The segregation was tested by means of the sieve test. In this test the concrete is poured into a sieve with 5mm square openings and the mass of mortar that falls through is compared to the mass of concrete poured into the sieve at the beginning of the test.

A total of forty cubes were cast and tested after being cured for 28 days in temperature controlled curing baths . The average cube strength of the concrete was 52.8 MPa with a standard deviation of 2.5 MPa.

3.3.2.2. STEEL

The structural hollow steel sections used in the experimental tests are produced in accordance with SANS 657: Part 1. The steel used for the inner and outer tube yields at 300 MPa with an ultimate strength of 450 MPa. It is noted that this was not verified through experimental testing.

3.4. TEST PROGRAMME

The casting of the specimen was conducted over two days. The 2.5 meter lengths were cast on day 1 while the 3.5 meter lengths were cast on day 2. Correspondingly the experimental tests also took place over two days. Because of safety concerns the columns were placed horizontally after three days. The concrete did settle slightly by ±3mm after curing. The columns were capped with an all purpose epoxy from Sika and sanded down with an orbital sander to ensure that the loading surfaces were smooth and perpendicular to the longitudinal axis. This also ensures that the entire cross section is loaded simultaneously. The finished surface is presented in Figure 3-1.

3.5.   TEST SETUP AND EQUIPMENT USED

The experiments were performed using a hydraulic actuator with a compression capacity of 2 MN. The actuator can be either load or displacement controlled. The tests were conducted using a displacement rate of 1mm/min to obtain quasi-static conditions. To simulate pinned end conditions, pot bearings were used at both ends of the test specimen. The dimensions for each type of column tested in this study is provided in Table 3-4.

Table 3-4: Dimentions of each type of CFDST column specimen

Specimen identification	Outer CHS (diam x thick) [mm]	Inner CHS (diam x tick) [mm]	Length [mm]	Thickness of concrete fill [mm]
LTK	177.8 x 3.0	76.2 x 3.0	3500	49.3
LTN	177.8 x 3.0	127.0 x 3.0	3500	23.9
STK	177.8 x 3.0	76.2 x 3.0	2500	49.3
STN	177.8 x 3.0	127.0 x 3.0	2500	23.9

Figure 3-2 shows the 3.5 meter length column in the hydraulic actuator before testing commenced. To ensure that the columns do not pop out from the test setup, chains are attached to the column.

Figure 3-2: 3.5m long CFDST column setup in testing rig

The bearing plates at the top and bottom supports have alignment pins attached to ensure that each test specimen is consistently loaded with the same eccentricity. The setup of the load cell and bearing set up is shown in Figure 3-3 below.

Figure 3-3: Load cell and bearing setup

In order to include a pot bearing and load cell at the bottom configuration a total of three base plates were used. To include the alignment pin at the top support one base plate was required. The entire setup introduces ten possible sources of misalignment. The schematic diagram shown in Figure 3-4 below helps to identify these sources:
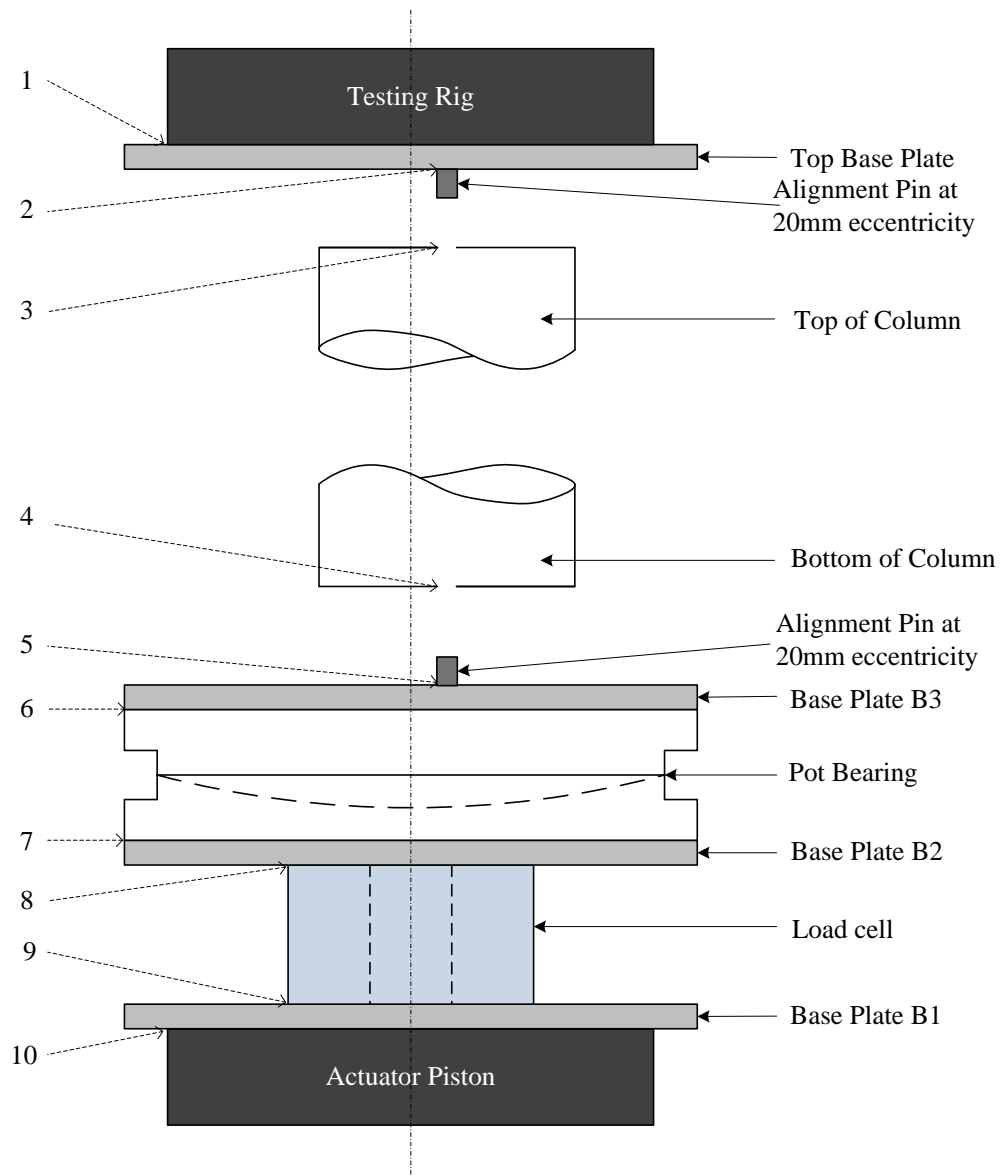
Figure 3-4: Schematic of test setup

1. The centring of the top base plate to the testing rig.
2. The position of the alignment pin on the top base plate.
3. Position of the centring hole for the top of the test specimen.
4. Position of the centring hole for the bottom of the test specimen
5. The position of the alignment pin on base plate B3.
6. The alignment of base plate B3 onto the pot bearing.
7. The alignment of base plate B2 onto the pot bearing.
8. The centring of the load cell to base plate B2.
9. The centring of the load cell to base plate B1.

10. The centring of base plate B1 to the testing rig.

Precautions were taken to ensure that other misalignment would not occur. However, to reduce the affect that any misalignment might have on the test results a relatively large eccentricity of 20mm was chosen. SABS 0100-Part1 states that, "*a minimum eccentricity of 5% of the height of the cross-section in the plane of bending should be used*". This would result in an eccentricity of almost 9mm. It was however decided to used a 20mm eccentricity.

The testing rig is equipped with load and displacement measuring devices. To ensure the correctness of the results an external load cell was used to measure the applied load while linear varying displacement transducers (LVDTs) were used to measure the axial and lateral displacements of the test specimens. The load cell is shown in Figure 3-3 while the lateral LVDTs were positioned at quarter intervals along the length of the column as shown in Figure 3-2. Figure 3-5 presents a closer view of how the LVDTs were positioned along the length of the column.
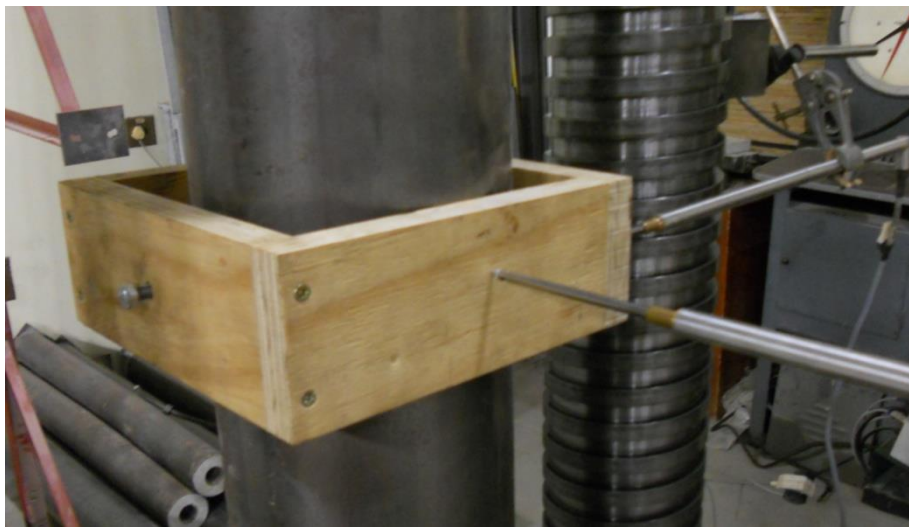
Figure 3-5: LVDT measurement setup

A LVDT was also positioned to measure the axial displacement of the testing rig's actuator as shown in Figure 3-6.

pg. 38

Figure 3-6: LVDT measuring the axial displacement of the actuator

3.6.   EXPERIMENTAL RESULTS AND DISCUSSION

This section presents the experimental results using the methodology explained earlier. All the responses are plotted starting at a load of 20 kN to ensure that the specimen has settled. Settling refers to the closing of any spaces between the specimen and the actuator piston that may be present after the specimen was setup.

3.6.1.   2.5M COLUMN TESTS

3.6.1.1. STK (2.5M SHORT, THICK CONCRETE ANNULUS)

Figure 3-7 and Figure 3-8 shows the axial load response versus axial displacement and midspan deflection of the 2.5m CFDST with the thick annulus. It should be noted the axial displacements refers to the vertical shortening between the column ends.

Figure 3-7 Axial load vs. axial displacement response for STK (2.5m with thick annulus) columns
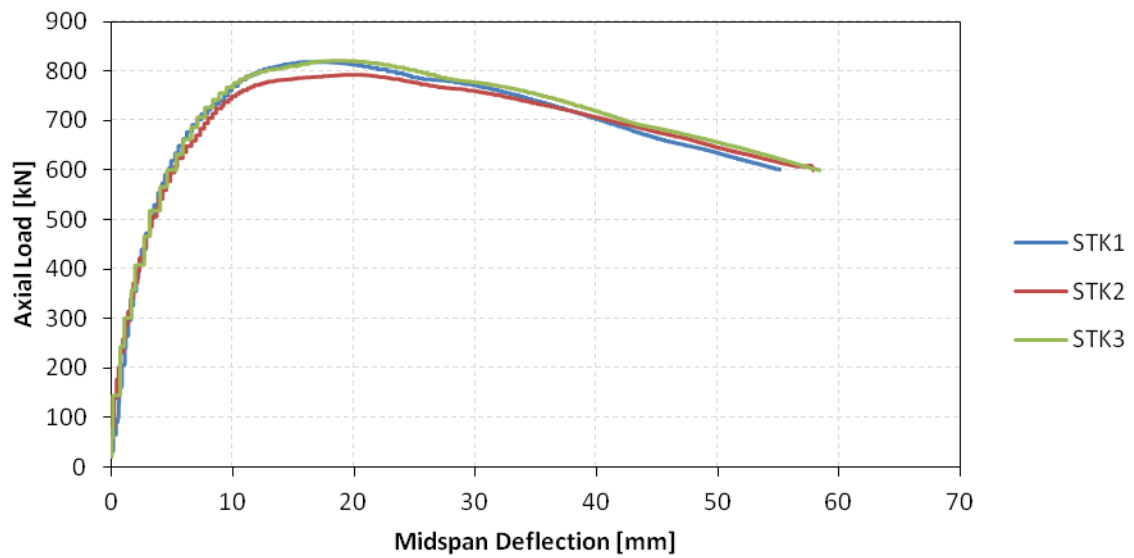
Figure 3-8 Axial load vs. midspan deflection for STK (2.5m with thick annulus) columns

Table 3-5 presents the peak load data from the responses shown in Figure 3-7 and Figure 3-8.

Table 3-5: Peak data from STK (2.5m with thick annulus) columns

Test specimen	Peak load [kN]	Displacement at peak load [mm]	Midspan deflection at peak load [mm]
STK1	818	5.9	16.9
STK2	794	6.3	19.9
STK3	823	6.3	18.6
Average	811	6.2	18.5

The results from Figure 3-7 Figure 3-8 shows that there are no outliers. The results also yield the expected behaviour, i.e. a linear behaviour until the load approaches its peak with high ductility after the ultimate load is achieved. Based on the similarity of the results, the test data is assumed correct and accurate.

The standard deviation of the peak load is $15.5 \ kN$ which is equal to 1.9% of the average peak load. The axial displacement at peak load had a standard deviation of $0.2 \ mm$ which equates to 3.2% of the average axial displacement at peak load. The midspan deflection at peak load has a standard deviation of $1.5 \ mm$ which is equal to 8.1% of the average midspan deflection at peak load. The difference in midspan deflections is relatively large when compared to the difference in peak loads and axial displacements. This is because the response of axial load versus midspan deflection has a relatively flat peak, meaning that subtle changes in axial load results in comparatively large changes in midspan deflection. The covariance between the peak load and the axial displacement and the midspan deflection are both negative. Indicating that a larger peak load resulted in a smaller displacement and deflection. This means the test specimen with larger peak loads were slightly stiffer than other specimen.

3.6.1.2. STN (2.5M SHORT THIN CONCRETE ANNULUS)

Figure 3-9 and Figure 3-10 shows the axial load response versus axial displacement and midspan deflection, respectively
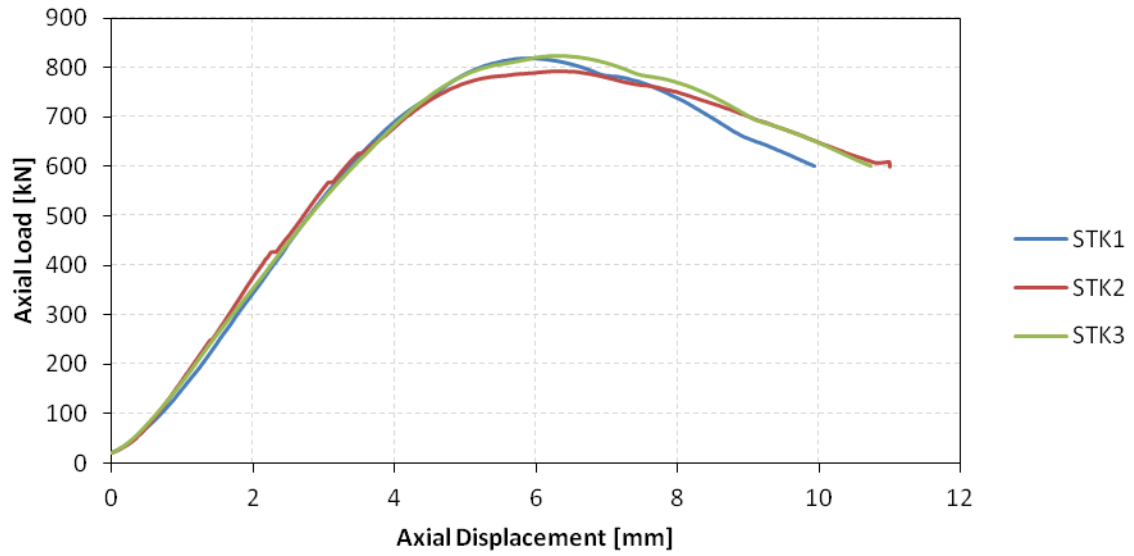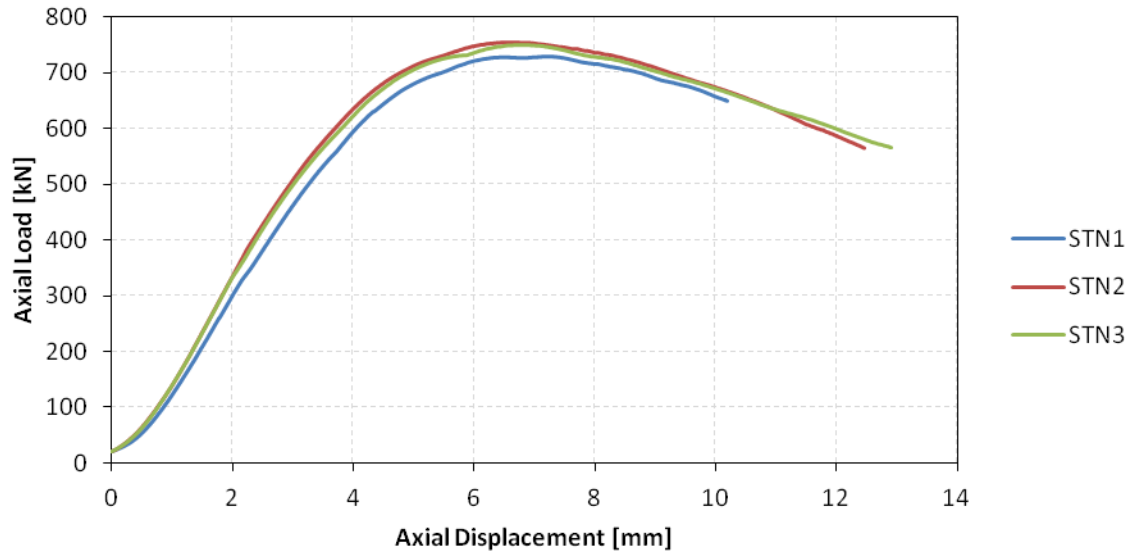
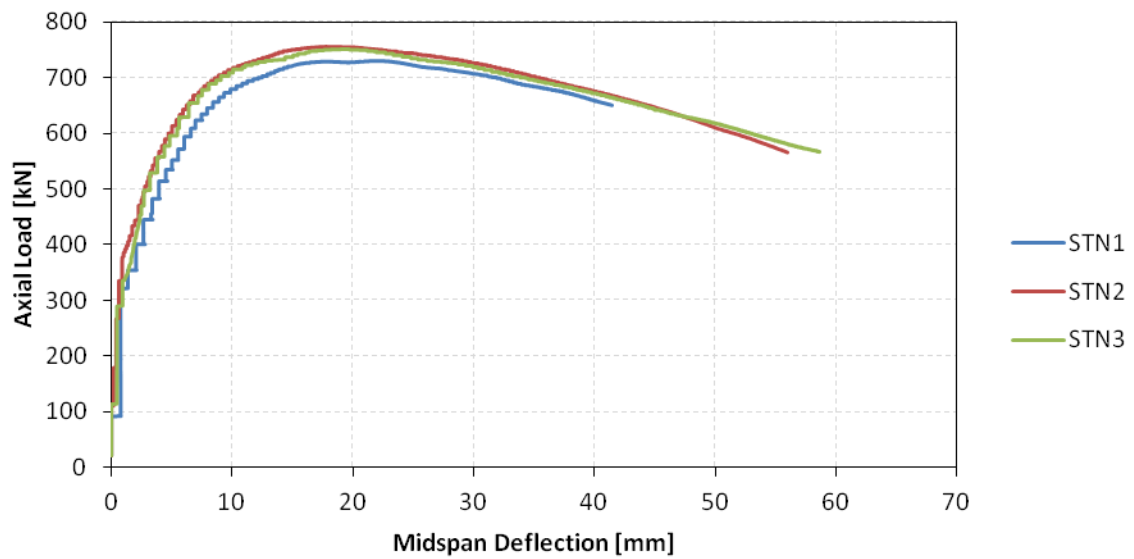*Figure 3-9 Axial load vs. axial displacement response for STN (2.5m with thin annulus) columns*

Figure 3-10 Axial load vs. midspan deflection for STN (2.5m with thin annulus) columns

Table 3-6 presents the peak load data from the responses shown in Figure 3-9 and Figure 3-10.

Table 3-6: Peak data from STN (2.5m with thin annulus) columns

Test specimen	Peak load [kN]	Displacement at peak load [mm]	Midspan deflection at peak load [mm]
STN1	729	7.2	22.1
STN2	756	6.6	17.8
STN3	751	6.9	19.3
Average without STN1	754	6.8	18.6

During the testing of STN1, the data logger experienced problems. This resulted in the anomaly of the results in Figure 3-9 Figure 3-10. Thus the data from STN1, although indicated in Table 3-6, will not be used to determine the average responses. With STN1 removed, the distribution of the results are similar and thus the test data is assumed accurate.

The standard deviation of the peak load is 3.5 kN which is equal to 0.5% of the average peak load. The axial displacement at peak load had a standard deviation of 0.2 mm which equates to 2.9% of the average axial displacement at peak load. The midspan deflection at peak load has a standard deviation of 1.1 mm which is equal to 5.9% of the average midspan deflection at peak load. The difference in midspan deflections is relatively large when compared to the difference in peak loads and axial displacements. This is because the response of axial load versus midspan deflection has a relatively flat peak, meaning that subtle changes in axial load results in comparatively large changes in midspan deflection. The covariance between the peak load and the axial displacement and the midspan deflection are both negative. Indicating that a larger peak load resulted in a smaller displacement and deflection. This means the columns with larger peak loads were slightly stiffer that the other specimen.

3.6.2.   3.5M COLUMN TESTS

3.6.2.1.   LTK (3.5M LONG THICK CONCRETE ANNULUS)

Figure 3-11 and Figure 3-12 shows the axial load response versus axial displacement and midspan deflection, respectively.
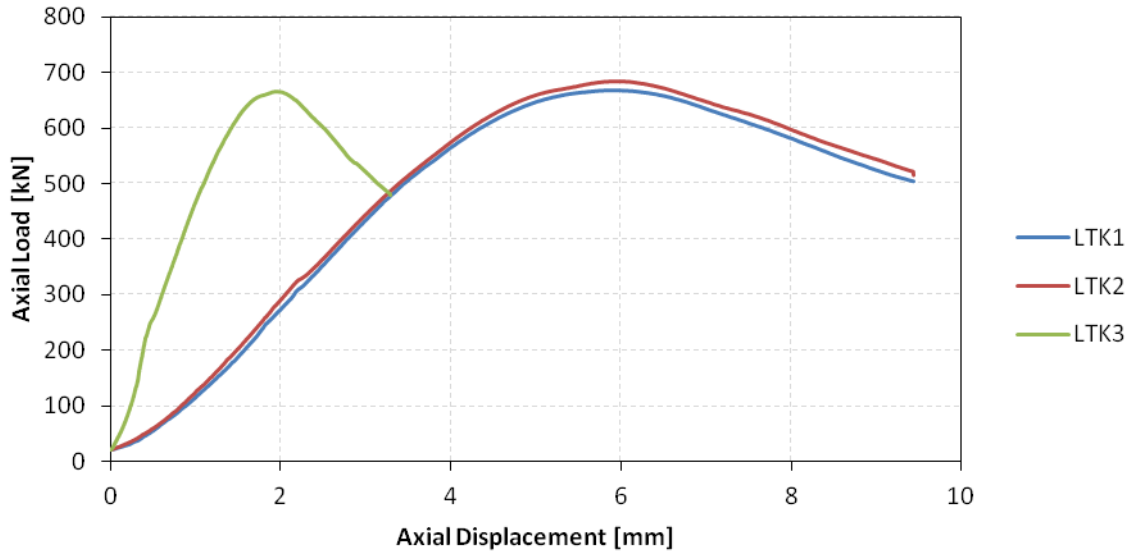
Figure 3-11 Axial load vs. axial displacement response for LTK (3.5m with thick annulus) columns
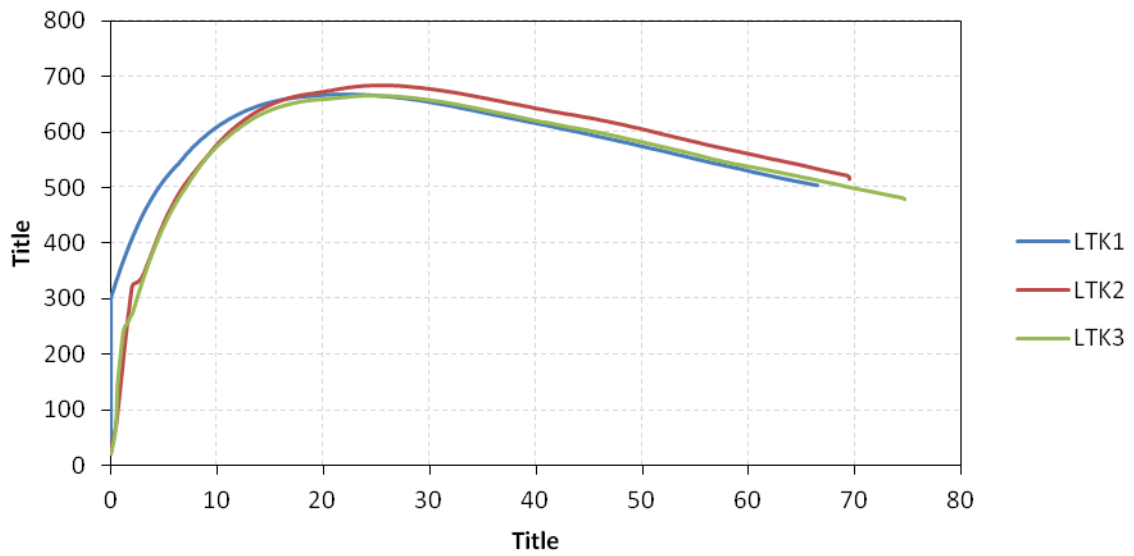

Figure 3-12 Axial load vs. midspan deflection for LTK (3.5m with thick annulus) columns

Table 3-7 presents the peak load data from the responses shown in Figure 3-11 and Figure 3-12

Table 3-7: Peak data for LTK columns

Test specimen	Peak load [kN]	Displacement at peak load [mm]	Midspan deflection at peak load [mm]
LTK1	669	5.9	22.1
LTK2	683	6.0	26.2
LTK3	666	1.9	24.1
Average without LTK3	676	6.0	24.2

Examining the test results from LTK3 it is clear that the readings collected from the LVDT are incorrect while the force seems correct. Both the load reading and midspan deflection reading are similar to readings obtained from LTK1 and LTK2. However, it is impossible to observe a midspan displacement of $24.1\ mm$ with an axial displacement of only $1.9\ mm$. Thus, the reading obtained of LTK3 is ignored for determining the averages. With LTK3 removed, the distribution of the results are similar and thus the test data is assumed correct.

The standard deviation of the peak load is $9.9\ kN$ which is equal to 1.5% of the average peak load. The axial displacement at peak load had a standard deviation of $0.1\ mm$ which equates to 1.2% of the average axial displacement at peak load. The midspan deflection at peak load has a standard deviation of $2.9\ mm$ which is equal to 12.0% of the average midspan deflection at peak load. The difference in midspan deflections is relatively large when compared to the difference in peak loads and axial displacements. This is because the response of axial load versus midspan deflection has a relatively flat peak, meaning that subtle changes in axial load results in comparatively large changes in midspan deflection. The covariance between the peak load and the axial displacement and the midspan deflection are both positive. Indicates that a larger peak load resulted in a larger displacement and deflection. This means that the test specimen with higher peak loads peaked slightly later than other specimen.

3.6.2.2. LTN (3.5M LONG THIN CONCRETE ANNULUS)

Figure 3-13 and Figure 3-14 shows the axial load response versus axial displacement and midspan deflection, respectively.
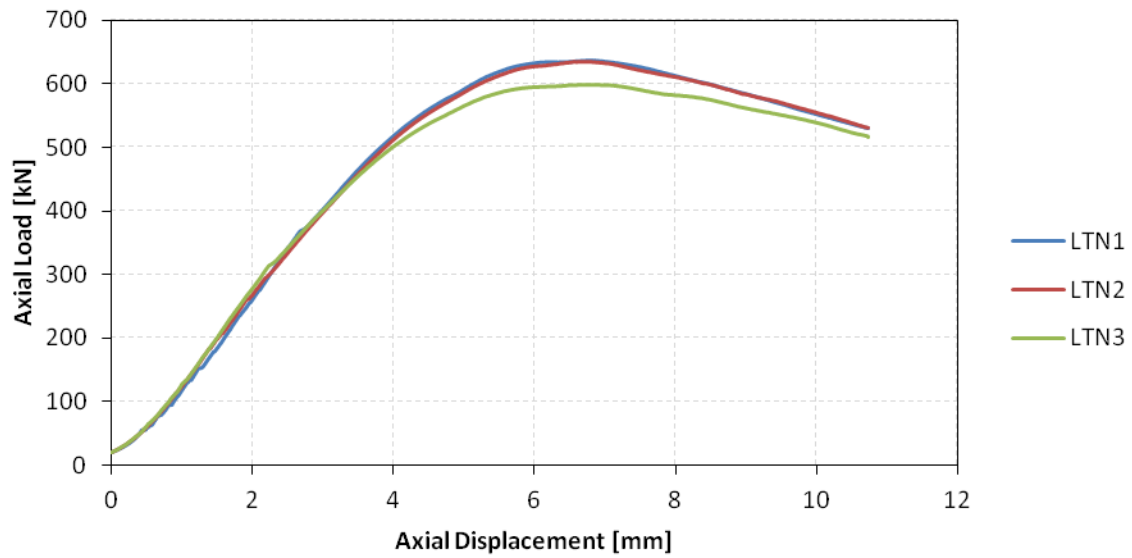
Figure 3-13 Axial load vs. axial displacement response for LTN (3.5m with thin annulus) columns
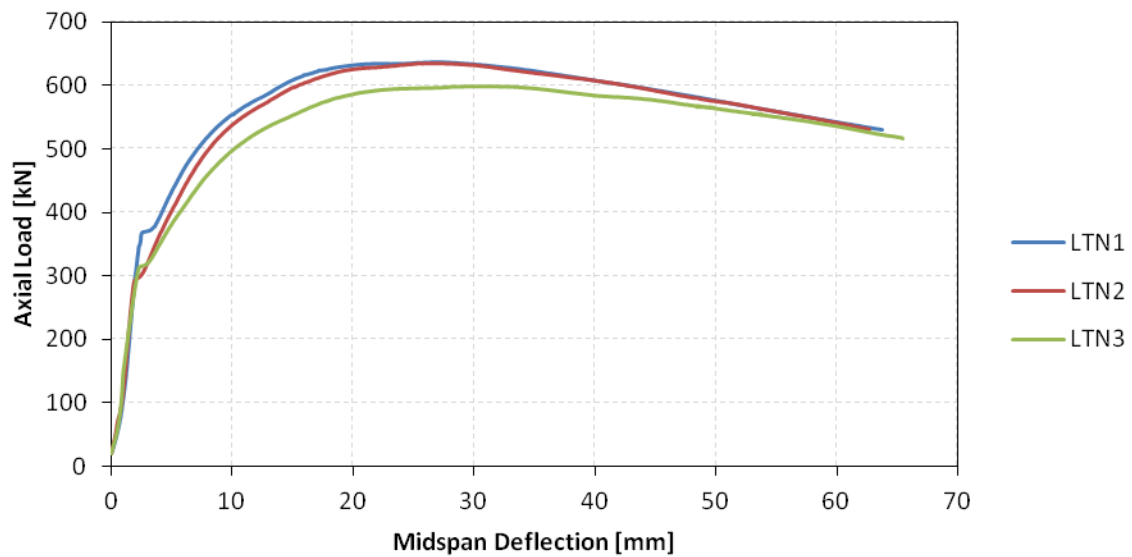

Figure 3-14 Axial load vs. midspan deflection for LTN (3.5m with columns

Table 3-8 presents the peak load data from the responses shown in Figure 3-13 and Figure 3-14

pg. 46

Table 3-8: Peak data from LTN columns

Test specimen	Peak load [kN]	Displacement at peak load [mm]	Midspan deflection at peak load [mm]
LTN1	637	6.8	26.9
LTN2	635	6.7	26.9
LTN3	599	6.8	31.1
Average	624	6.8	28.3

The results of LTN3 could be considered as an outlier when compared to LTN1 and LTN2. Since the difference is not significant, LTN3 was not removed to obtain the averages. The test results are similar therefore they are assumed correct and accurate.

The standard deviation of the peak load is $21.4\ kN$ which is equal to 3.4% of the average peak load. The axial displacement at peak load had a standard deviation of $0.1\ mm$ which equates to 0.9% of the average axial displacement at peak load. The midspan deflection at peak load has a standard deviation of $2.4\ mm$ which is equal to 8.6% of the average midspan deflection at peak load. The difference in midspan deflections is relatively large when compared to the difference in peak loads and axial displacements. This is because the response of axial load versus midspan deflection has a relatively flat peak, meaning that subtle changes in axial load results in comparatively large changes in midspan deflection. The covariance between the peak load and the axial displacement and the midspan deflection are both positive. Indicates that a larger peak load resulted in a larger displacement and deflection. This means the columns with larger peak loads were slightly stiffer that the other specimen.

3.7.   CONCLUDING SUMMARY

The CFDST column specimens were filled by hand with a SCC mix and capped with an all-purpose epoxy to achieve a smooth and even loading surface. The axial load was applied with an eccentricity of 20mm at both the top and bottom surfaces of each specimen about one axis. Data was collected with a 2 MN load cell and LVDTs to measure the axial displacement and midspan deflection.

The difference in the midspan deflection at peak load between the specimens of each test series seems large when compared to the difference in the peak load and axial displacement, respectively. When considering the responses it is observed that the curve of midspan

deflection against axial load is relatively flat. This explains how the difference in peak load can remain small while the midspan deflection at peak load seems relatively large. Barring the axial response curve of LTK3, when considering each test series on their own the results depicted in the graphs above all fall within an acceptable envelope.

Table 3-9 presents a summary of the average peak load data from all the experimental tests.

Table 3-9: Average peak load data from experimental tests

Test specimen	Average peak load [kN]	Average displacement at peak load [mm]	Average midspan deflection at peak load [mm]
STK	811	6.2	18.5
STN	754	6.8	18.6
LTK	676	6.0	24.2
LTN	624	6.8	28.3

The table shows that all the experimental test specimens buckled at approximately the same axial displacement. The thin walled columns (STN and LTN) reached ultimate load at an axial displacement of $6.8\ mm$, while the thick walled columns (STK and LTK) reached ultimate load at an average of $6.1\ mm$.

The percentage difference between average peak load are presented as:

- 7.0 %   decrease from STK to STN
- 16.6 % decrease from STK to LTK
- 7.7 %   decrease from LTK to LTN
- 17.2 % decrease from STN to LTN

The test data reveals that the short CFDST columns can sustain a greater load compared to long CFDST columns. The short CFDST columns can sustain an average of 16.9 % larger ultimate loads compared to the longer CFDST columns. If Euler theory is considered and keeping parameters E and I constant we obtain, $P_{cr\ 2.5m} = 0.16\pi^2 EI$ and $P_{cr\ 3.5m} = 0.08\pi^2 EI$ for the 2.5m and 3.5m column lengths. This shows a decrease of 50 % from the short CFDST column capacity to the long CFDST column capacity. This shows that Euler's theory is not suitable for CFDST column analysis.

Also the specimens with a thick annulus (TK) can sustain a greater ultimate load compared to specimen with a thin annulus (TN). The thick annulus section can sustain an ultimate load that is an average of 7.4 % larger than that of the column with a thin annulus. Since experimental testing is expensive and time consuming a FEA was also used in the investigation which is discussed in chapter 5.

Chapter 4

FINITE ELEMENT MODELLING

4.1. INTRODUCTION

This chapter describes the development of the finite element models of four different CFDST columns. Two different lengths and two different cross sections were modelled. The purpose of the finite element models is to predict the behaviour of slender eccentrically loaded CFDST columns. A sensitivity study, presented at the end of this chapter, was also conducted to assess the effects that various parameters have on the behaviour of the CFDST columns.

4.2. DEVELOPMENT OF THE FINITE ELEMENT MODEL

In conducting the literature study it was found that some work was conducted on finite element modelling of composite sections and that ABAQUS, a finite element (FE) program, was commonly used [(Hu, et al., 2003), (Ellobody & Young, 2006), (Ellobody, et al., 2006), (Han, et al., 2007), (Moon, et al., 2012), (Hu & Su, 2011), (Huang, et al., 2010), (Li, et al., 2012)]. The modelling techniques developed by Han (Han, et al., 2007) to model the behaviour of CFST stub columns was also used by other authors to model the axial behaviour of CFDST columns. It was used by Li (Li, et al., 2012) to model CFDST stub columns with a pre-load on the steel tubes and showed good correlation when compared to experimental results published by different authors. For this reason that the stress-strain relationship of the concrete core developed by Han (Han, et al., 2007) was used in the development of the FE model in this study.

4.2.1. GEOMETRY

A total of four columns with different dimensions were modelled. Two geometric properties were varied across the test series; namely the length of the CFDST columns and the diameters of the inner tubes.

A generic sketch of the column geometry is presented in Figure 4-1 while the dimensions of each model is given in Table 4-1 .
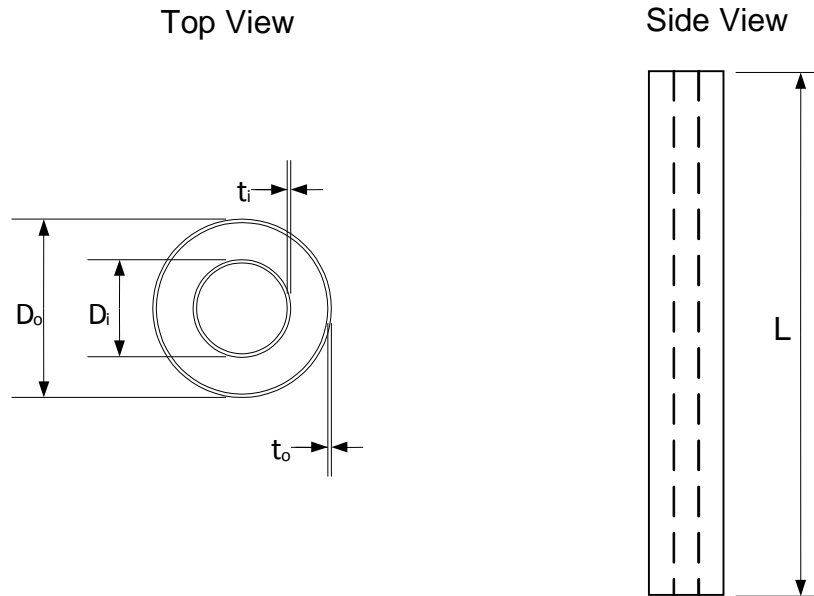
Top View   Side View

Figure 4-1: Column geometry

Table 4-1: Model dimensions

Geometric property	STK	STN	LTK	LTN
Length (L)	2500 mm	2500 mm	3500 mm	3500 mm
Outer tube (D_o x t_o)	177.8 x 3 mm	177.8 x 3 mm	177.8 x 3 mm	177.8 x 3 mm
Inner tube (D_i x t_i)	76.2 x 3 mm	127.0 x 3 mm	76.2 x 3 mm	127.0 x 3 mm

The slenderness ratio of the columns is determined by $\lambda = L/i$; where L is the length of the column, while i is the radius of gyration given by; $i = \sqrt{I_{sc}/A_{sc}}$. I_{sc} and A_{sc} are the moment of inertia and the cross sectional area of the entire CDSFT cross section, respectively. The slenderness ratio of each model is presented as:

- **STK** = 52.3
- **STN** = 46.5
- **LTK** = 73.2
- **LTN** = 65.1

4.2.2. ELEMENTS AND MESHING

To reiterate, CFDST sections are constructed using steel tubes with concrete infill between the steel tubes. The concrete infill is modelled with solid 4-node brick elements while the steel

pg. 51

tubes are modelled with 4-node shell elements. These were commonly used in other studies and provide sufficient accuracy while being computationally efficient. This section further elaborates on each element and the interface between them. The Figures 4-2 and 4-3 shows the meshed concrete infill and outer steel tube. The only difference between the outer and inner tube at this stage is their diameters.
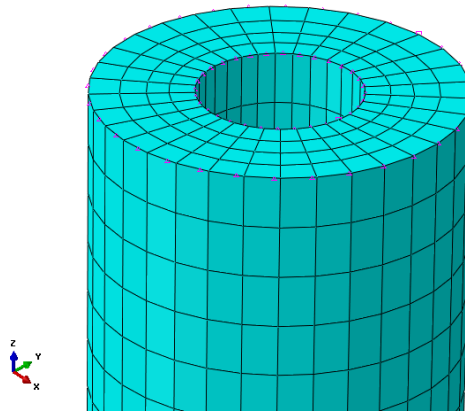

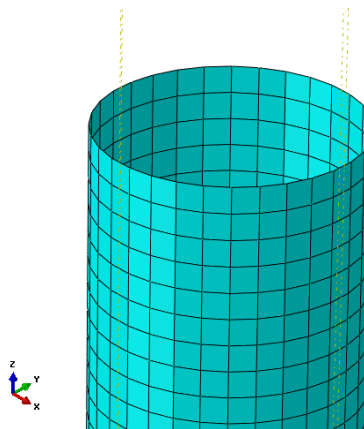*Figure 4-2: Meshed concrete infill*

Figure 4-3: Meshed outer steel tube

4.2.2.1. SHELL ELEMENTS

This section provides information on the shell element properties used in ABAQUS. The specific shell element used in the model is presented at the end of this section. Figure 4-4 shows a schematic view of a typical shell element with 6 degrees of freedom at each node.
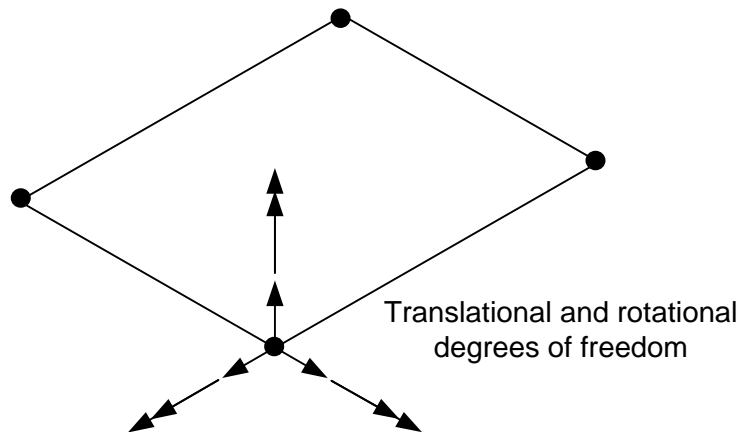
Figure 4-4: 4-node shell element

Shell elements are used to model structural parts in which the thickness dimension is significantly smaller than the other dimensions. Conventional shell elements in ABAQUS use this condition to discretize a body by defining the geometry at a reference surface. Thus, the element thickness is defined in the section property definition. The conventional shell elements in ABAQUS have displacement and rotational degrees of freedom. In contrast ABAQUS also has continuum shell elements, which discretize the entire three dimensional body. Thus, the thickness is determined from the node geometry. Continuum shell elements only have translational degrees of freedom. Therefore continuum shell elements look like continuum solid elements but has a behaviour similar to shell elements.

It was decided to use the S4R shell element, a 4-node general-purpose shell element with reduced first-order integration, hourglass control, finite membrane strains and second order accuracy to model the steel tubes. Reduced integration is used to form the element stiffness matrix, however the mass and distributed loadings are still integrated exactly. Reduced integration significantly reduces computation time, especially in the analysis of three dimensional models. The element accounts for finite membrane strains and arbitrarily large rotations; therefore, it is suitable for large-strain analyses.

4.2.2.2. SOLID ELEMENTS

This section provides information on the solid elements properties used in ABAQUS. The specific solid element used in the model is provided at the end of this section. Figure 4-5 shows a schematic view of a typical solid element with 6 degrees of freedom at each node.
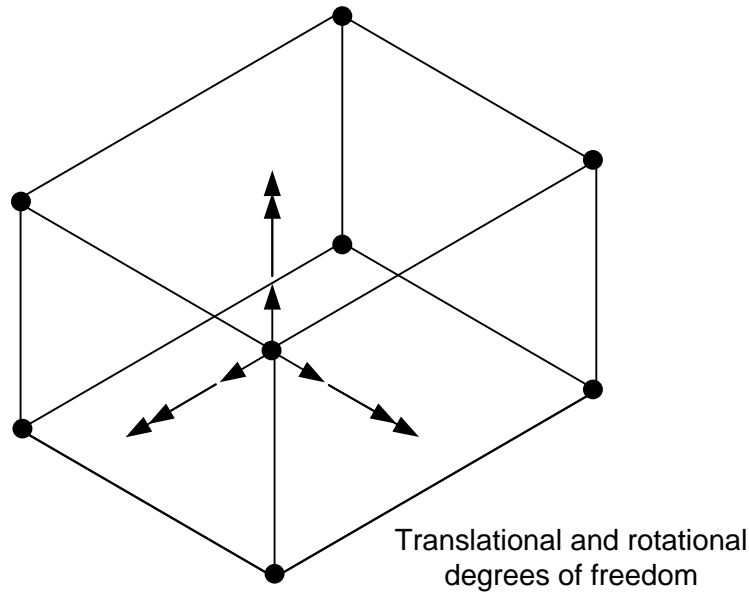
pg. 53

Translational and rotational
degrees of freedom

Figure 4-5: 8-node solid element

The solid elements in ABAQUS can be used for linear analysis and for complex nonlinear analysis involving contact, plasticity and large deformations. ABAQUS includes first-order/linear interpolation elements and second-order/quadratic interpolation. Reduced integration is also available for solid elements.

Second-order elements provide greater accuracy for problems that do not involve severe element distortions. These elements capture stress concentrations more accurately and are better for modelling geometric features because quadratic elements can have curved edges, resulting in the use of less elements to model a curved surface. Second-order elements are also highly effective in modelling bending dominated problems.

Reduced integration for solid elements is the same as for shell elements, i.e. it uses a lower order integration to form the element stiffness matrix, but the mass matrix and distributed loadings still use full integration. Second-order reduced integration elements in ABAQUS generally yield more accurate results than their full integration counterparts. However, for first-order elements the accuracy achieved is largely dependent of the nature of the problem.

The solid elements used to model the concrete infill is C3D8R, a 8-node solid element with reduced first-order integration.

4.2.2.3. STEEL-CONCRETE INTERACTION

This section provides information on interface modelling properties in ABAQUS. The specific interface properties used in the model is mentioned at the end of this section.

Where two surfaces are in contact they transmit shear forces as well as a normal forces across their interface which results in a relationship between the two forces. In the default friction model of ABAQUS the coefficient of friction is directly defined by equation 4-1 as:

$$\mu = \mu(\dot{\gamma}_{eq}, p, \bar{\theta}, \bar{f}^{\alpha}) \hspace{3cm} \text{EQ 4-1}$$

where $\dot{\gamma}_{eq}$ is the equivalent slip rate, p is the contact pressure, $\bar{\theta}$ is the average temperature at the contact point defined as $\bar{\theta} = \frac{1}{2}(\theta_A + \theta_B)$ and $\bar{f}^{\alpha}$ is the average predefined field variable α defined as $\bar{f}^{\alpha} = \frac{1}{2}(f_A^{\alpha} + f_B^{\alpha})$. The subscript 'A' and 'B' refers to two points. Point A is a node on the slave surface and point B corresponds to the nearest node on the opposing master surface. The formulation of the friction coefficient μ is dependant on the slip rate, the contact pressure, the temperature and the field variables.

In ABAQUS it is possible to define a shear stress limit $\bar{\tau}_{max}$. This implies that sliding will occur if the magnitude of the equivalent shear stress reaches $\bar{\tau}_{max}$, regardless of the magnitude of the contact pressure. The specified value of $\bar{\tau}_{max}$ cannot be zero. Figure 4-6 illustrates the shear stress limit.
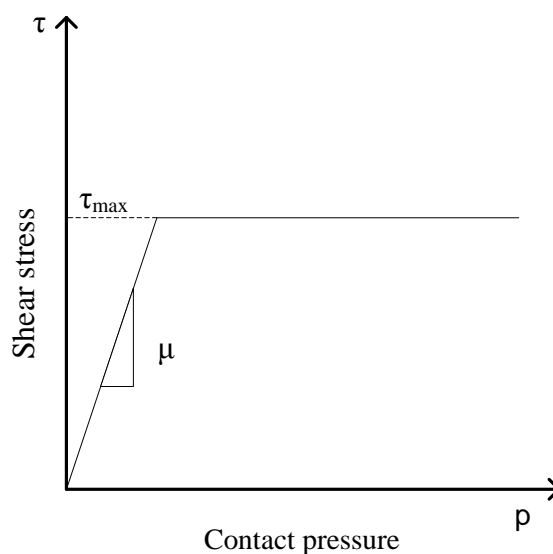

Figure 4-6: Shear stress limit at interface (SIMULIA, 2012)

pg. 55

It could be that some incremental slip may occur even though the friction model determines that the current frictional state is "sticking". The slope of the frictional shear stress versus total slip may be finite while in the sticking stage. This is demonstrated in Figure 4-7. It is possible to specify an elastic slip value in ABAQUS, where a smaller elastic slip value would result in a steeper slope in the "sticking" state.
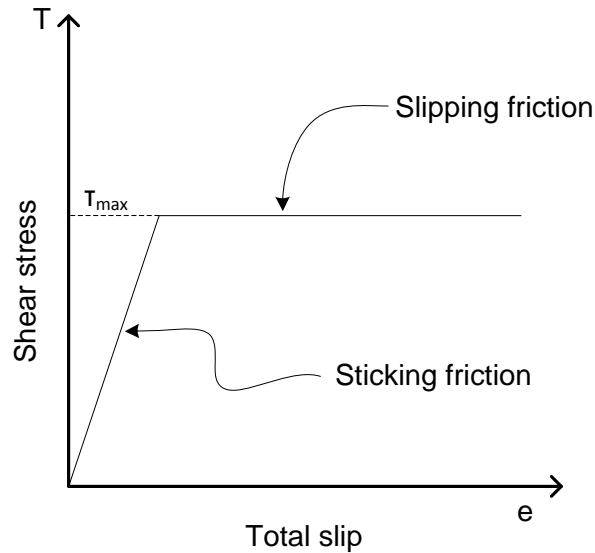

Figure 4-7: Shear stress over total slip

The most common contact pressure-overclosure relationship is the hard-contact relationship, shown in Figure 4-8. When surfaces are in contact any contact pressure can be transmitted between the two surfaces. Once the surfaces are in contact and the pressure reduces to zero the surfaces are allowed to separate.
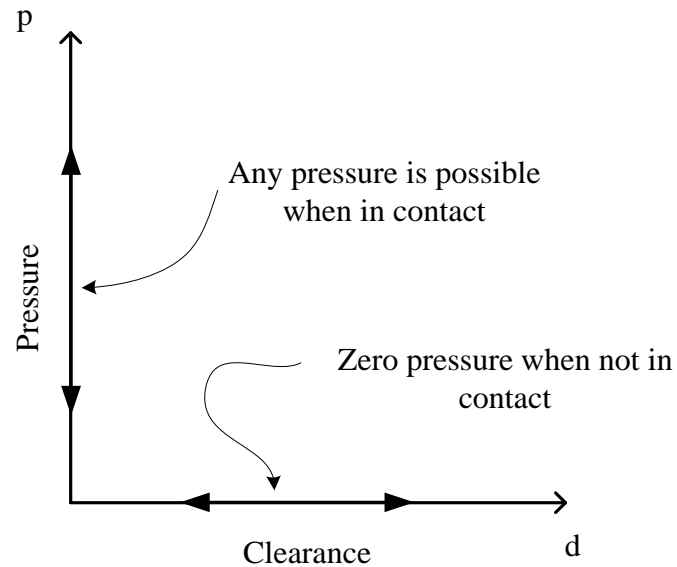
Figure 4-8: Interface pressure over clearance relationship (SIMULIA, 2012)

It was decided to use hard-contact to model the normal behaviour of the steel-concrete interface and the default friction model of ABAQUS. The friction coefficient was chosen as 0.25 which is the same magnitude used by Ellobody (Ellobody & Young, 2006). To decide on a shear stress limit it was assumed that the contact behaviour between the steel tube and concrete would be similar to the contact behaviour between a normal R-bar (smooth reinforcing steel). According the MC-2010 (fib Special Activity Group 5, 2011) the shear stress limit between a R-bar and concrete can be estimated by $0.3\sqrt{f_{cm}}$, where f_{cm} is the mean concrete strength. The model was constructed assuming the mean strength of the concrete infill is $41.5 \ MPa$, giving a shear stress limit of $1.93 \ MPa$. To closely model a so called sticky friction, where there is no elastic slip between the two surfaces, a small elastic slip value of 1×10^{-5} was specified.

4.2.3. MATERIAL MODELLING

This section describes the stress-strain behaviour used to model the concrete and steel respectively.

4.2.3.1. CONCRETE MATERIAL MODEL

Under low confining pressures concrete behaves in a brittle manner. The main failure mechanism is cracking in tension and crushing in compression. The brittle behaviour of concrete becomes more ductile when confining pressures are significantly large to prevent crack propagation. Under these circumstances failure is initiated by consolidation and collapse of the concrete microporous microstructure leading to macroscopic response that resembles a

ductile material. In finite element modelling, the strength improvement observed at a state of triaxial loading can be achieved by the proper definition of the yielding surface and the description of the plastic behaviour of the equivalent stress-strain relationships of the core concrete (Han, et al., 2007). The plasticity of core concrete increases due to passive confinement in the following manner (Han, et al., 2007).

- The strain corresponding to maximum stress increases.
- The descending branch of the stress-strain curves trend to the horizontal.

The increase in the plastic behaviour depends on the level of confinement which is related to the confinement factor given in equation 2-2 from Chapter 2 and is repeated for ease of reference as:

$$\xi = \frac{A_{so} \cdot f_{syo}}{A_{c,nominal} \cdot f_{ck}} \qquad \text{EQ 4-2}$$

The equivalent stress strain model proposed by Han (Han, et al., 2007) showed good agreement to experimental test conducted on CFDST stub columns (Huang, et al., 2010). The model has also been verified by Li (Li, et al., 2012). Therefore, the same confinement model will be used to verify if it is applicable to eccentrically loaded slender columns. The model can be described:

$$\sigma/f_c' = \begin{cases} 2 \cdot (\varepsilon/\varepsilon_0) - (\varepsilon/\varepsilon_0)^2, & (\varepsilon/\varepsilon_0 \leq 1) \\ (\varepsilon/\varepsilon_0)/\beta_0(\varepsilon/\varepsilon_0 - 1)^2, & (\varepsilon/\varepsilon_0 > 1) \end{cases} \qquad \text{EQ 4-3}$$

where $\quad \varepsilon_o = \varepsilon_c + 800\xi^{0.2} \times 10^{-6}$,

$\quad \varepsilon_c = (1300 + 12.5f_c') \times 10^{-6}$, and

$\quad \beta_0 = (2.36 \times 10^{-5})^{[0.25+(\xi-0.5)^7}(f_c')^{0.5} \times 0.5 \quad \geq 0.12$

in the equations the term f_c' is the cylinder strength of the concrete with units of MPa. The cylindrical strength of concrete typically falls between 0.7 and 0.9 of the cube strength. A cylinder strength of 0.8 of the cube crushing strength is widely accepted (Robberts & Marshall, 2009). Using the dimensions given in Table 4-1; a cube strength of 50 MPa and S355W steel properties for the outer tube the stress-strain behaviour shown in Figure 4-9 was obtained for a confinement factor (ξ) of 0.753.
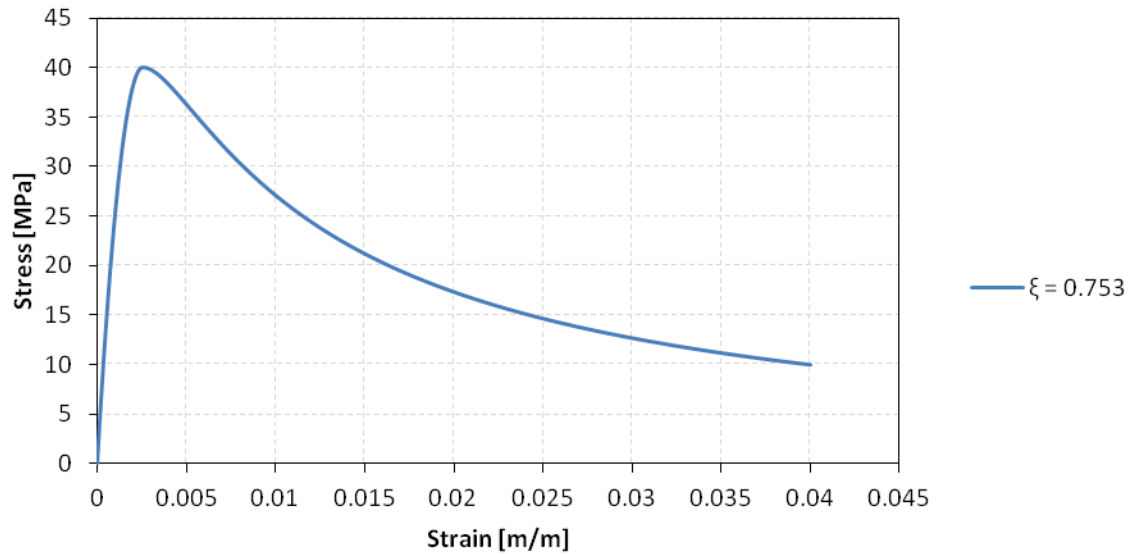
Figure 4-9: Stress-Strain relationship of concrete infill

4.2.3.1.1. INCORPORATION INTO ABAQUS

The concrete damaged plasticity model in ABAQUS was used to model the concrete infill. A description of the model is now presented.

Modelling the behaviour of concrete under large hydrostatic pressures is outside the scope of the damaged plasticity model in ABAQUS. The model aims to capture the effects of irreversible damage associated with the failure mechanisms that occur in concrete under confining pressures less than five times the ultimate compressive stress in uniaxial compression loading. These effects are exhibited in the following macroscopic properties:

- Different yield strengths in tension and in compression.
- Softening behaviour in tension as opposed to initial hardening followed by softening in compression.
- Different degradation of the elastic stiffness in tension and compression.
- Stiffness recovery during cyclic loading
- Rate sensitivity, especially an increase in peak strength with strain rate.

The plastic-damage model in ABAQUS is based on work proposed by Lubliner (Lubliner, et al., 1989) and by Lee and Fenves (Lee & Fenves, 1998).

pg. 59

4.2.3.1.2. DEFINING CONCRETE DAMAGED PLASTICITY IN ABAQUS

As mentioned in Chapter 2 the concrete damaged plasticity (CDP) model in ABAQUS is a modification of the Drucker-Prager model. The evolution equations of the hardening variables $\tilde{\varepsilon}_t^{pl}$ and $\tilde{\varepsilon}_c^{pl}$ are conveniently formulated by considering uniaxial loading conditions first and then extended to multiaxial conditions.

The CDP model in ABAQUS was used to model the concrete core. The model is a continuum, plasticity-based, damage model for concrete. It assumes that the main two failure mechanisms are tensile cracking and compressive crushing of the concrete material. The evolution of the yield surface is controlled by two hardening variables, the tensile and compressive equivalent plastic strains. These variables are linked to failure mechanisms under tension and compression loading respectively.

The following parameters are used to describe the concrete's performance under multiaxial loading:

- K_c: The failure surface in the deviatoric cross section is governed by K_c. The parameter K_c can be interpreted as the ratio of the distances between the hydrostatic axis and the compression and tension meridians, respectively. This must always larger than 0.5 and smaller than 1.0. With a value of 1.0 the cross sectional shape is circular as in the Drucker-Prager model. Figure 4-10 shows a deviatoric cross section of the failure surface defined in the CDP model.
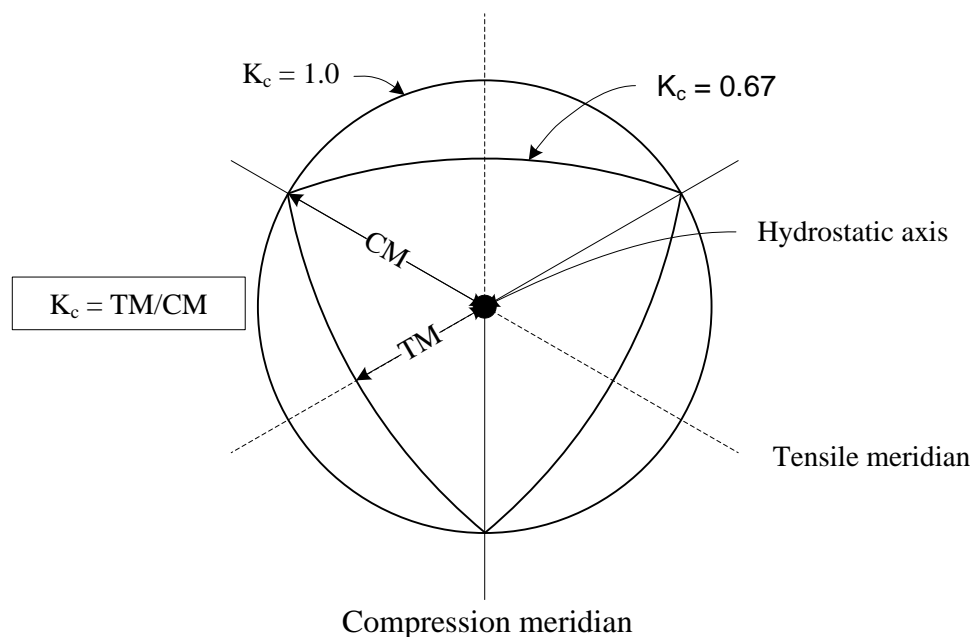

Figure 4-10: Deviatoric cross section of failure surface in CDP model (SIMULIA, 2012)

pg. 60

The CDP model in ABAQUS recommends a value of $K_c = 2/3$.

- **Plastic potential eccentricity**: The eccentricity parameter (ϵ) changes the shape of the meridians of the plastic potential surface in the stress space. In the CDP model the plastic potential surface in the meridional plane assumes the form of a hyperbola. The eccentricity parameter is a small positive value which expresses the rate of approach of the plastic potential hyperbola to its asymptote. It is defined as the distance, measured along the hydrostatic axis, between the centre of the hyperbola and its vertex. The centre of a hyperbola is where the asymptotes intersect. Figure 4-11 shows the plastic potential surface in the meridional plane.
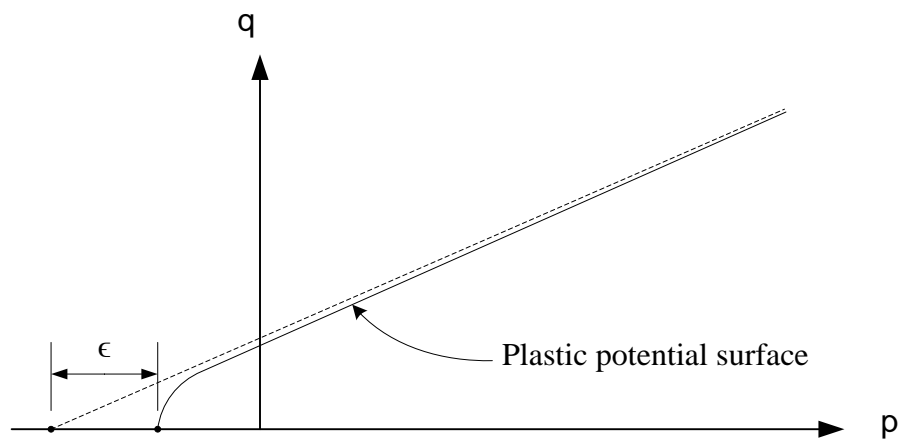

Figure 4-11: Hyperbolic plastic potential surface in the meridional plane (SIMULIA, 2012)

The eccentricity parameter (ϵ) can be calculated as a ratio of tensile strength to compressive strength (Jankowiak, et al., 2005). The CDP model recommends a value of $\epsilon = 0.1$. When $\epsilon = 0.0$, the plastic potential surface in the meridional plane becomes a straight line, as in the Drucker-Prager model.

- **fb0/fc0**: Is a ratio of the strength in biaxial state to the strength in the uniaxial state. This parameter describes the point at which the material undergoes failure under biaxial compression. The CDP model uses $f_{b0}/f_{c0} = 1.16$ as default.
- **Dilation angle**: The dilation angle (ψ) is the angle of inclination of the failure surface to the hydrostatic axis measured in the meridional plane. The angle is interpreted as the concrete internal friction angle. In an analysis a value of $\psi = 36°$ or $\psi = 40°$ is usually assumed (Kmiecik & Kaminski, 2011).

pg. 61

- **Viscosity parameter**: Convergence issues may arise when full nonlinearity of the concrete material with gradual degradation under increased stress is assumed, especially with tensile stress. Reducing the size of the increment or increasing the maximum number of steps when solving the problem using Newton-Raphson may prove to be insufficient. The CDP model uses the viscosity parameter (μ) to allow the model to slightly exceed the plastic potential surface in certain, sufficiently small solution steps. In other words, μ is used for the viscoplastic regularization of the constitutive equations. It is necessary to use a trial and error approach to find the correct viscosity parameter since the minimum value of μ should be used.

The following values were chosen for the parameters discussed earlier:

- **Dilation angle**: 36°
- **Eccentricity**: 0.078
- **fb$_0$/fc$_0$**: 1.16 (default value)
- **K**: 0.67 (default value)
- **Viscosity parameter:** 0.0005

The stress-strain model in Figure 4-9 is used as an input parameter in ABAQUS in two stages namely, the elastic stage and the plastic stage. The elastic stage is entered using two variables, namely:

- The elastic modulus of the concrete
- The initial Poisson's ratio of concrete.

The elastic modulus of the concrete was obtained from the stress-strain curve shown in Figure 4-9 by fitting a straight line to the linear region of the initial slope. An elastic modulus of $21.26\ GPa$ was obtained from Figure 4-9. The initial Poisson's ratio of the concrete was taken as 0.2. The plastic region of the model is given in tabular form as the yield stress versus the inelastic strain, where inelastic strain is only the strain after the elastic strain. In other words the inelastic strain starts as zero at the yield stress. To ensure that ABAQUS interpreted the input data correctly a quick check was performed. A single brick element was modelled with the concrete material model described above and a strain applied. The stress-strain output of the element is plotted against the calculated stress-strain relationship from Figure 4-9 in Figure 4-12. The results were almost identical and thus assumed correct.
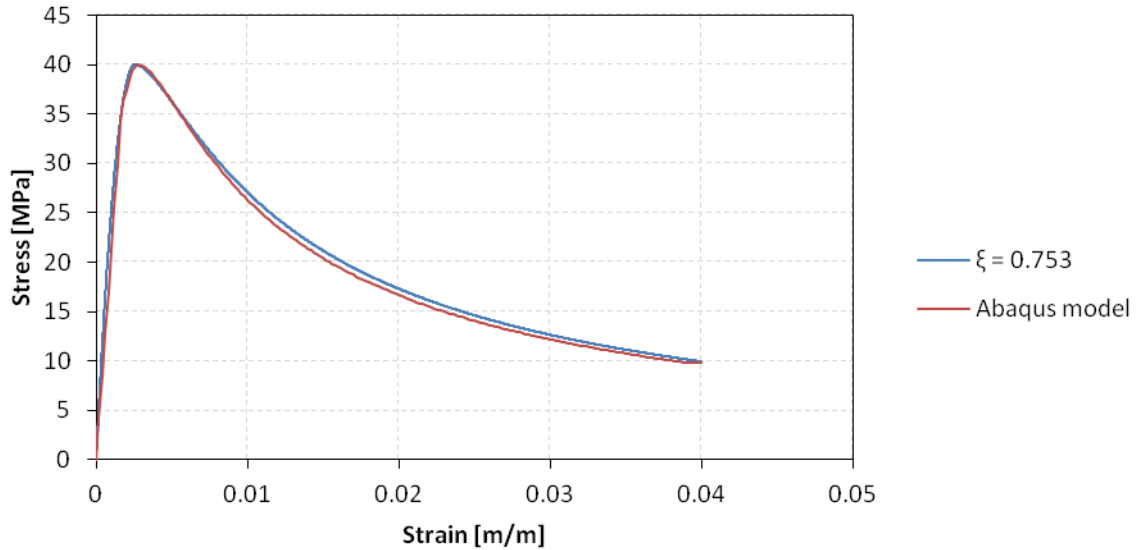
Figure 4-12: Comparing output from ABAQUS to desired stress-strain relationship

The tensile behaviour of the concrete can be specified using the yield stress and cracking strain or the yield stress and displacement or the yield stress and fracture energy. The tensile behaviour of the concrete was defined using yield stress and fracture energy. The tensile strength of the concrete can be estimated from the characteristic strength as $0.3(f_{ck})^{2/3}$, obtained from the Model Code 2010 (fib Special Activity Group 5, 2011), where the characteristic strength, f_{ck}, is taken as 67% of the cube strength f_{cu}. Using $f_{cu} = 50\ MPa$ yields a tensile strength of $f_{ctm} = 3.118\ MPa$. The fracture energy was estimated in a similar manner, also from the Model Code 2010 (fib Special Activity Group 5, 2011), with $G_f = 73 \cdot (f_{ck} + 8)^{0.18}$, where G_f is the fracture energy. This yields a fracture energy equal to $G_f = 142.748\ N/m$.

4.2.3.2. STEEL MATERIAL MODELLING

The material model for structural steel proposed by Liang (Liang, 2009) was used. The transition from the elastic to the plastic region is represented by a smooth curve described by the equation 4-4 as.

$$\sigma_s = f_{sy}\left(\frac{\varepsilon_s - 0.9\varepsilon_{sy}}{\varepsilon_{st} - 0.9\varepsilon_{sy}}\right)^{\frac{1}{45}} \qquad (0.9\varepsilon_{sy} < \varepsilon_s \leq \varepsilon_{st}) \qquad \text{EQ 4-4}$$

where σ_s is the stress in the steel, ε_s is the strain in the steel, f_{sy} is the yield stress, ε_{sy} is the yield strain and ε_{st} is the hardening strain taken as 0.005.
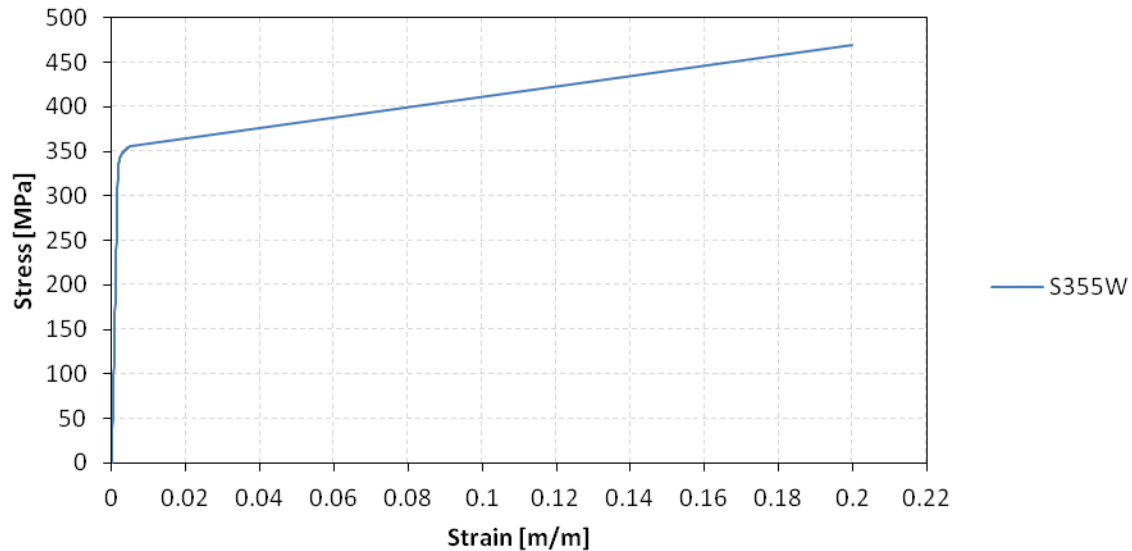
pg. 63

Figure 4-13: Stress strain relationship of S355W steel

The stress-strain relationship in Figure 4-13 uses equation 4-4 to obtain the curved transition. With the yield stress taken as $f_{sy} = 355\ MPa$ and the elastic modulus taken as 200 GPa. The ultimate stress is taken as $f_{su} = 470\ MPa$ and the ultimate strain as $\varepsilon_{su} = 0.2$. The reasoning for using the curved transition between the elastic and plastic regions of the stress-strain relationship is that the smoother transition is thought to help with convergence in finite element analysis.

4.3.   FINITE ELEMENT RESULTS

Base models were developed where after individual parameters were independently varied to determine the affect on the failure load of the CFDST columns.

4.3.1.   DESCRIPTION OF BASE MODEL

The following parameters were used to obtain load versus displacement curves for the various lengths and annulus sections:

Concrete material: The stress-strain model has the following parameters:

$f_{cu} = 50\ MPa$ Cube strength of concrete.

$\nu = 0.2$ Initial Poisson's ratio.

$E = 21.26\ GPa$ Elastic modulus.

$G_f = 142.748\ N/m$ Fracture energy.

pg. 64

$$f_{ctm} = 3.118 \, MPa \quad \text{Tensile strength}$$

Steel material: The stress-strain model has the following parameters:

$$f_{sy} = 355 \, MPa \qquad \text{Yield strength.}$$

$$f_{su} = 470 \, MPa \qquad \text{Ultimate strength.}$$

$$\nu = 0.3 \qquad \text{Poisson's ratio.}$$

$$E = 200 \, GPa \qquad \text{Elastic modulus.}$$

Steel-concrete interface: The steel-concrete interface has the following parameters.

$$\mu = 0.25 \qquad \text{Friction coefficient.}$$

$$\bar{\tau}_{max} = 1.93 \, MPa \qquad \text{Shear stress limit.}$$

$$e_s = 1.0 \times 10^{-5} \qquad \text{Elastic slip.}$$

4.3.2.   AXIAL LOAD VERSUS AXIAL DISPLACEMENT

Figure 4-14 presents the FE simulations of the axial load against the axial displacement of the CFDST columns.
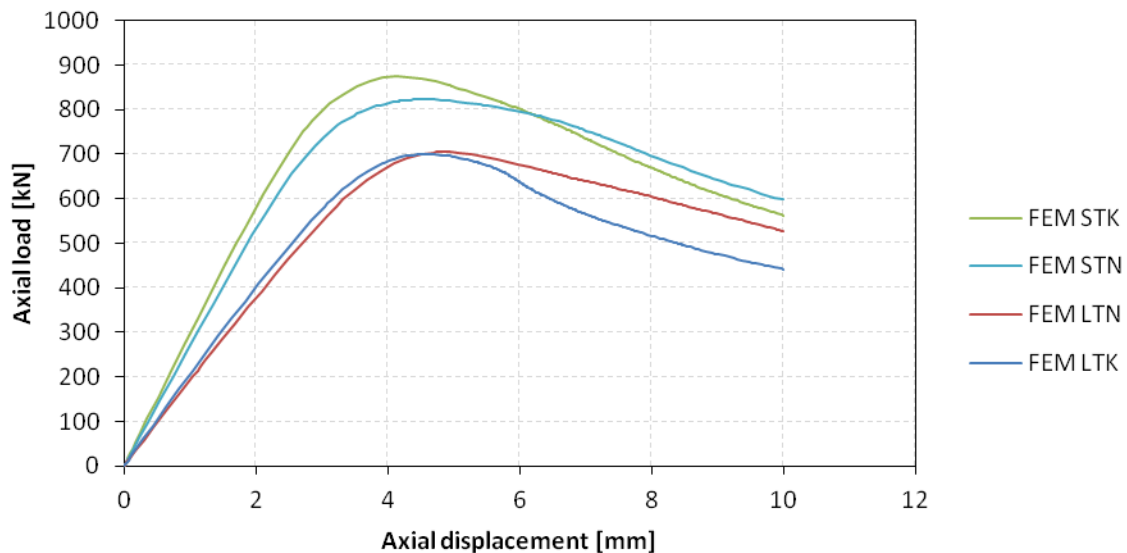

Figure 4-14: Axial load vs. axial displacement response from FEM

pg. 65

Table 4-2 presents the load and axial displacement in tabular form

Table 4-2: Axial load and axial displacement of CFDST column

Column description	Peak Load [kN]	Axial displacement at peak load [mm]
LTN	705	5
LTK	700	5
STN	823	5
STK	874	4

The results show that the short CFDST columns yield greater ultimate load capacities compared to the longer CFDST columns. As expected the STK column yields a higher ultimate load capacity compared to the STN column. However the LTK column yields an insignificantly smaller ultimate load capacity compared to the LTN column. This indicates that the FE model does not accurately simulate the CFDST columns. This could be as a result of numerous parameters which are not correctly modelled in the FE model. The most likely cause of the inconsistency is within the confined concrete model, which was adopted without any changes from the CFDST stub columns.

4.4. SENSITIVITY ANALYSIS

A sensitivity analysis was conducted to determine reasons for the discrepancies in the FE simulation results before the results are compared with the experimental results. This section will also provide insight into the influence that certain parameters have on the behaviour of the model. The LTK model was chosen for the sensitivity analysis since it yielded the outlier FE simulation result.

The changes made to the different parameters with respect to the *Base* model are;

- The friction coefficient used in the concrete-steel interface changed to $\mu = 0.5$ and $\mu = 0$.
- The eccentricity was varied by plus and minus 10%.
- The fracture energy of the concrete was doubled and halved.
- The tensile strength of the concrete was doubled.
- Two yield stresses for the steel was considered.
    - $f_{sy} = 300\ MPa$ $f_{su} = 450\ MPa$
    - $f_{sy} = 250\ MPa$ $f_{su} = 365\ MPa$

pg. 66

In all the models the inner and outer tube were both given the same material properties.

- The shear limit of the steel-concrete interface was doubled and halved.

4.4.1. SENSITIVITY TO CHANGES IN THE FRICTION COEFFICIENT

Figure 4-15 shows the axial load response from finite element model LTK with varying coefficients of friction (μ). The *Base* model with a coefficient of friction equal to 0.25 is compared to the '$\mu = 0$' *model* that has a coefficient of friction of zero (frictionless) and the '$\mu = 0.5$' *model* that has a friction coefficient of 0.5.
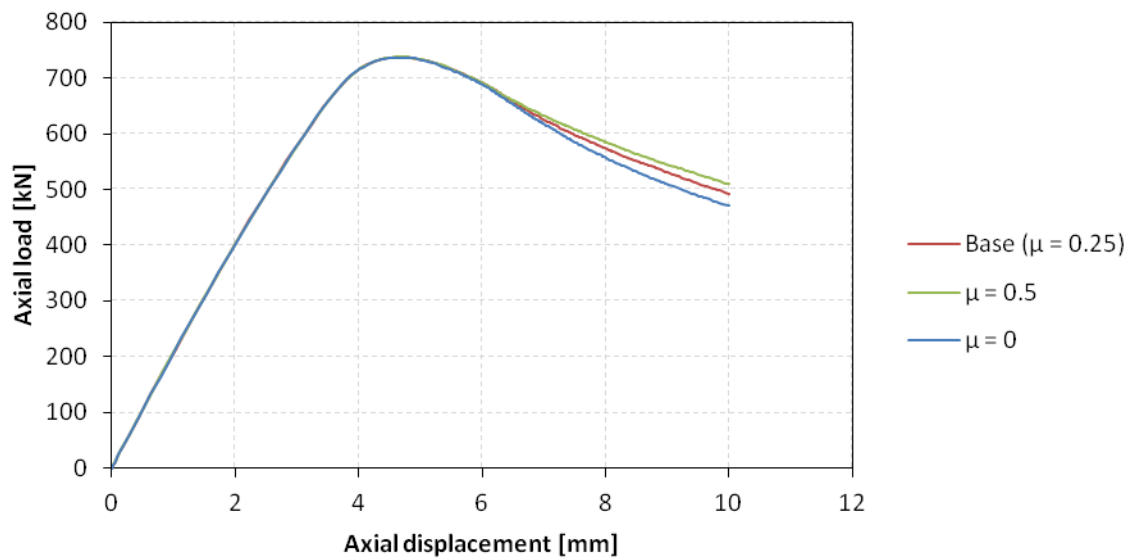

Figure 4-15: Comparison of axial load response for different friction coefficients

Figure 4-16 compares the midspan deflection versus axial load from the finite element model LTK with different friction coefficients.
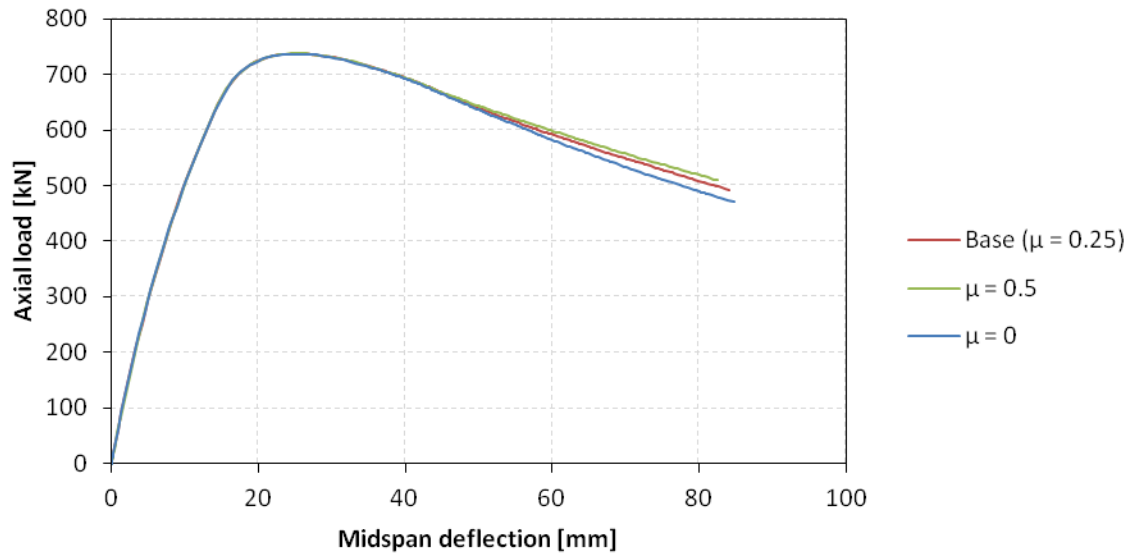
pg. 67

Figure 4-16: Comparison of midspan deflection versus axial load for different friction coefficients

Figure 4-15 and Figure 4-16 shows that changes to the friction coefficient does not affect the pre-peak behaviour however the post peak behaviour in insignificantly affected. During the literature study friction coefficients ranging from 0.25 (Ellobody, et al., 2006) to 0.6 (Han, et al., 2007) was used in FE simulations. This parameter study shows that the model is not sensitive to changes in the friction coefficient.

4.4.2. SENSITIVITY TO CHANGES IN THE ECCENTRICITY OF THE APPLIED LOAD

Figure 4-17 shows the axial load response of the LTK's finite element model with the load applied at different eccentricities (e). The *Base* model, which has an eccentricity of 20mm, is compared to the '$e = 18mm$' model and the '$e = 22mm$' model, where the load is applied at an eccentricity of 18mm, and 22mm, respectively.
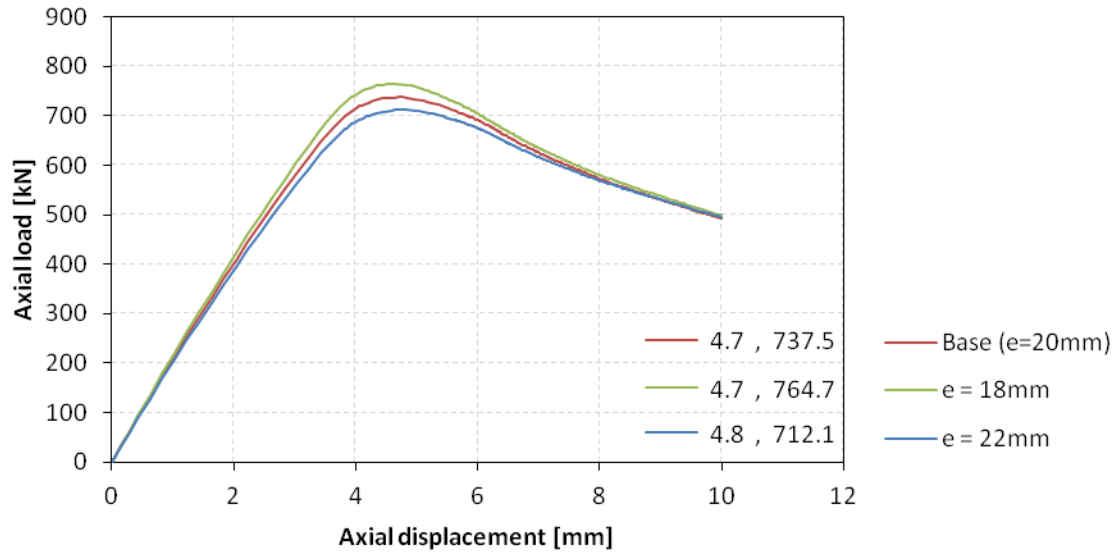
Figure 4-17: Axial load response under different eccentricities

As expected, Figure 4-17 reveals that reducing the eccentricity results in a greater peak load while increasing the eccentricity results in a smaller peak load. The coordinates shown in the graph are the peak load coordinated for each response. The change in eccentricity resulted in a linear difference of approximately 3.5 % in both cases. The 10% changes in eccentricity, i.e. 2mm, applied in this study has an insignificant affect on the displacement at peak load. It is interesting to note that after buckling the all three responses have the same slope. In Figure 4-18 the axial load versus the midspan deflection is plotted. This figure also shows that the three responses have the same slope some time after the peak load has been reached.
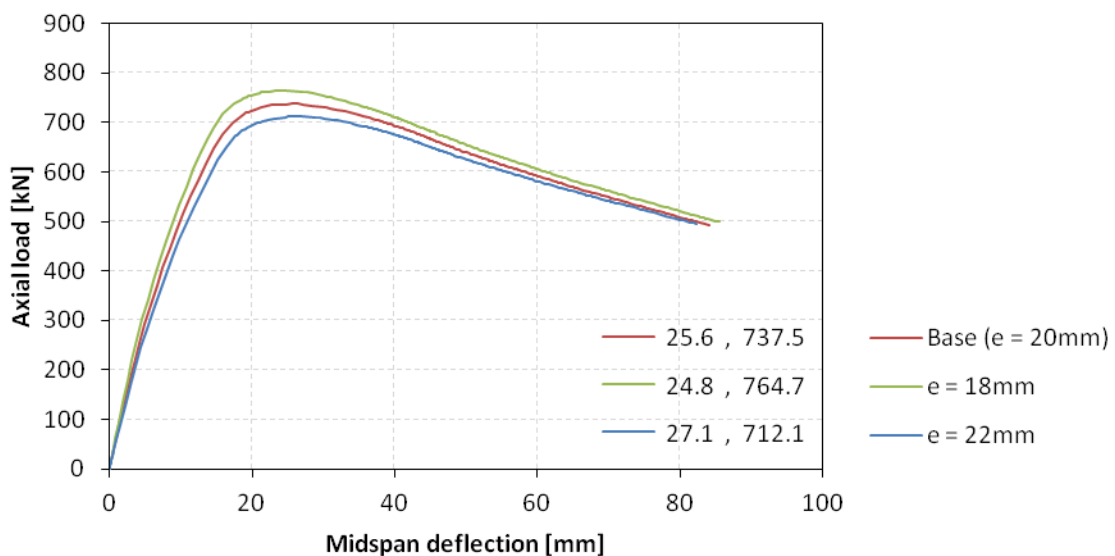

Figure 4-18:Midspan deflection under different eccentricities

The "slope convergence" seen both in Figure 4-17 and Figure 4-18 indicates that a plastic hinge has formed at midspan due to the yielding moment being reached in that region. The coordinates shown in the graph are the peak load coordinated for each response.

In Figure 4-19 the deflected shape of the column is shown for different stages during the analysis. At approximately $2.5mm$ axial shortening, the column curves smoothly along its length. By the end of the analysis, at 10mm axial shortening, the bending in the column is concentrated at midspan where the material has entered the plastic region, called a plastic hinge.
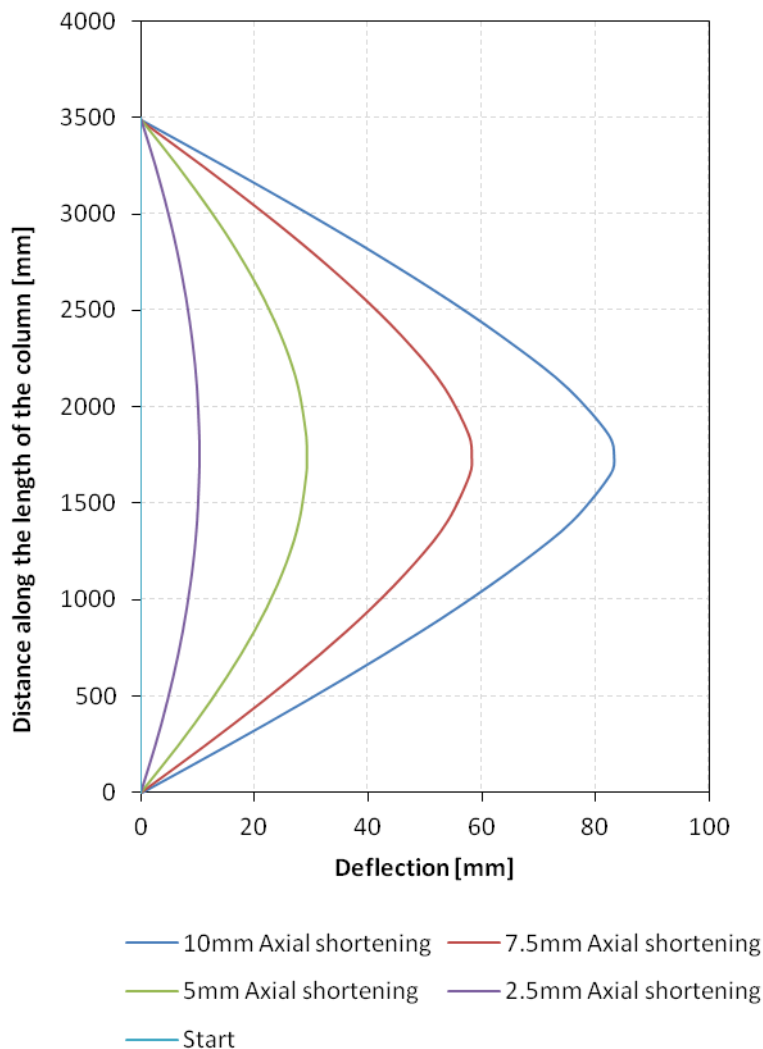

Figure 4-19: Column deflection at different stages during the analysis

The changes in peak load, displacement at peak load and deflection at peak load are presented in Table 4-3.

Table 4-3: Comparison of results from eccentricity parameter study

Model	Peak load [kN]	Displacement at peak load [mm]	Midspan deflection at peak load [mm]
Base	738	4.7	25.6
e = 18mm	765	4.7	24.8
e = 22mm	712	4.8	27.0

This parameter study shows expected levels of sensitivity to the eccentricity of the applied load. This shows that changes in the eccentricity is captured by the FE model.
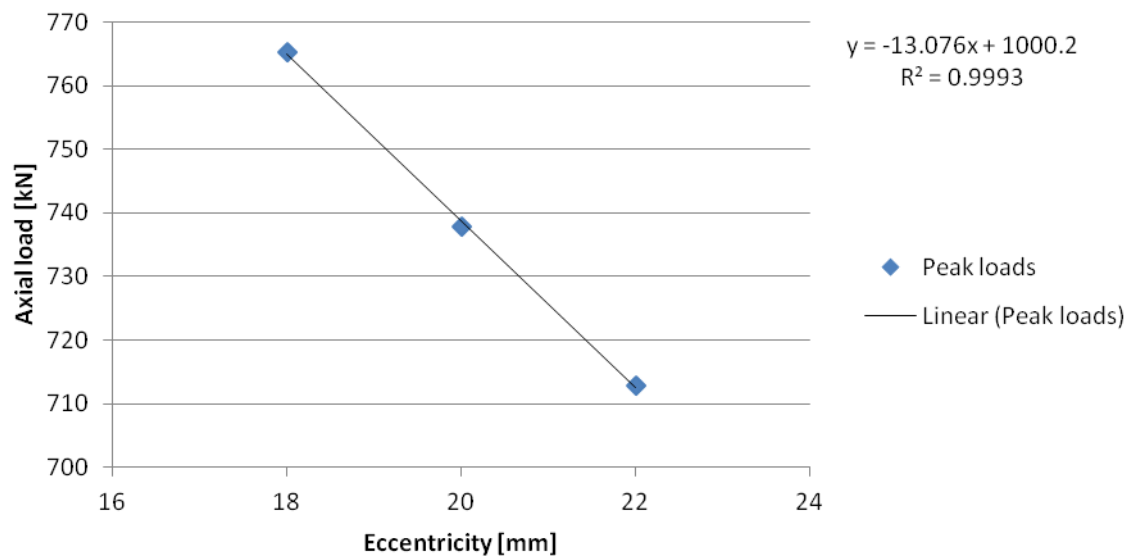
Figure 4-20: Correlation between peakloads for different eccentricities

Figure 4-20 shows a good linear correlation between the peak loads obtained at different eccentricities.

4.4.3. SENSITIVITY TO CHANGES IN THE CONCRETE FRACTURE ENERGY

Figure 4-21 shows the axial load response of the LTK finite element model with different fracture energies specified for the concrete infill. The *Base* model, which uses a fracture energy of $142.75 \ N/m$, is compared to the $F.E \times 2$ model with a fracture energy of $285.5 \ N/m$, respectively.

Figure 4-21: Comparison of axial load response from 'Base', 'F. E.× 0. 5' and 'F. E.× 2' models
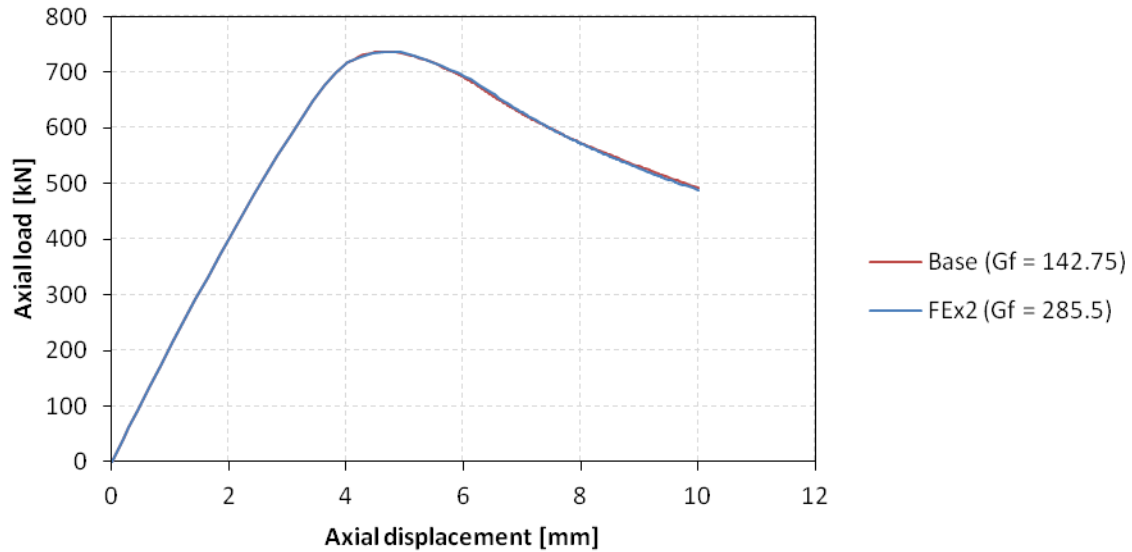
Figure 4-21 shows no noticeable difference in the response. This parameter study shows no sensitivity to changes in the fracture energy of the concrete infill.

4.4.4. SENSITIVITY TO CHANGES IN THE TENSILE STRENGTH OF THE CONCRETE

The axial load response is shown in Figure 4-22 while the axial load versus midspan deflection is shown in Figure 4-23 for the LTK finite element model when the tensile strength of concrete is adjusted. Different ultimate tensile strengths were specified for the concrete infill. The *Base* model, with a concrete tensile strength of $3.118 \, MPa$, is compared to '$Tensile \times 2$' where the concrete has a tensile strength of $6.236 \, MPa$.
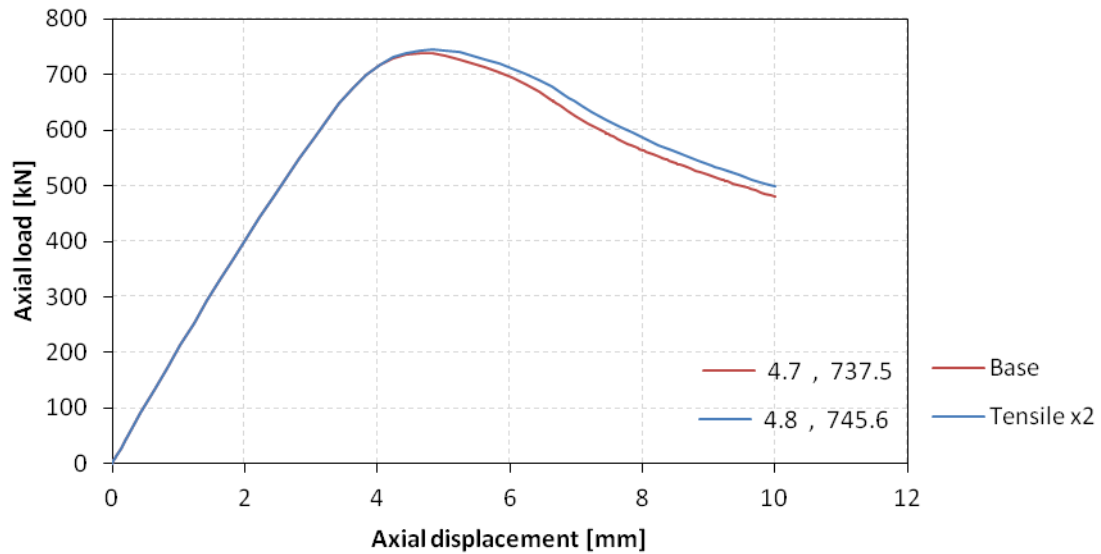
Figure 4-22: Comparison of axial load response of the Base and Tensile x2 models
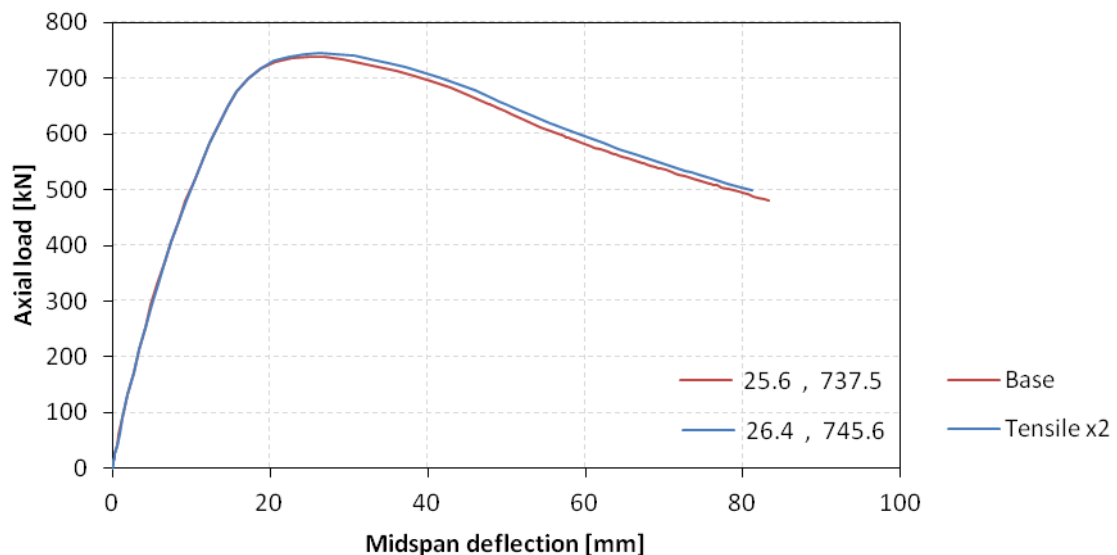
Figure 4-23: Comparison of midspan deflection from Base and Tensile x2 models

The difference shown in Figure 4-22 and Figure 4-23 is most prominent in the post peak region of the response. The coordinates shown in each graph are the peak load coordinated for each response. This parameter study shows that the model is insignificantly sensitive to the tensile strength of the concrete infill prior to the ultimate load being achieved.

4.4.5. SENSITIVITY TO CHANGES IN YIELD STRENGTH OF THE STEEL TUBES

Figure 4-24 shows the axial load response of the LTK finite element model with different types of steel, with different yield stresses used to model the steel tubes. The *Base* model, with a steel

yield strength of 355 MPa, is plotted against the *250 MPa* model and the *300 MPa* model with a steel yield strength of 250 MPa and 300 MPa, respectively.

Figure 4-24: Comparison of axial load response between Base, 250 MPa and 300 MPa models

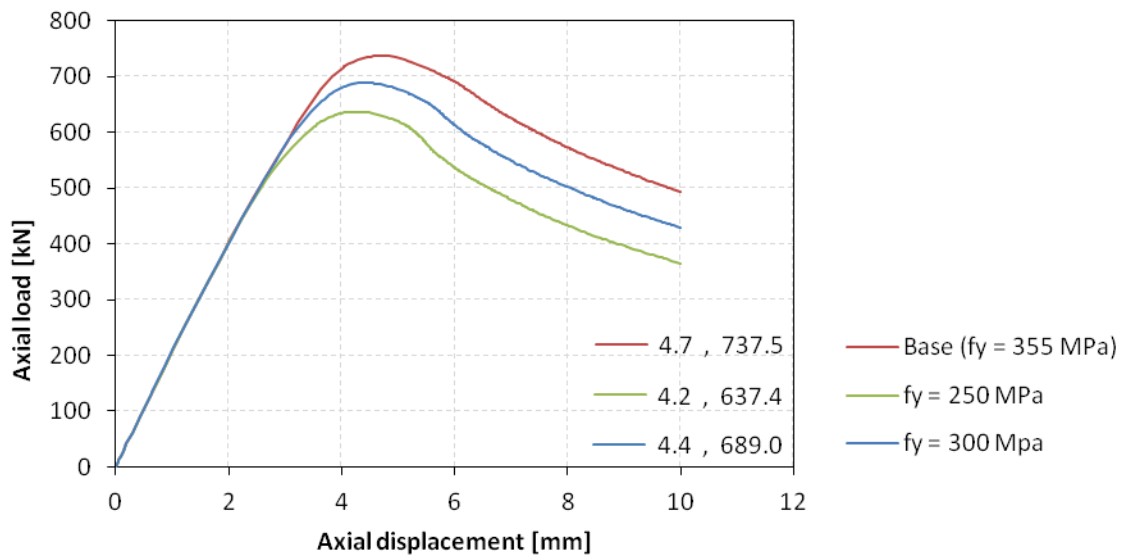Figure 4-25 shows the midspan deflection versus axial load for the *Base*, *300 MPa* and *250 MPa* models. The coordinates shown in the graph are the peak load coordinated for each response.
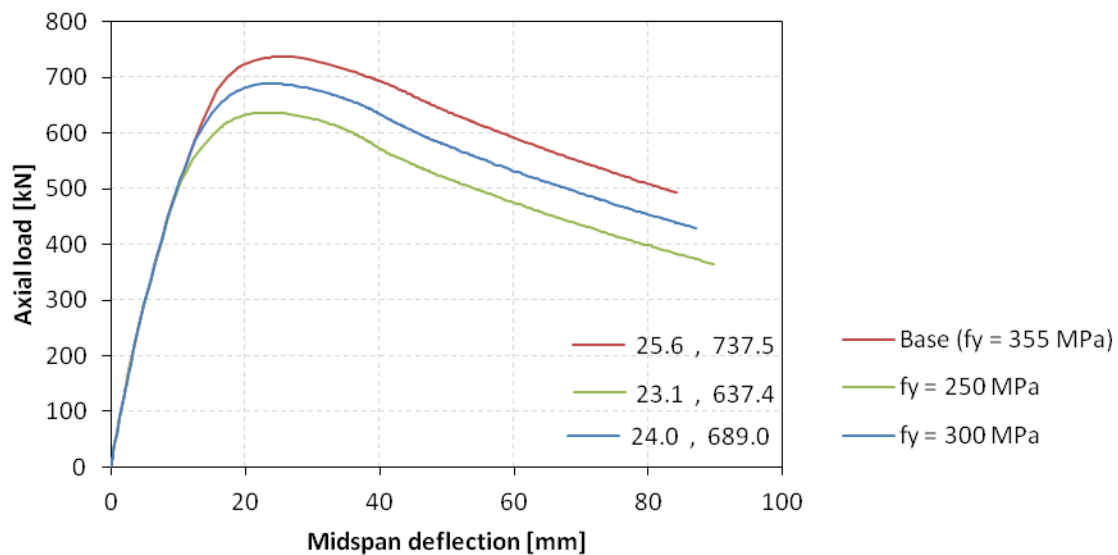

Figure 4-25: Comparison of midspan deflection from Base, 300 MPa and 250 MPa models

Significant differences in the peak load is observed in Figure 4-24 and Figure 4-25. The coordinates shown in the graph are the peak load coordinated for each response. The slope of all three plots are similar in the pre and post-buckling regions. This is due to the material behaviour of the steel in the three different models being the same in the elastic region and the post-yield strain hardening behaviour of all three material models being similar. The differences in peak load data is presented in Table 4-4.

Table 4-4: Comparison of results from Base, 300 MPa and 250 MPa models

Model	Peak load [kN]	Displacement at peak load [mm]	Midspan deflection at peak load [mm]
Base	737.5	4.6	25.6
250 MPa	637.4	4.2	23.1
300 MPa	689.0	4.4	24.0

The changes in the displacement and midspan deflection at peak load is insignificant. However, the peak load itself is influenced by the yield strength of the steel sections as shown in Figure 4-26.
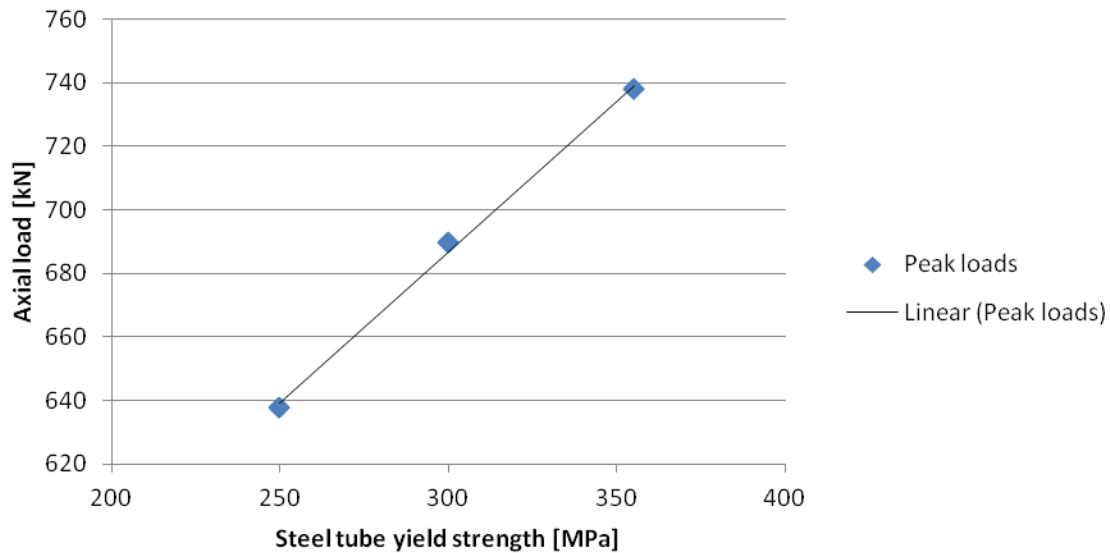
Figure 4-26: Correlation between peak loads from CFDST with different steel tube yield strengths

Figure 4-26 shows good linear correlation between the peak loads and the steel yield strength.

It is worth noting that the confinement model used to obtain the stress-strain relationship for the concrete also changes with different yield strengths for the outer tube. However, the changes are very subtle, as shown in Figure 4-27 .

pg. 75
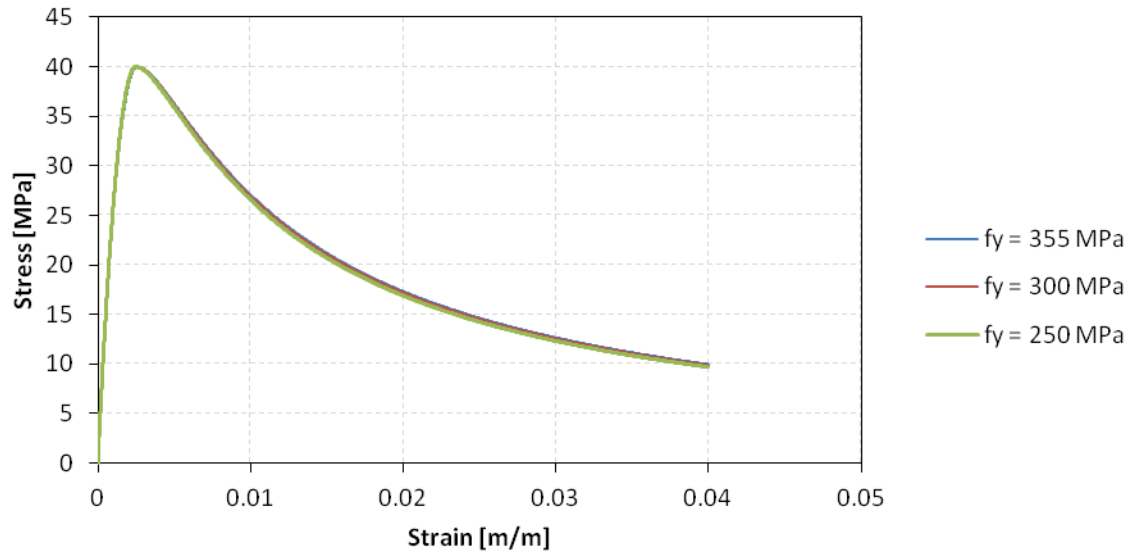
Figure 4-27: Comparison of confinement models for different steel tube yield strengths

This parametric study shows that the FE model is sensitive to changes in the yield strength of the steel tubes being used. However, the confinement model for the stress-strain model of the concrete infill is not sensitive to differences in the yield strength of the confining steel tubes.

4.4.6. SENSITIVITY TO CHANGES IN THE STEEL-CONCRETE INTERFACE SHEAR LIMIT

Figure 4-28 shows the axial load response of the LTK finite element model with different shear limits specified for the steel-concrete interface. The *Base* model, with a shear limit of $1.93\ MPa$, is plotted against the $SL \times 0.5$ model and the $SL \times 2$ model which uses a shear limit of $0.965\ MPa$ and $3.86\ MPa$, respectively. Figure 4-28 compares the response from these models.

pg. 76
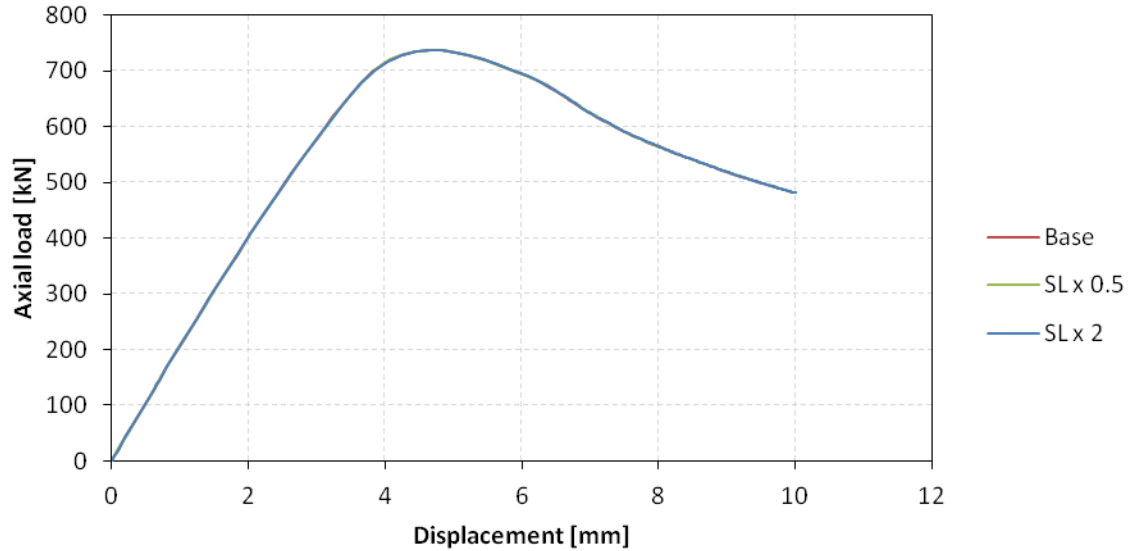
Figure 4-28: Comparison of axial load response between Base, SL x0.5 and SL x2 models

The three responses plotted in Figure 4-28 are identical, showing no sensitivity to the shear limit of the steel-concrete interface for the considered magnitudes.

As discussed in *Section 4.2.2.3* the shear limit was adopted from the fib MC 2010 as $\tau_{max} = 1.93\ MPa$.

however, Han (Han, et al., 2007) uses equation 4-5 to estimate the shear limit as:

$$\tau_{max} = 2.314 - 0.0195(\frac{D_o}{t_o}) \qquad\qquad \text{EQ 4-5}$$

which yields $\tau_{max} = 1.16\ MPa$.

This sensitivity analyses shows that there will be no difference in using either value.

4.5.   CONCLUDING SUMMARY

The sensitivity study shows that the friction coefficients, fracture energy and the shear limit of the steel-concrete interface have an insignificant affect on the response of the column. The tensile strength of the concrete has a moderate influence on the peak load and post peak behaviour. The eccentricity affects the slope of the response before the peak and it affects the peak load but has moderate affect on the post peak behaviour. The yield strength of the steel tube only influenced the peak load and post peak behaviour.

pg. 77

Chapter 5

COMPARISON OF RESULTS

5.1. INTRODUCTION

Chapter 4 discussed the finite element model developed in this study and presented a parameter study to determine the model's sensitivity to changes in certain parameters. In *Chapter 3* the experimental work was presented. This chapter will compare the predictions from the finite element model to experimental results. The axial load, the axial and midspan lateral deflections are used to compare each model to the corresponding experimental test. The peak load data is also compared. The capacity of CFDST columns under concentric loading can be estimated with the model described by the equations in *Section 2.5.3*. These capacities are also used in this chapter as a comparative tool.

5.2. COMPARISON OF RESULTS

The FEM predictions are compared to the experimental results in this section. Three experimental tests per specimen were conducted to obtain an average value for LTK, LTN, STK and STN. The average responses for each set of columns are compared to their respective FE model.

The dimensions and designations of the columns constructed and modelled in this study are repeated in Table 5-1 for ease of reference.

Table 5-1: Dimensions of the different CFDST columns

Specimen identification	Outer CHS (diam x thick) [mm]	Inner CHS (diam x tick) [mm]	Length [mm]	Thickness of concrete fill [mm]
LTK	177.8 x 3.0	76.2 x 3.0	3500	49.3
LTN	177.8 x 3.0	127.0 x 3.0	3500	23.9
STK	177.8 x 3.0	76.2 x 3.0	2500	49.3
STN	177.8 x 3.0	127.0 x 3.0	2500	23.9

5.2.1. COMPARISON OF PEAK LOAD

This section compares the experimental results to the FEM predictions as well as the axial capacity under concentric loads, determined from the model presented in *Section 2.5.3,* as a comparative tool.

Table 5-2 compares the calculated concentric axial load capacity to the experimental test results.

Table 5-2: Comparison between the calculated concentric axial load capacity to the axial capacities obtained from experimental tests

Column ID	Concentric axial capacity determined from equations [kN]	Experimental test results (eccentric loading) [kN]	Percentage difference [%]
LTN	954	624	35
LTK	1024	676	34
STN	1 066	754	30
STK	1174	815	31

The trend in Table 5-2 suggests that an estimated strength reduction of 32.5 % could be assumed for an eccentricity of 20 mm. The longer columns have an average reduction in strength of 34.3 % with an insignificant difference of 0.61 % between the LTK and LTN models. The shorter columns have an average reduction of 30.6 % with an insignificant difference of 0.85 % between the STK and STN models. The nature of the relationship between the column length and the reduction in axial capacity, whether it is linear or not, cannot be commented on, without further experimental tests.

Table 5-3 presents a comparison between the peak loads obtained from the experimental results and the FEM predictions.

Table 5-3: Comparison between peak loads obtained from Experimental results and FEM results

Column ID	Experimental test results (eccentric loading) [kN]]	FEM predictions (eccentric loading) [kN]	Percentage difference [%]
LTN	624	705	13.0
LTK	676	700	3.6
STN	754	823	9.2
STK	811	874	7.8

pg. 79

Table 5-3 reveals that the FE model constantly predicts un-conservative peak loads. The average over prediction is 8.4 % with a maximum of 13.0 % and a minimum of 3.6 %. It is established that the results from the FE model predicts the peak loads of the columns with thick annulus (STK and LTK) with greater accuracy compared the predictions of thin annulus (STN and LTN).

5.2.2.   RESPONSE COMPARISON FOR LTN (3.5M LONG THIN CONCRETE ANNULUS)

Figure 5-1 and Figure 5-2 presents a comparison between the response predicted by the FE model and the average experimental response.

Figure 5-1: Comparison of the average experimental response to the FEM response for LTN
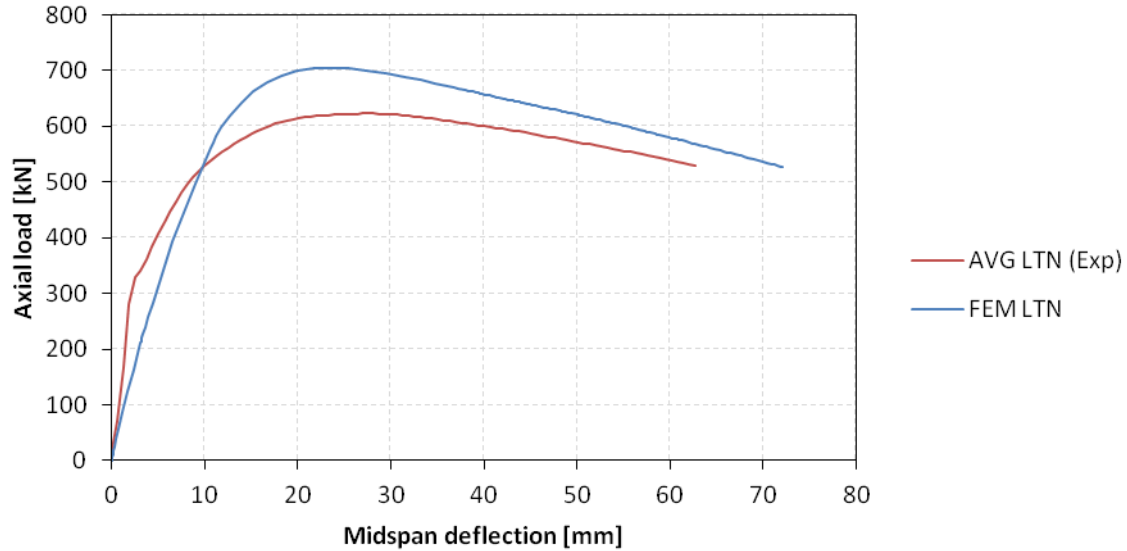
Figure 5-2: Comparison of the average experimental results to FEM predictions, for midspan deflection vs. axial load of the LTN model

Table 5-4 presents a comparison of the peak loads obtained from the FE model and average experimental results respectively for the LTN column.

Table 5-4: Peak load data comparison for LTN specimen

Set of results	Peak Load [kN]	Axial displacement at peak load [mm]	Midspan deflection at peak load [mm]
Experimental	624	7	27
FEM	705	5	23
% Difference	13.0 %	28.6 %	14.8 %

There is a clear discrepancy between the average experimental results and the FEM result for the LTN column. In the FE model the column buckles earlier and at a higher load. Since the three experimental test results were similar, it suggests that the FE model requires refinement to accurately to replicate the experimental response.

5.2.3. RESPONSE COMPARISON FOR LTK (3.5M LONG THICK CONCRETE ANNULUS)

Figure 5-3 and Figure 5-4 presents a comparison between the response predicted by the FE model and the average experimental response.
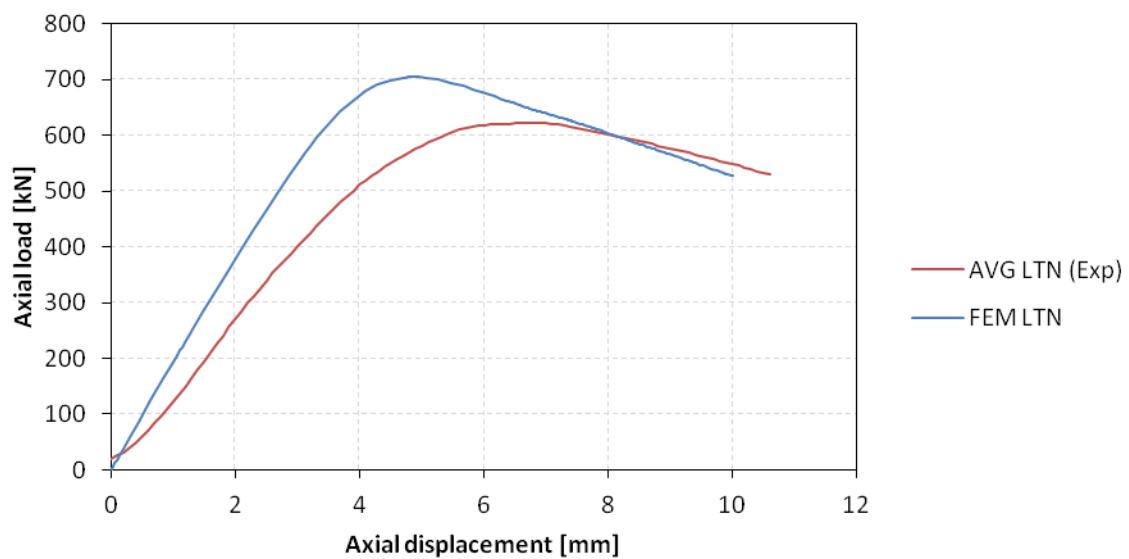
pg. 81

Figure 5-3: Comparison of the avarage experimantal response to the FEM response for the LTK model

Figure 5-4: Comparison of the average experimental results to FEM predictions, for midspan deflection vs. axial load of the LTK model

Table 5-5 presents a comparison of the peak loads obtained from the FE model and the average experimental results respectively for the LTK column.

pg. 82

Table 5-5: Peak load data comparison for model LTK

Set of results	Peak Load [kN]	Axial displacement at peak load [mm]	Midspan deflection at peak load [mm]
Experimental	676	6	24
FEM	700	5	26
% Difference	3.6 %	16.7 %	8.3 %

The LTK model yields a smaller discrepancy compared to the LTN model. However, the axial displacement at peak load is smaller in the FE model. The FE results for this column is questionable as it yielded outlier results compared to the other FE simulation results.

5.2.4. RESPONSE COMPARISON FOR STN (2.5M SHORT THIN CONCRETE ANNULUS)

Figure 5-5 and Figure 5-6 presents a comparison between the response predicted by the FE model and the average experimental response.
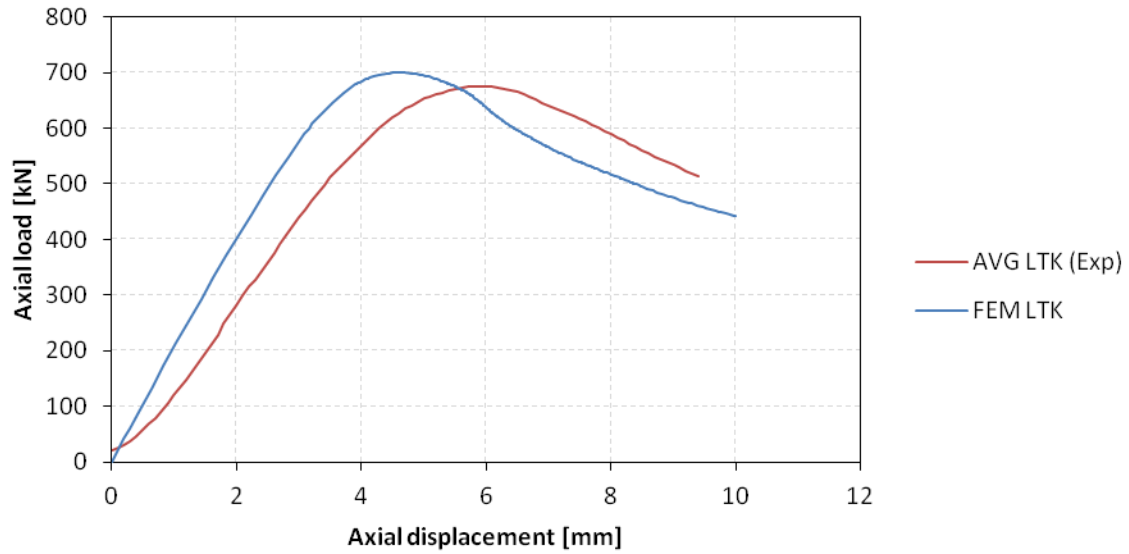

Figure 5-5: Comparison of the average experimental response to the FEM response of the STN model
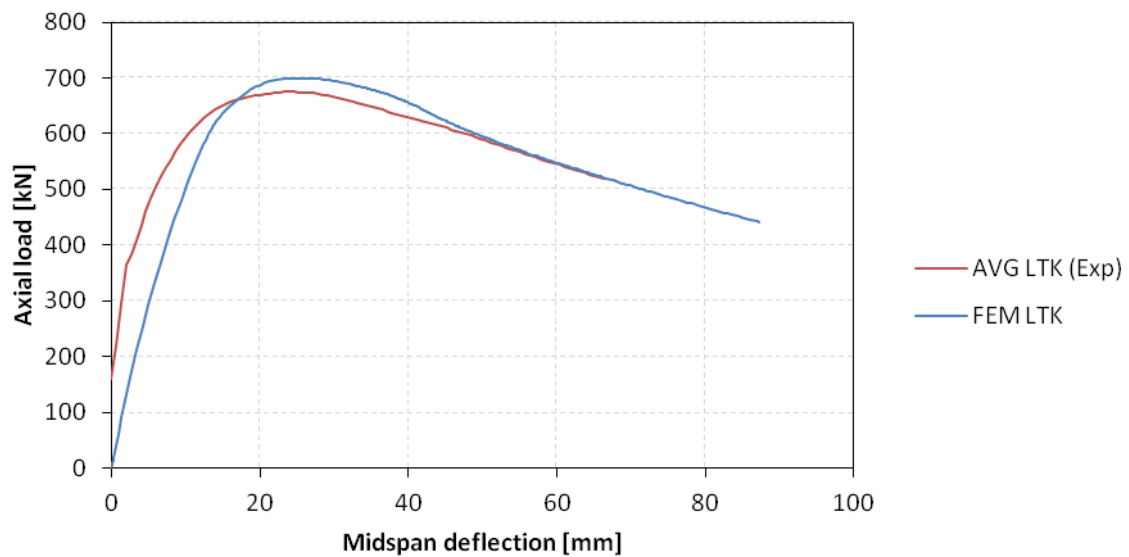
Figure 5-6: Comparison of the average experimental results to FEM predictions, for midspan deflection vs. axial load of the STN model

Table 5-6 presents a comparison of the peak loads obtained from the FE model and the average experimental results respectively for the STN column.

Table 5-6: Peak load comparison for STN specimen

Set of results	Peak Load [kN]	Axial displacement at peak load [mm]	Midspan deflection at peak load [mm]
Experimental	754	7	19
FEM	823	5	15
% Difference	9.2 %	28.6 %	21.1 %

There is a clear discrepancy between the average experimental results and the FEM results for the STN column in terms of the axial and lateral midspan displacements. The difference in peak load is acceptable. In the FE model the column buckles earlier and at a higher load.

5.2.5. RESPONSE COMPARISON FOR STK (2.5M SHORT THICK CONCRETE ANNULUS)

Figure 5-7 and Figure 5-8 presents a comparison between the response predicted by the FE model and the average experimental response.
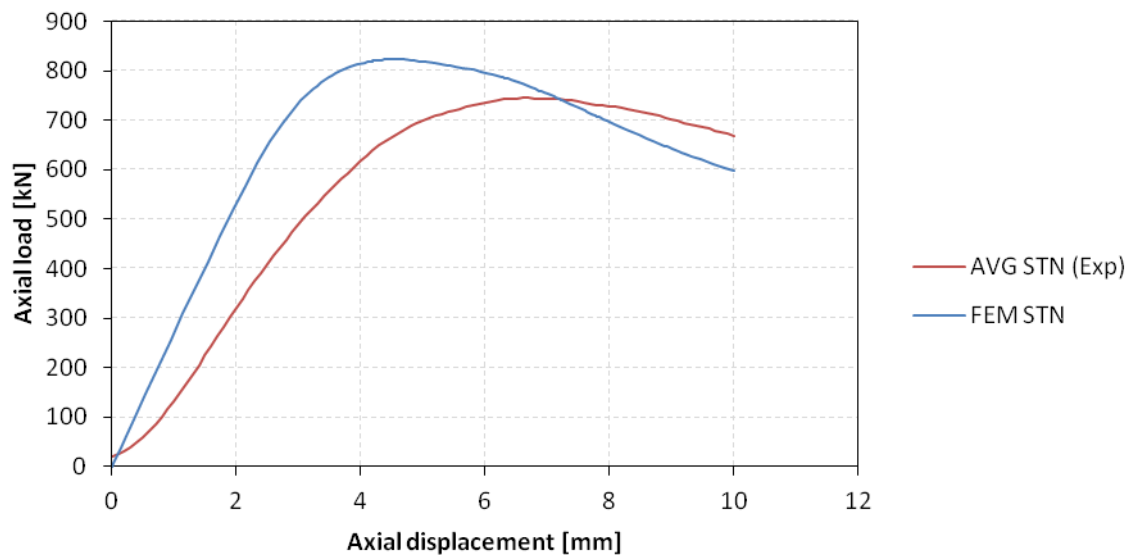
Figure 5-7: Comparison of the average experimental response to the FEM response of the STK model
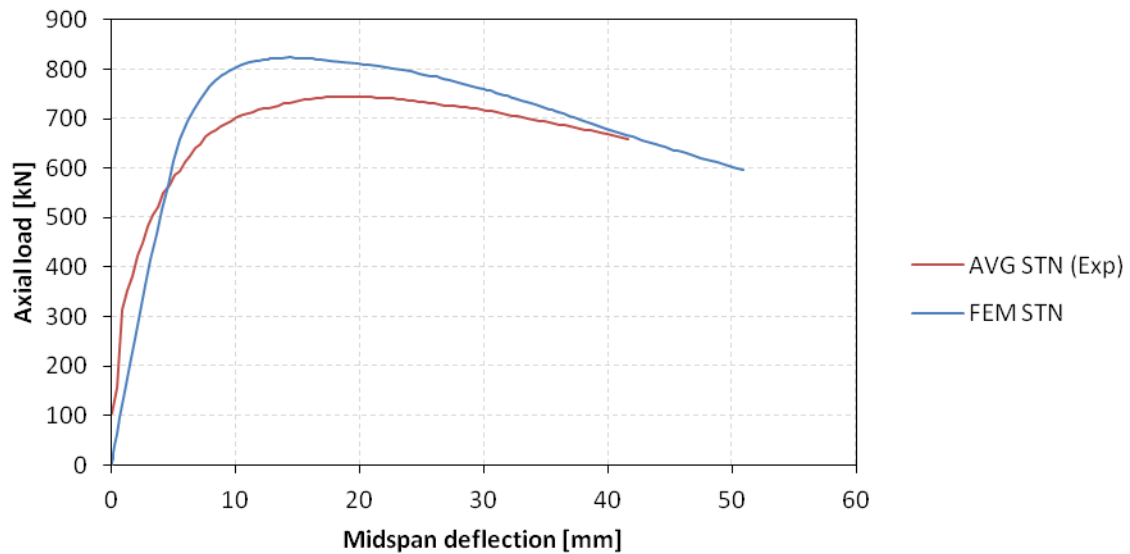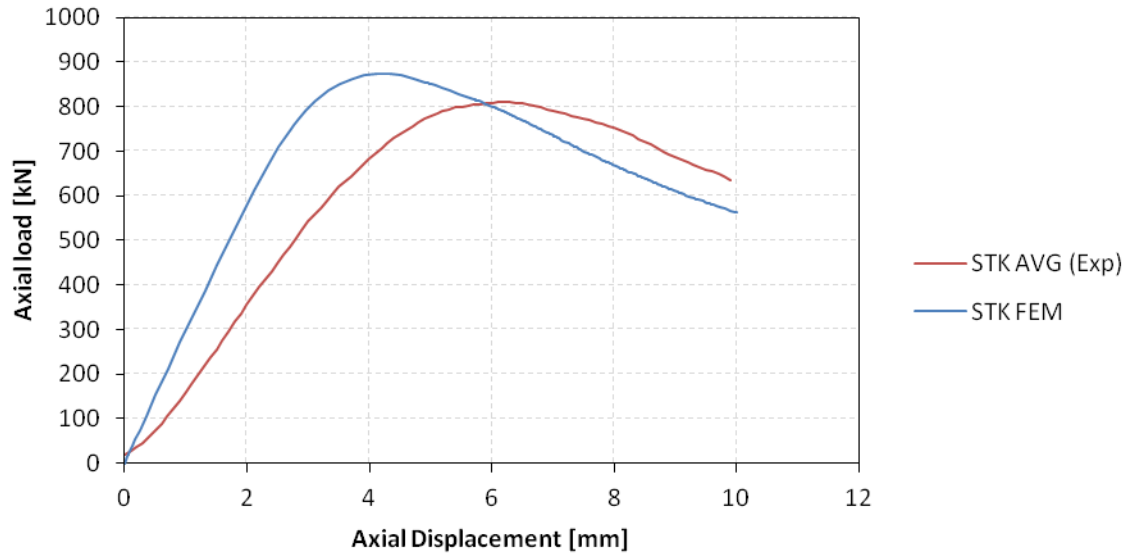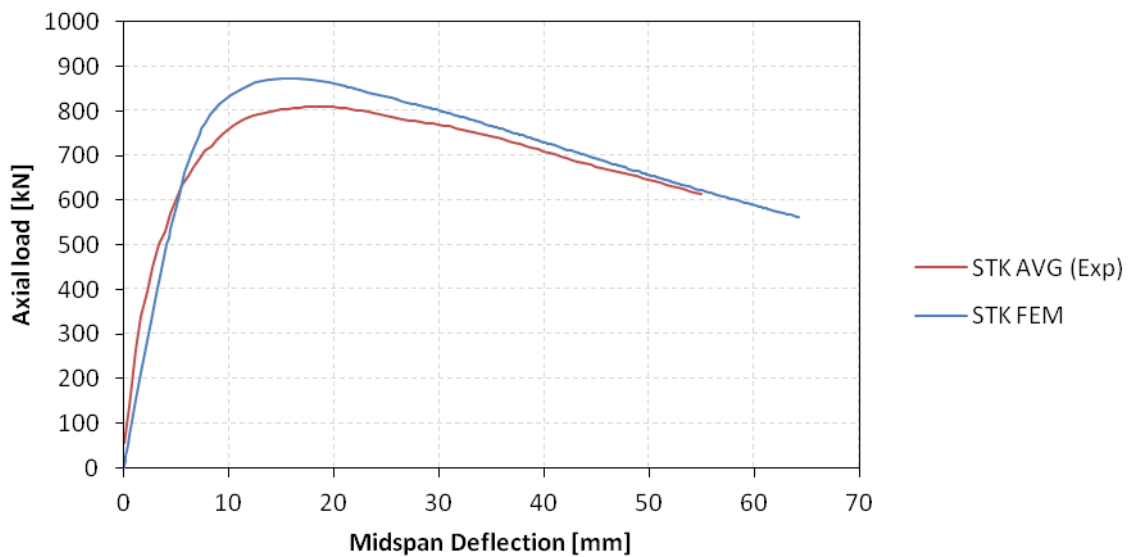

Figure 5-8: Comparison of the average experimental results to FEM predictions, for midspan deflection vs. axial load of the STK model

Table 5-7 presents a comparison of the peak loads obtained from the FE model and the average experimental results respectively for the STK column.

Table 5-7: Peak load data comparison for model STK

Set of results	Peak Load [kN]	Axial displacement at peak load [mm]	Midspan deflection at peak load [mm]
Experimental	811	6	18
FEM	874	4	15
% Difference	7.8 %	33.9 %	17.5 %

Table 5-7 shows discrepancies in peak load which are acceptable. However the axial and midspan deflections are not. In the FE model the column buckles earlier and at a higher load.

5.3. CONCLUDING SUMMARY

This chapter compared the experimental results to the FEM predictions and used the calculated axial capacity under concentric loading to draw comparisons. When considering the comparison between the experimental results and the FEM predictions, the following observations can be made.

- The stiffness of the experimental results is not the true stiffness of the test specimen. The axial displacement of the hydraulic actuator's piston is measured. As the test specimen is compressed between the piston and the crosshead of the testing frame, the frame itself undergoes slight elongation. The elongation of the testing frame is included in the axial displacement measurement of the piston which is used to plot the experimental results. Thus no comment can be made on the discrepancies in stiffness between the experimental results and the FE results.

- It was observed that the FE model with the thicker concrete annulus yielded more accurate results compared with the thin concrete annulus columns. This could suggest that the FE model has trouble with the higher stress concentrations that are present in the thin walled columns, whereas the eccentric force is distributed over a greater area in the thick walled columns.

- When comparing the entire response behaviour, the FE model does not predict the behaviour of the CFDST columns adequately. There are clear discrepancies in the slope of the response which results in inaccurate axial displacements at peak loads. this could be due to the over predictions of the elastic stiffness of the CFDST's

During the sensitivity study none of the chosen parameters affected the slope without influencing the peak load. The slope discrepancy is present in the pre-peak region of the response while the material is still in the elastic stage. This could indicate that the material

model presented by Han (Han, et al., 2007) is not suitable for modelling eccentrically loaded slender CFDST columns.

When comparing experimental results to the axial capacity under concentric loading as calculated by the method described in *Section 2.5.3* the following observations are made:

- For the experimental test specimen in this study, there is a predictable reduction in load carrying capacity between the eccentrically loaded test results and the calculated concentrically loaded axial capacity. Approximately 30% for the STK and STN specimens and approximately 34% for the LTK and LTN specimens.
- The percentage reduction from the calculated capacity to the experimental results is directly proportional to the length of the column, but not to the hollow section ratio. This confirms that the method takes the affect of the hollow section ratio into account.

Chapter 6

CONCLUSIONS AND RECOMMENDATIONS

6.1. OBJECTIVES

The objective of this study was:

1. To determine the axial capacity of eccentrically loaded CFDST columns by means of experimental tests.

2. Find a material model for concrete used to model the behaviour of CFDST columns. Apply this model to eccentrically loaded slender members to verify the material model's validity under these conditions.

3. Find expressions that are able to predict the concentrically loaded axial capacity of slender CFDST columns and determine whether a correlation can be found between the calculated capacities and those determined experimentally.

6.2. CONCLUSIONS

The results from the FEM analysis show that the material model does not accurately capture the behaviour of eccentrically loaded CFDST columns. It over predicted the peak load for every column type. This could be a result of the way the material model was implemented. The material model was incorporated into ABAQUS using the Concrete Damaged Plasticity model, this model can capture the effect of confinement under confining pressures of less than 5 times the ultimate compressive stress of the concrete in uniaxial compression. However the stress-strain relationship incorporated also took confinement effects into account. This could lead to an over estimation of the concrete ductility and strength, leading to the overestimation of the column capacity observed in the results. The confining pressures in the concrete of a stub CFDST column would be much greater than in an eccentrically loaded slender CFDST column, as the member fails from crushing rather than buckling. The higher confinement pressure could exceed that which the Concrete Damaged Plasticity model is capable of capturing. Thus the concrete material model used from Han should be altered to accurately model the behaviour of stub columns, where confinement pressures are much greater.

Comparison of the experimental data to the calculated concentric capacity of the considered CDFST columns show a predictable reduction in load carrying capacity. Approximately 30% for the shorter specimens and approximately 34% for the longer specimens. The percentage reduction from the calculated capacity to the experimental results is directly proportional to the length of the column, but not to the hollow section ratio. This confirms that the method successfully takes the affect of the hollow section ratio into account.

6.3. RECOMMENDATIONS

- In the sensitivity study a good linear correlation between the steel yield strength and the peak load was observed. Further investigation needs to be conducted.

- This study did not draw any comparisons between CFDST columns and any other type of column. A comparison between CFDST columns and RC columns, showing the advantages and disadvantages of both (including construction costs), could go a long way in promoting the use of concrete filled composite sections in South Africa.

- This study showed a clear correlation between the reduction in axial load capacity predicted by the model presented by Zhao (Zhao, et al., 2010) and the length of the column for the applied eccentricity. Further investigation into the trend of this correlation between different lengths and for different eccentricities is necessary to be able to formulate a model to capture this correlation.

- FE models developed in this study needs further development to accurately predict the axial load capacity of CFDST's. I suggest starting with the modelling concentrically loaded stub columns with thick walls and gradually moving towards slender, eccentrically loaded columns with thin walls.

Chapter 7

WORK CITED

Cement and Concrete Institute, 2009. *Fulton's concrete technology.* 9 ed. s.l.:s.n.

Ellobody, E. & Young, B., 2006. Nonlinear analysis of concrete-flled steel SHS and RHS columns. *Thin-Walled Structures,* Volume 44, pp. 919-930.

Ellobody, E., Young, B. & Lam, D., 2006. Behaviour of normal and high strength concrete-filled compact steel tube circular stub columns. *Jounal of Constructional Steel Research,* Volume 62, pp. 706-715.

fib Special Activity Group 5, 2011. *The Model Code 2010,* s.l.: s.n.

Giakoumelis, G. & Lam, D., 2004. Axial capacity of circular concrete-filled tube columns. *Journal of Constructional Steel Research,* Issue 60, pp. 1049-1068.

Gopal, S. & Manoharan, P., 2006. Experimental behaviour of eccentrically loaded slender circular hollow steel columns in-filled with fibre reinforced concrete. *Journal of Constructional Steel Research,* Issue 62, pp. 513-520.

Gupta, P., Sarda, S. & Kumar, M., 2007. Experimantal and computational study of concrete filled steel tubular columns under axial loads. *Journal os Contructional Steel Research,* Issue 63, pp. 182-193.

Han, L., Huang, H., Tao, Z. & Zhao, X., 2006. Concrete-filled double skin steel tubular (CFDST) beam-columns subjected to cyclic bending. *Engineering Structures,* 28(12), pp. 1698-1714.

Han, L., Huang, H. & Zhao, X., 2009. Analytical behaviour of concrete-filled double skin steel tubular (CFDST) beam-columns under cyclic loading. *Thin-Walled Structures,* Volume 47, pp. 668-680.

Han, L. & Huo, J., 2003. Concrete-Filled Hollow Structural Steel Columns after Exposure to ISO-834 Fire Standard. *Journal of Structural Engineering,* 129(1), pp. 68-78.

Han, L., Liao, F. & Tao, Z., 2009. Behaviour and Calculations of Concrete-Filled Double Skin Steel Tubeular (CFDST) Members. *China Steel Construction Society.*

Han, L.-H. & Li, Y.-J. L. F.-Y., 2011. Concrete-filled double skin steel tubular (CFDST) columns subjected to long-term sustained loading. *Thin-Walled Structures,* Volume 49, pp. 1534-1543.

Han, L.-H. & Yao, G.-H., 2004. Experimental behaviour of thin-walled holow structural steel (HSS) columns filled with self-consolodating concrete (SCC). *Thin-Walled Structures,* Issue 42, pp. 1357-1377.

Han, L., Yao, G. & Tao, Z., 2007. Performance of concrete-filled thin-walled steel tubes under pure torsion. *Thin-Walled Structures,* Volume 45, pp. 24-36.

Han, L., Yao, G. & Zhao, X., 2005. Tests and calculations for hollow structural steel (HSS) stub columns filled with self-consolidating concrete (SCC). *Journal od Constructional Research,* Volume 61.

Han, L., Zhao, X. & Tao, Z., 2001. Test and mechanics model for concrete-filled SHS stub columns, columns, and beam columns. *Steel abd Composite Structures,* 1(1), pp. 51-74.

Huang, H., Han, L., Zhong, T. & Zhao, X., 2010. Analytical behaviour of concrete-filled double skin steel tubular (CFDST) stub columns. *Journal of Constructional Steel Research,* Volume 66, pp. 542-555.

Hu, H., Huang, C., Wu, M. & Wu, Y., 2003. Nonlinear Analysis of Axially Loaded Concrete-Filled Tube Colunms with Confinement Effect. *Journal of Structural Engineering,* Volume 129, pp. 1322-1329.

Hu, H. T. & Su, F. C., 2011. Nonlinear analysis of short concrete-filled double skin tube columns subjected to axial compressive forces. *Marine Structures,* Volume 24, pp. 319-337.

Jankowiak, I., Kakol, W. & Madaj, A., 2005. *Identification of a continuos composite beam numerical model based on experimental tests,* Zielons Gora: 7th Conference on Composite Structures.

Kmiecik, P. & Kaminski, M., 2011. Modeling of reinforced concrete structures and composite structures with concrete strength degradation taken into consideration. *Archives of civil and mechanical engineering,* 11(3), pp. 623-636.

Lee, J. & Fenves, L., 1998. Plastic_Damage Model for Cyclic Loading of Concrete Structures. *Journal of Engineering Mechanics,* 124(8), pp. 892-900.

Liang, Q. & Fragomeni, S., 2009. Nonlinear analysis of circular concrete-filled steel tubular short columns under axial loading. *Journal of Constructional Steel Research,* Volume 65, pp. 2186-2196.

Liang, Q. Q., 2009. Perfomance-based analysis of concrete-filled steel tubular beam-columns. Part I: Theory and algorithms.. *Journal of Constructional Steel Research,* 65(2), pp. 363-373.

Liang, Q. Q. & Fragomeni, S., 2009. Nonlinear analysis of circular concrete-filled steel tubular short columns under axial loading. *Journal of Constructional Steel Research,* Volume 65, pp. 2186-2196.

Li, W., Han, L. & Zhao, X., 2012. Axial strength of concrete-filled double skin steel tubular (CFDST) columns with preload on steel tubes. *Thin-Walled Structures,* Volume 56.

Lubliner, J., Oliver, J., Oller, S. & Onate, E., 1989. A Plastic-Damage Model for Concrete. *Journal of the Engineering Mechanics Division of the ASCE,* August.pp. 859-877.

Mander, J., Priestly, M. & Park, R., 1988. Theoretical stress-strain model for confined concrete. *Journal of Structural Engineering,* 114(8), pp. 1804-1826.

Mehta, P. & Monteiro, P., 2006. *Concrete Microstructure, Properties and Materials.* 3 ed. s.l.:McGraw-Hill.

Mirmiran, A. & Naguib, W., 2003. Creep modeling for concrete-filled steel tubes. *Journal of Constructional Steel Research,* Volume 59, pp. 1327-1344.

Mirmiran, A. & Shahawy, M., 1997. Dilation characteristics of con®ned concrete. *Mechanics of cohesive-frictional materials,* Volume 2, pp. 237-249.

Mirmiran, A. & Shahawy, M., 1997. Dilation characteristics of confined concrete. *Mechanics of cohesive-frictional materials,* Volume 2, pp. 237-249.

Moon, J., Roeder, C. W., Lehman, D. E. & Lee, H., 2012. Analytical modeling of bending of circular concrete-filled steel tubes. *Engineering Structures,* Volume 42, pp. 349-361.

Okamura, H. & Ouchi, M., n.d. *Self-compacting concrete: development, present use and future..* Stockholm, Sweden, s.n., pp. 3-14.

Robberts, J. M. & Marshall, V., 2009. *Analysis and Design of Concrete Structures.* s.l.:Cement and Concrete Institute.

Roberts, T., Edwards, D. & Narayanan, R., 1996. Testsing and analysis of steel-concrete-steel sandwich beams.. *Journal of Constructional Steel Research,* 38(3), pp. 257-279.

Schneider, S., Kramer, D. & Sarkkinen, D., 2004. *The design and construction of concrete-filled steel tube column frames.* s.l., 13th World Conference on Earthquake Engineering. Paper number 252.

SIMULIA, 2012. *ABAQUS 6-12 Documentation.* s.l.:s.n.

Tao, Z., Han, L.-H. & Zhao, X.-L., 2007. Behaviour of concrete-filled double skin (CHS inner and CHS outer) steel tubular stub columns and beam-columns. *Journal of Constructional Steel Research,* Issue 60, pp. 1129-1158.

Uy, B., Tao, Z. & Han, L., 2011. Behaviour of short and slender concrete-filled stainless steel tubular columns. *Journal of Constructional Steel Research,* pp. 360-378.

Vrcelj, Z. & Uy, B., 2002. Strength of slender concrete-filled steel box columns incorporating local buckling. *Journal of Constructional Steel Research,* Issue 58, pp. 375-300.

Wang, Y., 1999. Tests on slender composite columns. *Journal of Constructional Steel Research,* Issue 49, pp. 25-41.

Wang, Y. & Moore, D., 1997. A design method for concrete-filled, hollow section, composite columns. *The Structural Engineer,* pp. 368-373.

Xiao, J. & Zhang, C., 2008. Seismic behavior of RC columns with circular, square and. *Construction and Building Materials,* Issue 22, pp. 801-810.

Xiong, D. & Zha, X., 2007. A Numerical Investigation into the Behaviour of Concrete-Filled Steel Tubular Columns Under Initial Stresses. *Journal of Constructional Steel Research,* Volume 63.

Yu, Z.-w., Ding, F. x. & Cai, C. S., 2007. Experimental behaviour of circular concrete-filled steel tube stub columns. *Journal of Constructional Steel Research,* Issue 63, pp. 165-174.

Zhao, X., Han, B. & Grzebieta, R., 2002. Plastic mechanism analysis of concrete-filled double-skin (SHS inner and SHS outer) stub columns. *Thin Walled Structures,* 40(10), pp. 815-33.

Zhao, X. & Han, L., 2006. Double skin composite construction. *Progress in Structural Engineering and Materials,* Volume 8, pp. 93-102.

Zhao, X.-L., Han, L.-H. & Lu, H., 2010. *Concrete-filled Tubular Members and Connections.* s.l.:Spon Press.

Zhao, X. & Packer, J., 2009. Tests and design of concrete-filled elliptical hollow section stub columns. *Thin-Walled Structures,* Issue 47, pp. 617-628.

Zhao, X.-L., Wilkinson, T. & Hancock, G., 2005. *Cold-Formed Tubular Members and Connections Structural Behaviour and Design.* 1 ed. Kidington: Elsevier.

Zhi-wu Yu, F. x. D. C. C., 2007. Experimental behaviour of circular concrete-filled steel tube stub columns. *Journal of Constructional Steel Research,* Issue 63, pp. 165-174.

Zhou, F. & Young, B., 2009. Concrete-filled aluminium circular hollow section column tests. *Thin-Walled Structures,* Issue 47, pp. 1272-1280.